



National Library  
of Canada

Acquisitions and  
Bibliographic Services Branch

395 Wellington Street  
Ottawa, Ontario  
K1A 0N4

Bibliothèque nationale  
du Canada

Direction des acquisitions et  
des services bibliographiques

395, rue Wellington  
Ottawa (Ontario)  
K1A 0N4

*Your file    Votre référence*

*Our file    Notre référence*

## NOTICE

The quality of this microform is heavily dependent upon the quality of the original thesis submitted for microfilming. Every effort has been made to ensure the highest quality of reproduction possible.

If pages are missing, contact the university which granted the degree.

Some pages may have indistinct print especially if the original pages were typed with a poor typewriter ribbon or if the university sent us an inferior photocopy.

Reproduction in full or in part of this microform is governed by the Canadian Copyright Act, R.S.C. 1970, c. C-30, and subsequent amendments.

## AVIS

La qualité de cette microforme dépend grandement de la qualité de la thèse soumise au microfilmage. Nous avons tout fait pour assurer une qualité supérieure de reproduction.

S'il manque des pages, veuillez communiquer avec l'université qui a conféré le grade.

La qualité d'impression de certaines pages peut laisser à désirer, surtout si les pages originales ont été dactylographiées à l'aide d'un ruban usé ou si l'université nous a fait parvenir une photocopie de qualité inférieure.

La reproduction, même partielle, de cette microforme est soumise à la Loi canadienne sur le droit d'auteur, SRC 1970, c. C-30, et ses amendements subséquents.

Canada

UNIVERSITY OF ALBERTA

**Investigation of Water in Poly(vinyl chloride) Based  
Ion-Selective Electrode Membranes**

BY

**Zhong Li**



**A Thesis Submitted  
To The Faculty of Graduate Studies and Research  
In Partial Fulfillment of The Requirements For The Degree of  
Doctor of Philosophy**

**Department of Chemistry**

**Edmonton, Alberta**

**Fall, 1994**



National Library  
of Canada

Acquisitions and  
Bibliographic Services Branch

395 Wellington Street  
Ottawa, Ontario  
K1A 0N4

Bibliothèque nationale  
du Canada

Direction des acquisitions et  
des services bibliographiques

395, rue Wellington  
Ottawa (Ontario)  
K1A 0N4

*Your file    Votre référence*

*Our file    Notre référence*

THE AUTHOR HAS GRANTED AN  
IRREVOCABLE NON-EXCLUSIVE  
LICENCE ALLOWING THE NATIONAL  
LIBRARY OF CANADA TO  
REPRODUCE, LOAN, DISTRIBUTE OR  
SELL COPIES OF HIS/HER THESIS BY  
ANY MEANS AND IN ANY FORM OR  
FORMAT, MAKING THIS THESIS  
AVAILABLE TO INTERESTED  
PERSONS.

L'AUTEUR A ACCORDE UNE LICENCE  
IRREVOCABLE ET NON EXCLUSIVE  
PERMETTANT A LA BIBLIOTHEQUE  
NATIONALE DU CANADA DE  
REPRODUIRE, PRETER, DISTRIBUER  
OU VENDRE DES COPIES DE SA  
THESE DE QUELQUE MANIERE ET  
SOUS QUELQUE FORME QUE CE SOIT  
POUR METTRE DES EXEMPLAIRES DE  
CETTE THESE A LA DISPOSITION DES  
PERSONNE INTERESSEES.

THE AUTHOR RETAINS OWNERSHIP  
OF THE COPYRIGHT IN HIS/HER  
THESIS. NEITHER THE THESIS NOR  
SUBSTANTIAL EXTRACTS FROM IT  
MAY BE PRINTED OR OTHERWISE  
REPRODUCED WITHOUT HIS/HER  
PERMISSION.

L'AUTEUR CONSERVE LA PROPRIETE  
DU DROIT D'AUTEUR QUI PROTEGE  
SA THESE. NI LA THESE NI DES  
EXTRAITS SUBSTANTIELS DE CELLE-  
CI NE DOIVENT ETRE IMPRIMES OU  
AUTREMENT REPRODUITS SANS SON  
AUTORISATION.

ISBN 0-612-06578-2

Canada

UNIVERSITY OF ALBERTA  
RELEASE FORM

NAME OF AUTHOR: **Zhong Li**

TITLE OF THESIS: **Investigation of Water in Poly(vinyl chloride)  
Based Ion-Selective Electrode Membrane**

DEGREE: **Doctor of Philosophy**

YEAR THIS DEGREE GRANTED: **1994**

Permission is hereby granted to the University of Alberta Library to reproduce single copies of this thesis and to lend or sell such copies for private, scholarly or scientific research purposes only.

The author reserves all other publication and other rights in association with the copyright in the thesis, and except as hereinbefore provided neither the thesis nor any substantial portion thereof may be printed or otherwise reproduced in any material from whatever without the author's written permission.

AUTHOR'S SIGNATURE:

A handwritten signature in dark ink, appearing to read 'Zhong Li', written over a horizontal line.

PERMANENT ADDRESS:

3A 9011 Hub  
Edmonton, Alberta  
T6G 2G2

DATE: **August 31 , 1994**

UNIVERSITY OF ALBERTA  
FACULTY OF GRADUATE STUDIES AND RESEARCH

The undersigned certify that they have read, and recommend to the Faculty of Graduate Studies and Research for acceptance, a thesis entitled **Investigation of Water in Poly(vinyl chloride) Based Ion-Selective Electrode Membranes** submitted by **Zhong Li** in partial fulfillment of the requirements for the degree of **Doctor of Philosophy**.

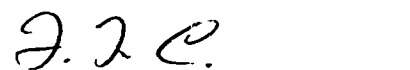
Supervisor:   
Dr. D. J. Harrison

  
Dr. F. F. Cantwell

  
Dr. J. A. Plambeck

  
Dr. S. Bergens

  
Dr. M. Williams

EXTERNAL EXAMINER:   
Dr. M. Arnold  
University of Iowa

Date: August 26, 1994

献给远方的亲人

*To my Family*

## **Abstract**

Poly(vinyl chloride) (PVC) based ion-selective electrode membranes are the key component of both conventional ion-selective electrodes (ISE) and ion-sensitive field-effect transistors (ISFET). In this thesis, the water transport phenomena in the membranes, an understanding of which is needed to improve the performance of these ion sensors, have been explored.

An equilibrium water uptake model based on osmotic pressure arguments has been proposed and experimental work using a spatial imaging photometer (SIP) and a UV-Visible spectrometer has been carried out to evaluate this model. Obtained results confirm that osmotic pressure effects are the main driving force for water uptake in PVC based ISE membranes. A dual-sorption model has also been proposed to describe the kinetics of water uptake in these membranes. The experimental results obtained using the SIP are consistent with the proposed models. A numerical analysis technique has been used to simulate the transport process described by the dual-sorption model in membranes doped with salts. An explicit-finite-difference method was used and the calculated results are in good agreement with the experimental ones.

Efforts have also been directed towards a better understanding of the water-rich surface region observed in PVC based ISE membranes. Effects of additives on this highly hydrated surface layer have been studied in detail. Results show that the additives in the membrane play a significant role in establishing a non-uniform water distribution. Studies of water distribution inside PVC based membranes plasticized with polymeric-plasticizer have demonstrated that loss of plasticizer from a membrane to an external aqueous solution may be a main source of the water-rich surface layer. A water uptake model incorporating this surface layer has been proposed. Results of numerical analysis of the model are presented.

## **Acknowledgments**

I would like to express my sincerely gratitude to the following people who have given me help and friendship, which have enabled my stay here to be an enjoyable and rewarding experience.

I thank my supervisor, Dr. D. Jed Harrison, for his guidance, encouragement, patient and help during these past four-plus years. His attitude towards work, his knowledge and keenness in science are always admired.

I thank Dr. F. F. Cantwell, my committee chairman, for his valuable help and suggestions throughout my program.

The friendship of the members of Harrison's research group, especially (in order of appearance) Xizhong Li, Paul Glavina, Sabeth Verpoorte, Dan Raymond, Alebachew Demoz, Andy Chan, Hugh Fan, Alem Teclemariam, Stan Tsai, Xiaodong Zhang, and Dr. Liang, contributed greatly to making my time in this group productive and fun.

I thank my friends, Mr. Haoran Yang, for his help in numerical analysis; Mr. Xiangrong Liu, for his help in 486PC, without their help my thesis would have been decidedly more difficult.

I am also indebted to the talented people in the Computer Service, the Machine Shop, the Electronic Shop, the Glass Shop and the General Office for their excellent service.

I dedicate this thesis especially to my parents who asked only that I do my best to achieve this. The other person to whom this work is dedicated is my wife, Yun Wang, who, although immersed in demanding graduate research of her own, always gave me motivation to overcome various trials and frustrations, and company to celebrate the successes.



## **Table of Contents**

<b>Chapter 1</b>	<b>Introduction .....</b>	<b>1</b>
1.1	The Ion-Selective Electrodes .....	3
1.2	PVC Based Liquid ISE Membranes and Water .....	7
1.3	Diffusion in Polymers and Measurements .....	9
	1.3-1 Basic Equations .....	9
	1.3-2 Methods of Measurement .....	11
1.4	Studies of Water Transport in PVC Based Ion-Selective Membranes .....	13
	1.4-1 Spatial Imaging Photometer (SIP) .....	13
	1.4-2 Water Uptake Model .....	16
	1.4-3 SIP Data Analysis .....	20
1.5	Scope of The Thesis .....	24
1.6	References .....	26
<b>Chapter 2</b>	<b>Modeling of Water Uptake in PVC Based Ion-Selective Membranes .....</b>	<b>29</b>
2.1	Introduction .....	29
2.2	Theory .....	31
	2.2-1 Equilibrium Water Absorption .....	31
	2.2-2 Kinetics of Water Absorption .....	36
	2.2-3 Mathematical Solutions of The Diffusion Models .....	41
2.3	Experimental .....	43
	2.3-1 Sample Preparation .....	43
	2.3-2 SIP Measurements .....	44
	2.3-3 UV-Visible Absorption Studies .....	48
	2.3-4 SIP Data Analysis .....	48
2.4	Results and Discussion .....	53
	2.4-1 Equilibrium Water Uptake .....	53
	2.4-2 Kinetics of Water Uptake .....	60

2.5	Conclusions .....	64
2.6	References .....	67

### Chapter 3 Water Distribution in PVC Based Ion-Selective Membrane and Effects of Polymer Matrices and Membrane Additives ..... 70

3.1	Introduction .....	70
3.2	Experimental .....	72
3.3	Results and Discussions.....	73
	3.3-1 Water Transport and Distribution in PVC/NPOE Membranes .....	73
	3.3-2 Effects of KBPh <sub>4</sub> on Water Transport and Distribution in PVC/DOA Membranes .....	82
3.4	Summary and Conclusions .....	85
	3.4-1 Summary .....	85
	3.4-2 Conclusions .....	90
3.5	References .....	91

### Chapter 4 Numerical Analysis in Water Transport in PVC Based ISE membranes ..... 93

4.1	Introduction .....	93
4.2	Theoretical .....	95
	4.2-1 Graphical Description of The System .....	95
	4.2-2 Finite-difference Solution: explicit method .....	99
4.3	Experimental .....	105
	4.3-1 Sample Preparation and Measurements .....	105
	4.3-2 Calculation of Profiles of Concentration of Water Transferred .....	105
4.4	Results and Discussions .....	106
	4.4-1 Stability of Method .....	106

4.4-2	Parameters for The Computations .....	112
4.4-3	Results of Numerical Simulations .....	117
4.5	Conclusions .....	126
4.6	References .....	129

## Chapter 5 Water-Rich Surface Region in PVC Based ISE Membranes and The Effect of Additives ..... 131

5.1	Introduction .....	131
5.2	Experimental .....	133
5.2-1	Sample Preparation .....	133
5.2-2	Instrumentation .....	133
5.3	Results and Discussion .....	135
5.3-1	Instrument and Edge Stability .....	138
5.3-2	Standard Membrane Compositions .....	140
5.3-3	Effect of Additives .....	146
5.3-4	Effect of Other Matrices .....	151
5.4	Conclusions .....	152
5.5	References .....	153

## Chapter 6 A Study of the Water-Rich Surface Region In PVC-Based Ion-Selective Membranes ..... 155

6.1	Introduction .....	155
6.2	Modeling and Numerical Methods of Analysis of The Surface Region .....	157
6.3	Experimental .....	161
6.4	Results and Discussions .....	163
6.4-1	Water Distributions in PVC/polymeric-Plasticizer ISE Membranes .....	163
6.4-2	Numerical Analysis of Surface Region.....	174
6.5	Conclusions .....	183
6.6	References .....	186

**Chapter 7 Conclusions .....188**

7.1	Summary of Contributions .....	188
7.2	Future Studies .....	190
7.3	References .....	193

**Appendix A. Computer Programs for SIP Experiments .....194**

Program A.1	SV.POT .....	198
Program A.2	FILETRAN.PRG .....	200

**Appendix B. Computer Programs for Numerical Simulations ..206**

Program B.1	ABXT.FOR .....	210
Program B.2	ZHONG1.FOR .....	211
Program B.3	ZHONG2.FOR .....	214
Program B.4	ZHONG3.FOR .....	217
Program B.5	BLOCK1.FOR .....	220
Program B.6	BLOCK2.FOR .....	223

## List of Tables

### Table

2.1	The diffusion coefficient of water as a function of $C_1^s$ .....	62
3.1	The apparent diffusion coefficients of dissolved water, $D_1$ , as a function of $\text{CoCl}_2$ concentration in the early stage of water uptake in PVC/NPOE membrane .....	76
3.2	The apparent diffusion coefficients of light scattering centers ( $D_2$ ) and maximum absorbance of water at the water/membrane interface ( $\Delta A_{2,\text{max}}$ ) as a Function of $\text{CoCl}_2$ concentration at 24 hours of water uptake in PVC/NPOE membranes .....	80
3.3	The apparent diffusion coefficients of water in the early stages of water uptake, $D_1$ , as a function of $\text{KBPh}_4$ concentration in PVC/DOA membranes.....	86
3.4	The apparent diffusion coefficients of water at 24 hours of water uptake, $D_2$ , as a function of $\text{KBPh}_4$ concentration in PVC/DOA membranes.....	88
4.1	Summary of water desorption data from a PVC/DOA/0.15% $\text{CoCl}_2$ membrane .....	113
4.2	Changes of $C^s$ in the PVC/DOA/0.15% $\text{CoCl}_2$ membranes as a function of time .....	115
4.3	Parameters of numerical calculation (Scheme I) .....	119
4.4	Parameters of numerical calculation (Scheme I) for Hg block experiment .....	127
5.1	Diffusion coefficients and absorbance of light scattering centers in a PVC/DOA membrane .....	145

5.2	Thickness of water-rich region and apparent diffusion coefficients .....	147
6.1	Types of plasticizers used and their properties .....	164
6.2	Apparent diffusion coefficients of dissolved water at initial stage of water uptake in PVC based ISE membranes.....	170
6.3	Apparent diffusion coefficients of water at late stage of water uptake in PVC based ISE membranes.....	175
6.4	Parameters of numerical calculation (Scheme III) .....	179
A.1	Curve fitting for water uptake .....	205

## **List of Figures**

### **FIGURE**

1.1	Schematic diagram of a membrane electrode measuring circuit and cell assembly .....	4
1.2	The schematic diagram of a spatial imaging photometer (SIP) ....	14
1.3	Water uptake model .....	17
1.4	Absorbance profile inside $\text{CoCl}_2$ containing membrane during the first 60 minutes .....	21
2.1	Cartoon illustrating different sized water droplets formed inside a membrane .....	33
2.2	The schematic diagram for membrane casting .....	45
2.3	Spatial imaging photometer with two laser sources .....	46
2.4	Absorbance profiles in membrane containing varying wt.% $\text{CoCl}_2$ after 24 hour's exposure to water .....	54
2.5	Absorbance due to light scattering with distance from the membrane/water edge .....	56
2.5a	Absorbance changes ( $\Delta A$ ) with time in the membrane .....	57
2.6	Absorbance due to light Scattering in an ammonium-selective membrane as a function of time between 250 and 700 nm .....	58
2.7	Effects of the ionic strength of external aq. solutions on the light scattering in a PVC/DOA/1%Nonactin/1.7%KTpCIPB membrane .....	59
2.8	Total absorbance changes for six consecutive steps .....	61
2.9	The apparent diffusion coefficient of water as a function	

	of salt concentration at the early stage .....	63
2.10	Diffusion coefficient vs. concentration of $\text{CoCl}_2$ (WT.%) in membrane for 24 hours associated with light scattering .....	65
3.1	Absorbance profile inside PVC/NPOE membrane during first 30 minutes .....	74
3.2	Diffusion coefficient vs. concentration of salt ( $C_1^*$ , mM) in membranes for the early stage of water uptake (in the bulk region) .....	77
3.3	The expanded plot of the absorbance profiles in a PVC/NPOE membrane containing 0.15 wt.% $\text{CoCl}_2$ during the later stages of water uptake .....	78
3.4	Apparent diffusion coefficient $D_2$ vs. concentration of $\text{CoCl}_2$ (wt.%) in the PVC/NPOE membrane for 24 hours of water uptake .....	81
3.5	Absorbance profiles in membrane containing varying wt.% $\text{CoCl}_2$ after 24 hours exposure to water .....	83
3.6	Absorbance profiles of a PVC/NPOE membrane (with no added dye) after the membrane was soaked in water for 24 hours .....	84
3.7	Plot of the effect of added $\text{KBPh}_4$ concentration on the initial diffusion coefficient for water uptake in a PVC/DOA membrane with 0.15 wt.% $\text{CoCl}_2$ added as an indicator dye .....	87
3.8	Apparent diffusion coefficient vs. concentration of $\text{KBPh}_4$ (wt.%) in PVC/DOA membrane for the 24 hour water uptake associated with light scattering .....	89
4.1	Schematic of one-dimensional diffusion process in membrane ...	97
4.2	Space-time diagram for numerical analysis .....	100
4.3	Scheme I of Numerical Calculation .....	107



4.4	Comparison of numerical and analytical results .....	110
4.5	Numerical simulations with different sizes of the grid .....	111
4.6	The plot of $C^s/C_{eq}^s$ as a function of time .....	116
4.7	Profiles of concentration of water developed through the thickness of membrane sheet calculated at various times .....	118
4.8	Profiles of concentration of water across the membrane calculated using the model of simple Fick's law diffusion process .....	120
4.9	Comparison of the concentration-distance curves for a membrane after water contacted on both sides .....	122
4.10	Comparison of the numerical results and experimental data .....	123
4.11	Comparison of the concentration-distance curves for a Hg blocked membrane cell after the membrane was contacted with water .....	124
5.1	Spatial imaging photometer with three laser sources .....	134
5.2	The structure of ET-30 .....	136
5.3	The structure of CoTPP(py)Br .....	137
5.4	Relative transmittance, $T/T_0$ , vs. diode number (one diode $= 3 \mu\text{m}$ ) as a function of time that both membrane faces were exposed to water .....	139
5.5	Absorbance due to light scattering in a PVC/DOA membrane with 1% valinomycin, 0.01% KBPh <sub>4</sub> as a function of time exposed to water .....	141
5.6	Absorbance Due to light scattering in a PVC/DOA membrane over 23 hours of water exposure .....	143
5.7	Comparison of changes in absorbance in the surface regions	

	induced by water uptake over 24 hours .....	147
5.8	Changes in absorbance over 28 hour exposure to water for membrane with 0.15 wt. % $\text{CoCl}_2$ added .....	150
6.1	Hypothetical concentration profiles of plasticizer and water across the thickness of membrane at the equilibrium water uptake.....	158
6.2	Scheme III of numerical calculation .....	162
6.3	The symbolized structures of polymeric plasticizers .....	165
6.4	Changes in absorbance over 121 hour exposure to water for a PVC/G-62 membrane with 0.15 wt.% $\text{CoCl}_2$ added .....	167
6.5	Changes in absorbance over 140 hour exposure to water for a PVC/G-25 membrane with 0.15 wt.% $\text{CoCl}_2$ added .....	168
6.6	Changes in absorbance over 100 hour exposure to water for a PVC/EVA-45 membrane with 0.15 wt.% $\text{CoCl}_2$ added.....	169
6.7	Absorbance due to light scattering in PVC/polymeric-plasticizer membranes after 24 hours of water exposure .....	171
6.8	Absorbance due to light scattering in PVC based membranes after 24 hours of water exposure .....	173
6.9	The plot of $C^s / C_{eq}^s$ as a function of time.....	177
6.10a	Profiles of concentration of water developed through the membrane calculated using scheme III and observed SIP data .....	180
6.10b	Profiles of absorbance of water developed through the membrane calculated using scheme III and observed SIP data .....	181
6.11	Comparasion of profiles of concentration of water developed	

	through the membrane calculated using different $D_2^s$ .....	182
6.12	Profiles of concentration of water developed through the membrane calculated using Scheme II .....	184

## **List of Symbols**

$A$	absorbance
$A_{\text{mean}}$	mean absorbance of the membrane
$\Delta A$	absorbance change
$\Delta A_1$	absorbance change due to dye bleaching
$\Delta A_{1,\text{max}}$	maximum absorbance change due to dye bleaching at the membrane/water interface
$\Delta A_2$	absorbance change due to light scattering
$\Delta A_{2,\text{max}}$	maximum absorbance change due to light scattering at the membrane/water interface
$\Delta A_{\text{surf}}$	absorbance change at the membrane/water interface
$\Delta A_{\text{eq}}$	equilibrium absorbance change
$\Delta A_2^{\text{b}}$	absorbance change due to light scattering in the bulk of a membrane
$\Delta A_2^{\text{s}}$	absorbance change due to light scattering near the surface of a membrane
$a_i$	activity of the analyte ion (mol/L)
$a_j$	activity of the $j$ th interfering ion (mol/L)
$b$	optical path length in the membrane (cm)
$C$	concentration of diffusion substance (mol/L)
$C_1$	concentration of dissolved water in the membrane (mol/L)
$C_2$	concentration of water immobilized in droplets averaged over the membrane volume (mol/L)
$C_2^{\text{eq}}$	equilibrium concentration of water in droplets averaged

	over the membrane volume (mol/L)
$C_{aq}$	concentration of the electrolyte in the external aqueous solution (mol/L)
$C_{eq}$	total (or average) equilibrium concentration of water in the membrane (mol/L)
$C_k$	concentration of water at the critical position $x_k$ where light scattering starts (mol/L)
$C^s$	average concentration of water in the droplets at the membrane/water interface (mol/L)
$C_{eq}^b$	average equilibrium concentration of water in the bulk of membrane (mol/L)
$C_{eq}^s$	average equilibrium concentration of water in the droplets at the membrane/water interface (mol/L)
$C_1^s$	concentration of dissolved water at the membrane/water interface (mol/L)
$C_w$	total (or average) concentration of water in the membrane (mol/L)
$C_i^s$	average concentration of salt impurity in the membrane (mol/L)
$D$	diffusion coefficient of diffusing substance (cm <sup>2</sup> /sec)
$D_1$	apparent diffusion coefficient of dissolved water (cm <sup>2</sup> /sec)
$D_2$	apparent diffusion coefficient of immobilized water (cm <sup>2</sup> /sec)
$D_2^b$	apparent diffusion coefficient of light scattering centers in the bulk of membrane (cm <sup>2</sup> /sec)
$D_2^s$	apparent diffusion coefficient of light scattering centers near the surface of membrane (cm <sup>2</sup> /sec)

$\bar{D}$	average diffusion coefficient (cm <sup>2</sup> /sec)
$E_{\text{cell}}$	cell potential (V)
$E^0$	formal redox potential (V)
$F$	Faraday constant (96487 C·mol <sup>-1</sup> )
$G$	elastic shear modulus of the membrane (dyne/cm <sup>2</sup> )
$h$	increment of space (cm)
$I$	light intensity (W·sr <sup>-1</sup> )
$J$	rate of transfer per unit area of section (flux) (mole·cm <sup>-2</sup> ·s <sup>-1</sup> )
$K_{ij}^{\text{pot}}$	selectivity coefficient
$l$	thickness of membrane (cm)
$M_t$	mass of the liquid taken up at the time $t$ (gram)
$M_{\infty}$	mass of the liquid taken up at the equilibrium (gram)
$M_i$	average molecular weight of impurity
$M_w$	molecular weight of water
$\tilde{N}$	Avogadro constant (6.022×10 <sup>23</sup> mol <sup>-1</sup> )
$n_{\text{DW}}$	molar ratio of the bleached dye to the absorbed water
$n_{\text{lc}}$	number of light scattering centers
$p$	average elastic pressure (dyne/cm <sup>2</sup> )
$R$	gas constant (8.314 J·K <sup>-1</sup> ·mole <sup>-1</sup> )
$r$	radius of water droplet (cm)
$s_0$	solubility of water in the membrane (mol/L)
$T$	absolute temperature (K)
$T$	transmittance
$t$	time (s)
$T_g$	glass transition temperature of polymer (°C)
$V_{\text{droplet}}$	volume of the droplet (cm <sup>3</sup> )

$V_{\text{mem}}$	volume of the membrane ( $\text{cm}^3$ )
$x$	space co-ordinate measured normal to the section (cm)
$x_k$	position where the diffusion coefficient of water changes (cm)
$z_i$	charge number of the analyte ion
$z_j$	charge number of the $j$ th interfering ion
$\alpha$	polarizability of the scattering center ( $\text{C}^2 \cdot \text{J}^{-1} \cdot \text{m}^2$ )
$\gamma$	average aggregation number of ions in the salt particles
$\epsilon$	molar absorptivity ( $\text{L} \cdot \text{mol}^{-1} \cdot \text{cm}^{-1}$ )
$\kappa$	ratio of the radius of droplets after it absorbs water to the radius before it absorbs water
$\lambda$	wavelength of light (nm)
$\pi_{\text{aq}}$	osmotic pressure of the external aqueous solution ( $\text{dyne}/\text{cm}^2$ )
$\pi_i$	osmotic pressure of the impurity-droplet solution ( $\text{dyne}/\text{cm}^2$ )
$\rho_i$	density of impurity ( $\text{gram}/\text{cm}^3$ )
$\rho_w$	density of water ( $\text{gram}/\text{cm}^3$ )
$\sigma$	turbidity ( $\text{cm}^{-1}$ )
$\tau$	increment of time (s)

## **Abbreviations**

Aq.	aqueous
CoTPP(py)Br	bromo(pyridine)-(5,10,15,20-tetraphenylporphyrinato) cobalt
DOA	bis(2-ethylhexyl) adipate
DOS	bis(2-ethylhexyl) sebacate
ET-30	2,6-diphenyl-4-(2,4,6-triphenyl-N-pyridinio)phenolate
ETH1001	(-)-(R,R)-N,N'-bis[11-ethoxycarbonyl]undecyl]- N,N',4,5-tetramethyl - 3,6-dioxaoctanediamide
EVA-45	ethylene/vinyl acetate (45%) copolymer
EVA-70	ethylene/vinyl acetate (70%) copolymer
G-25	a polyester of sebacic acid
G-62	an expoxidized soybean oil
ISE	ion-selective electrode
ISFET	ion-selective field effect transistor
KBPh <sub>4</sub>	potassium tetraphenylborate
KTpCIPB	potassium tetrakis( <i>p</i> -chlorophenyl)borate
NMR	nuclear magnetic resonance
NPOE	<i>o</i> -nitrophenyl octylether
PVC	poly (vinyl chloride)
SIP	spatial imaging photometer
THF	tetrahydrofuran
UV-vis	ultraviolet-visible
Val.	valinomycin



## **Chapter 1**

### **Introduction**

Over the past thirty years, the field of ion-selective electrodes (ISEs) has been one of the most active and flourishing branches of modern electrochemistry and several books and reviews have been written on this subject [1-8]. The development and applications of ISEs continue to provide excitement in expanding areas of analytical chemistry, because these ion sensors offer the advantages of simple design and maintenance, low cost, non-destructive analysis of test samples, and possible interfacing with automated and computerized systems. Nowadays, ion-selective membrane electrodes have become important and reliable devices for biomedical analysis, environmental testing, industrial process control, and laboratory research. The description "membrane" is used here to denote a thin section of electrically conducting material separating two solutions across which a potential develops in an ISE (see Figure 1-1 below). If this chemically selective membrane is directly applied onto the surface of microelectronic devices, *i.e.*, chips, an ion-selective field effect transistor (ISFET or CHEMFET) is obtained [1, 9-10]. ISFETs are now more than two decades old and have received much attention. One reason for their popularity is the general trend towards the

miniaturization of chemical sensors. Another is that they represent modern analogs of familiar ion-selective electrodes and other time-tested potentiometric devices.

In the applications of ion sensors, there are very stringent requirements for the selectivity, sensitivity, potential stability, reproducibility, response time and lifetime of the devices. Modern ion-selective membrane electrodes are not fully satisfactory in terms of these requirements, although many kinds of ISEs are now commercially available. Problems with ISEs include the interferences arising from other ions, fouling of the electrodes in harsh sample environments (such as urine or blood), and limited lifetimes [2]. On the other hand, ISFETs are still not commercially available because of the serious problems with encapsulation and stability [10]. Many efforts have been directed towards the solution of these problems. A fundamental knowledge of the response mechanisms of ion-selective membranes is required.

The working mechanism of ion-selective membrane electrodes has been the subject of scientific research since the first decade of the twentieth century [6], when the first glass electrode was developed [11]. To understand the fundamental processes associated with ion-selective membranes, it is essential to study the transport phenomena of relevant species inside these membranes. Theoretical treatments of ion-selective membranes have been developed to describe the observed membrane potentials and the behaviors of species inside the membranes [4-6,12-13]. These theories made different assumptions about the events occurring inside the membrane (*e.g.*, linear concentration gradients or linear potential gradients, no transport of species or dominant transport, *etc.*). However, there are relatively few studies that examine internal concentration profiles experimentally [14-15], so it is difficult to distinguish the theories. In addition, water is believed to play a significant role within those membranes and in relation to the miscibility of the membrane components and adhesion on solids [15-16]. These effects will be

important in determining lifetime of ion sensors made with these membranes. However, there is little quantitative data available on membrane bound water to truly understand these roles. The question of whether events inside the membranes obey any of the ideal models has not really been addressed.

It is the primary objective of this thesis to obtain better understanding of the transport of water inside ion-selective electrode membranes and how the transport is affected by the membrane matrix and additives. In the following sections, some background which is relevant to this work will be outlined.

## 1.1 THE ION-SELECTIVE ELECTRODE [4-6, 8]

Ion-selective electrodes (ISEs) are devices that permit the activity of a given ion in a solution (usually aqueous) to be determined potentiometrically despite the presence of other ions. The general layout of an ISE cell assembly is given in Figure 1-1. It consists of an ion-selective membrane, an internal standard solution of analyte ions, and an internal reference electrode. This is immersed, along with an external reference electrode, into a test solution containing analyte ions with an activity  $a_i$ . In this case, a Nernstian response is expected, and the measured cell potential is given by:

$$E_{\text{cell}} = E^0 + \frac{RT}{z_i F} \ln(a_i) \quad (1.1)$$

where  $E_{\text{cell}}$  is the measured cell potential.

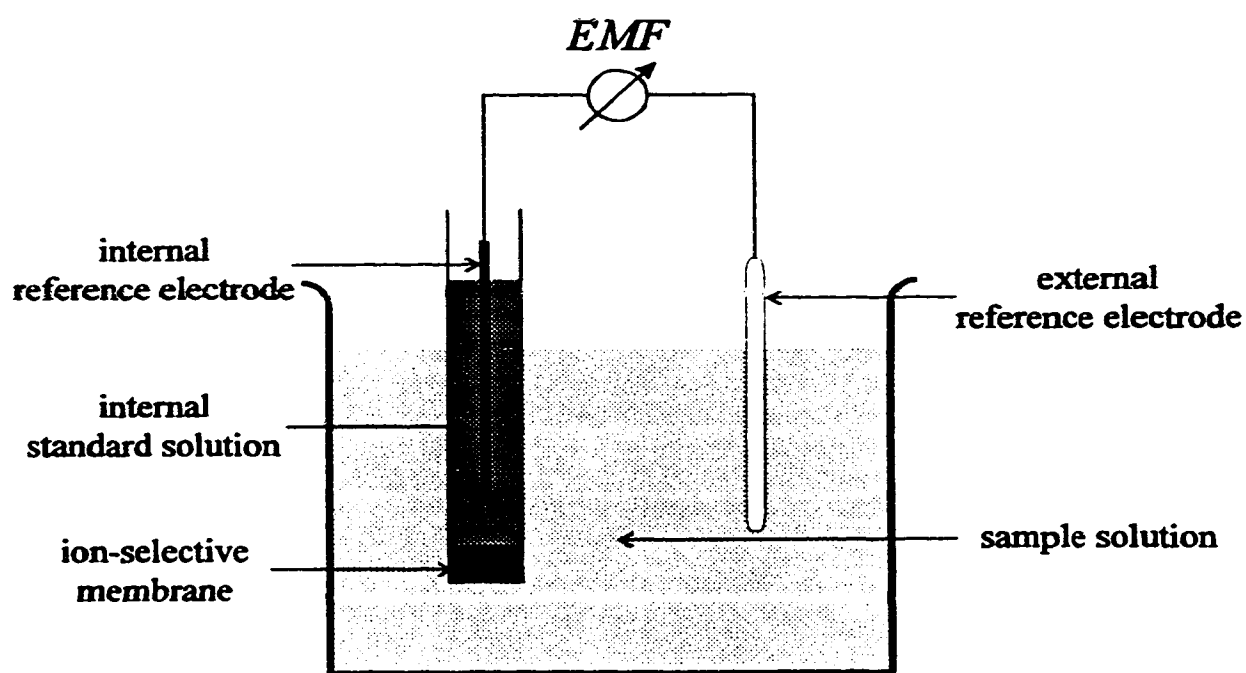


Figure 1.1 Schematic diagram of a membrane electrode measuring circuit and cell assembly

- $E^0$  is a constant depending on the reference electrode and the liquid junction potential.
- $R$  is the gas constant.
- $T$  is the absolute temperature.
- $F$  is the Faraday constant.
- $z_i$  is the charge of the analyte ion.

No ion-selective electrode responds exclusively to one kind of ion. In the presence of other interfering ions in the sample solution, the behavior of most ion-selective electrodes can be described by the Nikolsky-Eisenman equation:

$$E_{\text{cell}} = E^0 + \frac{RT}{z_i F} \ln \left[ a_i + \sum_{j \neq i} K_{ij}^{\text{pot}} (a_j)^{z_i/z_j} \right] \quad (1.2)$$

where

- $a_j$  is the activity of the  $j$ th interfering ion
- $z_j$  is the charge of the  $j$ th interfering ion
- $K_{ij}^{\text{pot}}$  is the selectivity coefficient

It can be seen from this equation that the more selective the ion-selective membrane electrode is for the analyte ion  $i$ , the lower the value of each selectivity constant  $K_{ij}^{\text{pot}}$  will be. The key to the successful design of an ion-selective membrane electrode is to select membranes that exhibit a specific and reproducible response to the ion of interest in the presence of the various other ions of the sample. Ion-selective electrodes may be roughly classified in the following way, according to the physical states of the substances (the electroactive materials) that form those membranes:

1. ***Ion-selective electrodes with solid membranes.***

Solid ISE membranes may be homogeneous as in a monocrystal (*e.g.*,  $\text{LaF}_3$  single crystal for  $\text{F}^-$ ), a sparingly soluble, polycrystalline or mixed crystal (*e.g.*,  $\text{Ag}_2\text{S}$  for  $\text{Ag}^+$  and  $\text{S}^{2+}$ ), or a glass (*e.g.*, silicate glasses for  $\text{Na}^+$  and  $\text{H}^+$ ), which is considered to be a solid because of the immobility of the ionic components. Alternatively, the membrane may be heterogeneous, by the incorporation of the electroactive substance within an inert matrix (*e.g.*,  $\text{AgCl}$  imbedded in polyethylene for  $\text{Ag}^+$ ).

2. ***Ion-selective electrodes with liquid membranes.***

Liquid ISE membranes were originally made by impregnating a porous inert solid support, *e.g.*, a disc of filter material, with a solution of the electroactive material in a water-immiscible solvent. As an alternative to the use of a porous disc as a rigid supporting medium, it has been found possible to immobilize the electroactive materials in plasticized polymer membranes. The electroactive substances in liquid membrane electrodes are of two kinds: (1) cationic or anionic ion-exchangers, and (2) electrically neutral, ion-specific complexing agents (ion carriers or ionophores). In ion-exchanger liquid membrane electrodes the selectivity depends on both the partition coefficient for the ions between water and the membrane, and the ion-exchanger's complexing abilities. In the case of neutral carrier membrane electrodes the selectivity is determined mainly by the complexation specificity of the carrier molecules.

## **1.2 PVC BASED LIQUID ISE MEMBRANES AND WATER**

Polymeric liquid membrane ion-selective electrodes are among the most successful approaches to ISEs [8, 17-19]. Currently, most liquid membrane electrodes are of this newer type. ISE membranes formed in this way behave in much the same way as those in which the electroactive material is held in the pores of a disk. However they offer the advantage of much simpler design and construction, and considerable economy of sensor materials due to the much slower loss of expensive electroactive substances. Increased lifetimes can also often be obtained using polymer-based membrane ISEs. Among the different polymer matrices used for neutral carrier based ion-selective membranes such as silicone rubber, copolymers of poly(bisphenol-A carbonated), poly(methylmethacrylate), poly(urethane), and poly(vinylisobutyl ether); poly(vinyl chloride) (PVC) is at present the most popular one [20-21].

PVC based ion-selective membranes usually consist of about 33% by weight PVC, which is "dissolved" in a plasticizing agent (plasticizer), as well as small quantities of ionophores and salts. The plasticizer is typically a relatively low dielectric, water-immiscible, high-boiling organic solvent such as dioctyladipate (DOA). One role of the PVC is to provide sufficient inherent mechanical strength for the membranes to be used in electrodes. The PVC is also important in raising the effective dielectric constant of the membranes to about 10 so that comparatively high ionic concentrations are supported, whereas that of pure DOA is close to 4 and that of rigid, pure PVC is between 3.2 and 3.4. The higher dielectric constant of the membrane compared with the pure materials arises from the liberation of the orientation polarization of the C-Cl bond in the composite material [22]. Commercial plasticized PVC products usually contain less than 33

wt.% plasticizer. ISE membranes, on the other hand, are typically made with 66 wt.% plasticizer and electrode performance deteriorates with decreasing plasticizer content [21-22]. It has been shown that ISEs are functional only when PVC-based ion-selective membranes have liquid like characteristics in terms of ionic conductivity [22]. In fact, the glass transition temperature of membranes,  $T_g$  (a transition temperature similar to the melting point of solids), must be below room temperature. Above the  $T_g$  plasticized PVC is in a liquid-like state, with the plasticizer molecules and PVC chains forming a true solution, with mixing at a molecular level, in which electroactive materials are dissolved. However, plasticized PVC is not simply an inert and pure matrix; both the physical structure and the chemical contaminants are important for the functioning of the membranes and must be considered when interpreting their behavior [22, 23].

When a PVC membrane is contacted by water then absorption of water molecules will occur. Water has been identified as playing significant roles in the potential determining equilibria within plasticized PVC-based ion-selective membranes [15-16]. It is a basic requirement that for either thermodynamic or kinetic reasons anionic sites (fixed or mobile) must be present in the membranes to compensate the ionophore-ion complex charges if Nernstian behavior is to be obtained [22]. Simon *et al.* have even suggested [14-15] that water immobilized in clusters in the membrane can be a source of those anionic sites, through the following type of reaction for a potassium-sensitive membrane:



where  $L$  is the ion carrier and (aq) and (mem) denote the aqueous and membrane phase, respectively. Very little work has been done to establish the validity of this hypothesis.



Phenomena related to water in ISE membranes such as surface gel layer formation, and abnormally high dissociation constants of weak acids in membranes have been invoked by a number of authors [24-25]. Harrison *et al.* have used optical instruments, NMR, and a gravimetric method to study the behavior of water in PVC based ion-selective membranes [26-28]. Their results show that there are at least two states of water inside the membrane. They also identified a water-rich surface region which leads to a considerable inhomogeneity within the membrane matrix. Their work demonstrates that water behaves in a very complex manner within PVC based ion-selective electrode membranes and will affect the performance of sensors made with these membranes.

## 1.3 MEASUREMENTS OF DIFFUSION IN POLYMERS

### 1.3-1 Basic Equations [29]

The mathematical theory of diffusion in isotropic substances is based on the hypothesis that the rate of transfer of diffusing substance through unit area of a section is proportional to the concentration gradient measured normal to the section, *i.e.*, *Fick's first law of diffusion*. For diffusion in one dimension,  $x$ , it becomes:

$$J = -D \frac{\partial C}{\partial x} \quad (1.4)$$

where  $J$  is the rate of transfer per unit area of section.  
 $C$  is the concentration of diffusing substance.

**x** is the space co-ordinate measured normal to the section.

**D** is the diffusion coefficient of diffusing substance.

If **J** and **C** are both expressed in terms of the same unit of quantity, then **D** is independent of the unit and has dimensions length<sup>2</sup>/time, *e.g.*, cm<sup>2</sup>/sec. Irreversible thermodynamics points to the gradient of chemical potential as the driving force rather than the concentration gradient, but for isothermal diffusion in a two-component system it is rarely necessary, although often instructive, to resort to the thermodynamic formulation. A material balance in a unit section of thickness **dx** yields:

$$\frac{\partial C}{\partial t} = - \frac{\partial J}{\partial x} \quad (1.5)$$

Combining equations 1.4 and 1.5 gives *Fick's second law of diffusion*:

$$\frac{\partial C}{\partial t} = \frac{\partial}{\partial x} \left( D \frac{\partial C}{\partial x} \right) \quad (1.6)$$

where the diffusion coefficient, **D**, may be constant or a function of concentration, **C**, or distance, **x**, or both. For a number of polymer systems [30-31], an adequate description of the diffusion process is not possible with **D**(**c**, **x**). Superficially **D** may appear to be a function of time as well as of concentration. Such behavior is classified as *non-Fickian diffusion* and is often associated with relaxation processes in the polymer which may become rate controlling. For a constant diffusion coefficient, equation 1.6 becomes:

$$\frac{\partial C}{\partial t} = D \frac{\partial^2 C}{\partial x^2} \quad (1.6a)$$

A large number of analytical solutions to equation 1.6a have been obtained for a variety of initial and boundary conditions [29]. For concentration-dependent diffusion coefficient strictly formal mathematical solutions are no longer possible and often graphical and numerical procedures are used [29-30, 32]. An analysis of the concentration dependence of the diffusion coefficient is often of value in the interpretation of mechanism of the transport process at a molecular level [23, 29].

### 1.3-2 Methods of Measurement [29-31]

Two techniques commonly used in the study of diffusion in polymers and membranes are sorption (desorption) kinetics and permeation methods. In the former, a thin sheet of membrane with thickness  $l$  is suspended in a liquid. The mass of the liquid taken up,  $M$ , is recorded as a function of time. For short times the solution with constant diffusion coefficient,  $D$ , reduces to:

$$\frac{M_t}{M_\infty} = 4 \left( \frac{Dt}{\pi l^2} \right)^{1/2} \quad (1.7)$$

giving the familiar initial  $t^{1/2}$  region; at longer times the plot becomes concave to the  $t^{1/2}$  axis as  $M_t$  approaches the equilibrium value  $M_\infty$ . When the diffusion coefficient,  $D$ , is a function of concentration, the initial  $t^{1/2}$  region is often still

obtained but equation 1.7 now yields some average diffusion coefficient,  $\bar{D}$ . Procedures have been developed which enable the concentration dependence of the diffusion coefficient,  $D$ , to be determined from that of  $\bar{D}$  [29].

In the permeation method a pressure difference of the vapor of a liquid is maintained across the polymer film or membrane with the downstream pressure  $p_2$  often much less than the upstream pressure  $p_1$ . The amount of material  $Q_t$  which has passed through the sheet in time  $t$  is recorded and after long times a linear steady-state region is approached, the slope of which,  $dQ/dt$ , is the steady-state flux  $J_{ss}$ . Using equation 1.5, and assuming virtually zero pressure on the downstream face:

$$J_{ss}l = \int_0^{C_1} D dC \quad (1.8)$$

where  $C_1$  is the concentration in the ingoing face. (Concentration of liquid at the membrane surface may be related to the vapor pressure by Henry's law,  $C = kp$ .) Measurement of  $J_{ss}$  as a function of  $p_1$  coupled with the sorption isotherm yields  $J_{ss}$  as a function of  $C_1$ . The concentration dependence of diffusion coefficient then follows from:

$$\left( \frac{dJ_{ss}l}{dC} \right)_{C=C_1} = D_{C=C_1} \quad (1.9)$$

Both methods described above can be used to obtain the diffusion coefficient (usually average value), but the distribution of diffusing substance can not be observed. Holographic techniques based the dependence of refractive index on penetrant concentration [14] and radiotracer techniques [15] have been used to

examine the concentration profiles of ions across liquid ISE membranes, but those methods were still limited to evaluate average distributions with low resolutions (about 250  $\mu\text{m}$  for the holographic method and about 40  $\mu\text{m}$  for the radiotracer method). X. Li *et al.* has developed an optical technique to directly probe the concentration profiles inside polymers or membranes [33] with a resolution of about 2  $\mu\text{m}$ . Their method will be introduced in the next section.

## **1.4 STUDIES OF WATER TRANSPORT IN PVC BASED ION SELECTIVE MEMBRANES [23,26]**

Although water is believed to play a significant role within plasticized, poly(vinyl chloride) (PVC) - based ion-selective membranes, relatively little quantitative information has been available about the rate of water transport, its distribution and its concentration within these membranes [23]. X. Li *et. al* in our laboratory reported experimental work using a spatial imaging photometer (SIP) to study the transport of water inside the PVC-based ion-selective electrode membranes [26, 33]. A simplified mathematical model for the water uptake in these membranes was developed and used to analyze the SIP data. The instrument and the transport model are presented below.

### **1.4-1 Spatial Imaging Photometer (SIP) [33]**

A spatial imaging photometer is essentially a digitized microscope which can be used to determine the spatial distribution of water within the membrane during the process of water uptake. The set up of the SIP is shown in Figure 1-2.

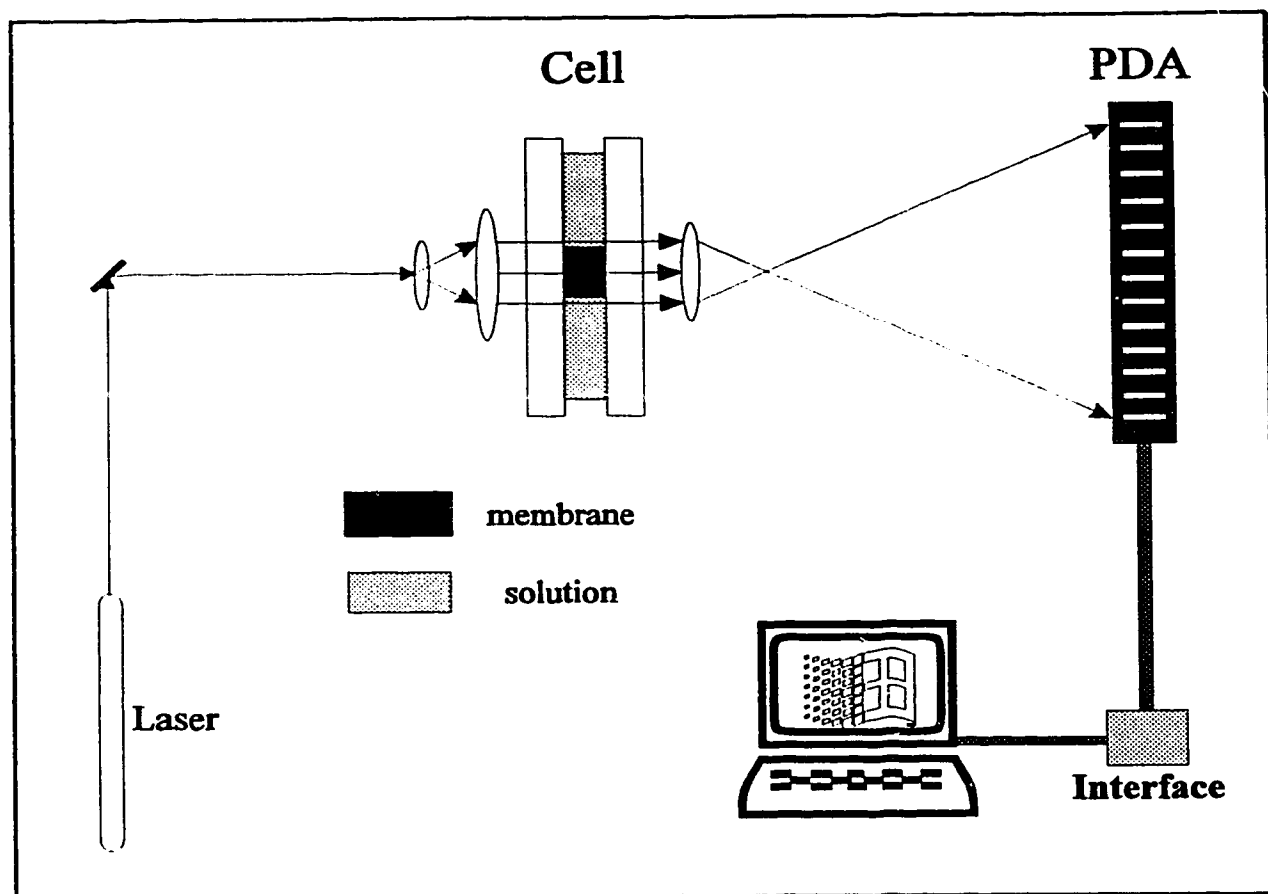


Figure 1-2. The schematic diagram of a Spatial Imaging Photometer (SIP)

Details of the instrument design and the electronic interface have been presented elsewhere [33]. A laser was used as the light source. An optical cell was prepared by sandwiching a thin slice of ion-selective membrane from a master membrane between two glass microscopic slides. The cell was mounted at the object plane of a lens, and a photodiode array detector, located in the image plane, was interfaced to a micro-computer for acquiring, manipulating and displaying the data. The direction of water transport in the cell was perpendicular to the laser light path. The magnification power of the optics is up to 20 times. The transmitted light was measured periodically and the absorbance was then calculated using the initial intensity of transmitted light as the reference. The absorbance change as a function of position inside a membrane was obtained.

Imaging of water concentration profiles with the SIP was done either by measuring the bleaching of a water-sensitive dye or the light scattering induced by the formation of water droplets inside the membranes [23, 26]. When the concentration of water was small, its distribution inside a membrane was imaged by the addition of a water-sensitive dye to the membrane. Anhydrous  $\text{CoCl}_2$ , which bleaches in the presence of water, was used most commonly. The decrease of absorbance observed by the SIP,  $\Delta A_1$ , could be related to the concentration change of water inside the membrane. When the concentration of water in a membrane became high, water droplets began to appear and act as light scattering centers. The scattering leads to an increase in absorbance,  $\Delta A_2$ , which can also be used to follow the progress of water uptake inside membranes (see discussion in 1.4-3).

The SIP provides a powerful means of probing the water distribution within membranes. Further, the method provides *in situ* measurement and so avoids errors due to evaporation of water when the membrane is transferred, as would occur in radio-labeling and gravimetric methods.

### 1.4-2 Water Uptake Model [23]

A model involving two stages of water uptake has been proposed by X. Li. Figure 1-3 is a schematic diagram of the concentration profiles expected using this model. When the concentration of water in the membrane is below a critical value,  $C_k$ , water is dissolved in the membrane matrix. At this stage, the dissolved water molecules diffuse rapidly through the membrane. The membrane remains as a homogenous "single phase". The concentration involved at this stage is relatively small, and the diffusion of water obeys Fick's laws. The diffusion coefficient of dissolved water at this stage has a constant diffusion coefficient  $D_1$ . As the concentration of water continues to increase above a critical value, clustering of water molecules occurs and water droplets that scatter light begin to form and grow. A front of those light scattering centers then apparently moves into the membrane. The penetration of the scattering centers at this second stage can be modeled as an apparent diffusion from the solution/membrane interface into the membrane bulk. However, this can not be the actual mechanism, since the scattering centers themselves are unlikely to move. Rather, water molecules must diffuse through the polymer phase from droplet to droplet nucleation site. The results of this model do provide a measure of the rate of transport of the water droplets into the membrane at this stage, even though the transport of water at the second stage must be described as a pseudo-Fickian diffusion process.

To describe these two stages of water uptake, X. Li has utilized an approximate model for which an analytical solution exists [29], in which the diffusion coefficient of scattering centers ( $D_2$ ) is constant, but changes in a step-wise fashion from  $D_1$  ( $\neq D_2$ ) for dissolved water at a moving boundary at position  $x_k$  within the membrane, where the water concentration has reached  $C_k$ . The equilibrium concentration of water at the membrane/water interface was also



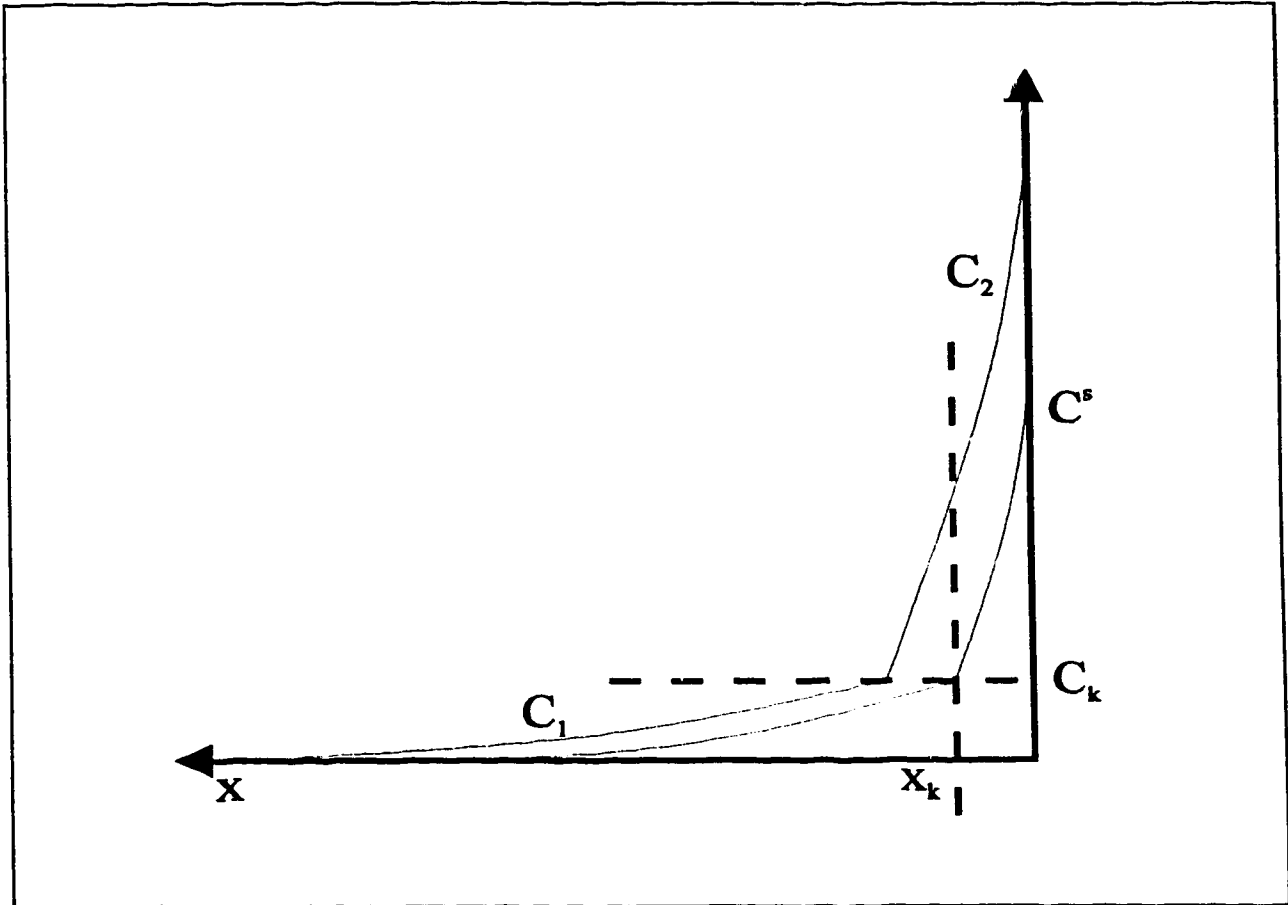


Figure 1-3. Water uptake model, showing the concentration profile inside a membrane.  $C_1$  is the concentration of dissolved water in the bulk region ( $x > x_k$ ),  $C_2$  is the concentration of water in droplets in the surface layer ( $0 < x < x_k$ ),  $C^s$  is the equilibrium concentration of water at the membrane/water interface,  $x$  is the distance from the interface, and  $C_k$  is the concentration of water at  $x_k$ , where the diffusion coefficient of water changes. (adapted from X. Li, Ph. D. Thesis, 1992, p59)

assumed to have a constant value. This approximation gave an average value of  $D_2$  in the surface region at any given time. Solutions to this moving boundary transport problem with the semi-infinite boundary conditions were given as [34]:

$$C_1(x, t) = \frac{C_k}{1 - \operatorname{erf}\left(x_k / 2\sqrt{D_1 t}\right)} \left(1 - \operatorname{erf} \frac{x}{2\sqrt{D_1 t}}\right) \quad x > x_k \quad (1.10)$$

$$C_2(x, t) = C^s - \frac{C^s - C_k}{\operatorname{erf}\left(x_k / 2\sqrt{D_2 t}\right)} \operatorname{erf} \frac{x}{2\sqrt{D_2 t}} \quad 0 < x < x_k \quad (1.11)$$

$$\frac{C_k \sqrt{D_1} \exp\left(-\frac{R_k^2}{4D_1}\right)}{1 - \operatorname{erf} \frac{R_k}{2\sqrt{D_1}}} - \frac{(C^s - C_k) \sqrt{D_2} \exp\left(-\frac{R_k^2}{4D_2}\right)}{\operatorname{erf} \frac{R_k}{2\sqrt{D_2}}} = 0 \quad (1.12)$$

- where
- $C_1(x, t)$  is the concentration of dissolved water in the bulk region ( $x > x_k$ ),
  - $C_2(x, t)$  is the concentration of water in droplets in the surface layer ( $0 < x < x_k$ ).
  - $C^s$  is the equilibrium concentration of water at the membrane/water interface.
  - $x$  is the distance from the membrane/water interface.
  - $C_k$  is the concentration of water at  $x_k$ , where the diffusion coefficient of water changes.

$R_k$  is equal to  $\frac{x_k}{\sqrt{t}}$  and is determined by 1.12 and reflects the correlation between the diffusion parameters in the two stages.

The solution for  $C_1$  using plane-sheet boundary conditions, with water entering from both sides, was also given as

$$C_1(x, t) = C_1^0 \left\{ 1 - \frac{4}{\pi} \sum_{n=1}^{\infty} \frac{1}{(2n-1)} \exp \left[ -\frac{D_1 (2n-1)^2 \pi^2 t}{l^2} \right] \sin \frac{(2n-1)\pi x}{l} \right\} \quad (1.13)$$

where

$$C_1^0 = \frac{C_k}{1 - \frac{4}{\pi} \sum_{n=1}^{\infty} \frac{1}{(2n-1)} \exp \left[ -\frac{(2n-1)^2 \pi^2 D_1 t}{l^2} \right] \sin \frac{(2n-1)\pi x_k}{l}} \quad (1.14)$$

$l$  is the thickness of the membrane,  $x$  is the distance from one edge towards the bulk of the membrane, and  $n = 1, 2, 3, \dots$

At the late stages of water uptake, light scattering was observed within the bulk [35]. To further complicate the situation, experimental results also show that there is a surface region that develops at the later stages of water uptake. Two diffusion coefficients,  $D_2^s$  and  $D_2^b$ , were introduced to describe this complicated transport problem.  $D_2^s$  describes the diffusion of light scattering centers near the surface,  $D_2^b$  describes the diffusion of light scattering centers in the bulk and  $D_2^s \neq D_2^b$ . This stage of development of light scattering can again be modeled by

equation 1.10 (or equation 1.13), where  $D_1$  is replaced by  $D_2^b$  and equation 1.11, where  $D_2$  is replaced by  $D_2^s$ .

### 1.4-3 SIP Data Analysis [23, 26]

Figure 1.4 shows the observed uptake of water into a membrane containing 0.78%  $\text{CoCl}_2$  as a water sensitive dye after a short period of time. The decrease of absorbance observed in the bulk of the membrane ( $\Delta A_1$ ) arises from the bleaching of  $\text{CoCl}_2$ , on reacting with water. It has been assumed that  $\Delta A_1$  is proportional to the concentration of water in the membrane [23]. At the surface the absorbance increase ( $\Delta A_2$ ) corresponds to the growth of light scattering centers in the membrane as the concentration of water increases, leading to an increase in absorbance. Formation of these scattering centers deeper and deeper within the membrane over time provides evidence of the transport of water from the surface onto the bulk region. When absorbance due to these centers is proportional to the concentration of water equations 1.15 and 1.16 can be obtained from equations 1.10 and 1.11, assuming semi-finite boundary conditions [36]:

$$\Delta A_1(x, t) = \Delta A_{1, \max}(x, t) \left[ 1 - \operatorname{erf} \frac{x}{2\sqrt{D_1 t}} \right] \quad x > x_k \quad (1.15)$$

$$\Delta A_2(x, t) = \Delta A_{2, \max}(x, t) \left[ 1 - \frac{1}{\operatorname{erf} \frac{x_k}{2\sqrt{D_2 t}}} \operatorname{erf} \frac{x}{2\sqrt{D_2 t}} \right] \quad 0 < x < x_k \quad (1.16)$$

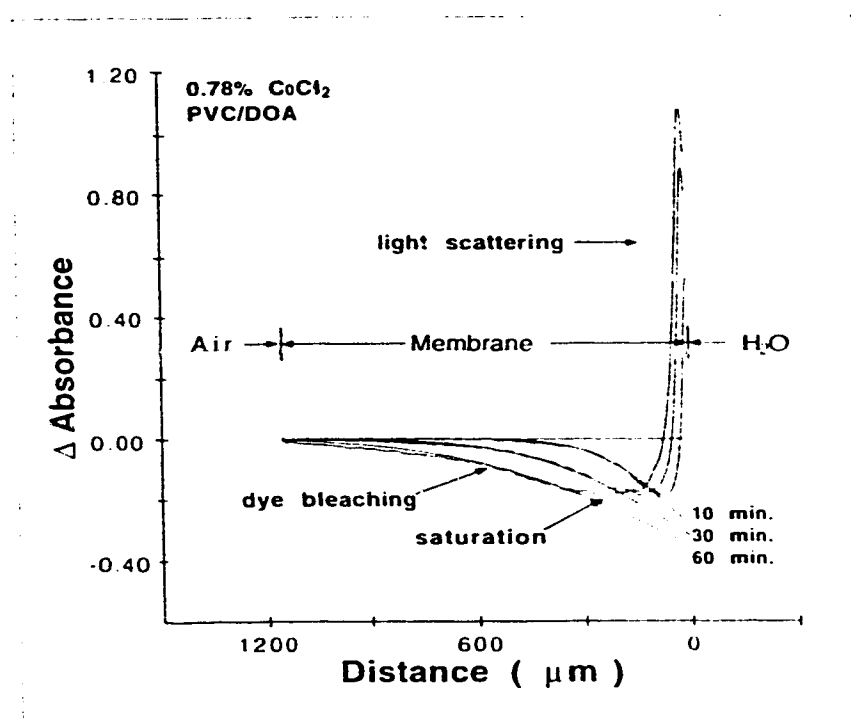


Figure 1-4 Absorbance profile inside  $\text{CoCl}_2$  containing membrane during the first 60 min. Water entered from the right side. Smooth curves are fits to equation 1.15 for dye bleaching (adapted from X. Li's thesis, 1992, p75)

where  $\Delta A_{1,\max}$  is the maximum absorbance that would be observed at the membrane surface if other effects were not present.  
 $\Delta A_{2,\max}$  is the maximum absorbance due to scattering at the membrane surface.

During the later stages of water uptake, water droplets begin to form throughout the bulk of the membrane, but a surface region often remains in which the diffusion coefficient is smaller than in the bulk. The water droplets still represent the transport of water. When absorbance due to the scattering centers is proportional to water concentration, equations 1.17 and 1.18 may be used to describe transport in the bulk and surface regions [37]. Given plane sheet boundary conditions, equation 1.17 has the same form as equation 1.13, except it describes light scattering instead of dye bleaching.

$$\Delta A_2^b(x, t) = \Delta A_b^0 \left\{ 1 - \frac{4}{\pi} \sum_{n=1}^{\infty} \frac{1}{(2n-1)} \exp \left[ -\frac{D_2^b (2n-1)^2 \pi^2 t}{l^2} \right] \sin \frac{(2n-1)\pi x}{l} \right\} \quad (1.17)$$

$$\Delta A_2^s(x, t) = \Delta A_{2,\max}(x, t) \left[ 1 - \frac{1}{\operatorname{erf} \frac{x_k}{2\sqrt{D_2^s t}}} \operatorname{erf} \frac{x}{2\sqrt{D_2^s t}} \right] \quad (1.18)$$

where  $\Delta A_2^b(x, t)$  is absorbance change due to light scattering in the bulk.  
 $\Delta A_2^s(x, t)$  is absorbance change due to light scattering in the surface.  
 $\Delta A_b^0$  is a constant in units of absorbance.

These equations arise from equations 1.13 and 1.11. The assumption of linear proportionality between water concentration and light scattering is clearly a critical one. The scattering cross-section is a function of the size and concentration of scattering centers [38]. For weak scattering the concentration of scattering centers of a constant size is proportional to the observed absorbance. However, the dependence of scattering on particle size is complex. Larger particles on the scale of micrometers show a weak dependence of the scattering cross-section on size, whereas particles smaller than 100 nm may show a dependence proportional to the particle size raised to the sixth power [39]. It has been shown [27] that the droplets range in size from 16 nm to many micrometers, so that changes in the droplets size with increasing water content will also cause an increase in scattering intensity. Consequently, an increase in absorbance due to scattering will reflect an increase in the amount of water, but the linear approximations may be poor.

Data analysis can be done by fitting the SIP data according to equation 1.15 or 1.17 in the bulk and equation 1.16 or 1.18 in the surface region. Equations 1.15 and 1.16 are used at early times when there is dye bleaching, while equation 1.17 and 1.18 are used when light scattering is present throughout a membrane. Analysis of the data gives observed diffusion coefficients which are functions of time and position [23]. It was recognized that the diffusion coefficients obtained are empirical parameters describing the different stages of water uptake, rather than the true diffusion coefficient for water [23]. The values obtained for  $D_2$  from the analysis represent the apparent diffusion rate of the water droplets. The value of  $D_2$  depends on the assumption that it is the number of droplets that is increasing, not their size, so that the water concentration is directly proportional to the absorbance change. Consequently equations 1.16, 1.17 and 1.18 essentially refer to the concentration of droplets. As discussed in Chapter 2 these assumptions may not be fully valid.

Analysis of the data shows that the apparent migration of light scattering centers is several orders of magnitude lower in rate than is the transport of dissolved water. Analysis also identifies a surface region where the apparent diffusion coefficient of scattering centers is different from the one in the bulk, so that three diffusion coefficients ( $D_1$ ,  $D_2^b$  and  $D_2^s$ ) were introduced to describe water transport [23]. These are empirically useful parameters, but may not be of fundamental significance due to the reason discussed above.

## 1.5 SCOPE OF THIS THESIS

The work presented in this thesis is concentrated on the phenomena of water transport inside PVC based ion-selective electrode membranes. Experimental research has been directed towards developing a model to understand the non-homogeneous behavior observed in ion-selective electrode membranes and the factors that govern water behavior in those membranes. These include membrane additives, ionic strength effects, and the plasticized polymer compositions. This work will aid in providing a framework of quantitative information about water in PVC based ISE membranes and should help development of longer lived ion sensors employing these membranes.

In Chapter 2, a dual-sorption model of water uptake in PVC based ion-selective electrode membranes has been presented and compared with X. Li's two stage model. An equilibrium water uptake model based on the osmotic pressure arguments is also presented. The experimental results are reported for PVC/DOA membranes using both the spatial imaging photometer and a UV-Visible spectrophotometer, and the results used to evaluate the proposed theories.



In Chapter 3, the transport behavior of water through PVC/o-nitrophenyloctylether (NPOE) membranes is studied in detail using the spatial imaging photometer. The effects of lipophilic salt, potassium tetraphenylborate ( $\text{KBPh}_4$ ), on the water distribution in PVC/DOA ISE membranes are also investigated. The results of this work provide further support of the models of water uptake in PVC based ISE membranes presented in Chapter 2.

In Chapter 4, a numerical analysis of water uptake in PVC based ISE membranes is presented. The explicit-finite-difference method is used to develop a finite-difference equation for simulation of the water transport process inside ISE membranes containing hydrophilic salt,  $\text{CoCl}_2$ . This was necessary since in the later stages of water uptake the differential equations are non-linear. The calculated results have been compared with the experimental ones.

Chapters 5 to 6 report studies of the water-rich surface region observed in PVC based ion-selective electrode membranes.

In Chapter 5, the effect of additives and membrane matrices on the water-rich surface region are presented. Quantitative analysis of experimental results is also given.

In Chapter 6, the effects of polymeric plasticizers on the formation of water-rich surface region in PVC based ISE membranes are investigated. Several polymeric plasticizers have been tested. Preliminary results of numerical analysis of water transport process inside PVC based ISE membranes with water-rich surface region present are also reported.

Chapter 7 provides a final summary of the conclusions of this thesis.

## 1.6 REFERENCES

- [1] Janata, J.; Joscowicz M.; Devaney, D. M. *Anal. Chem.* **1994**, *66*, 207R-228R.
- [2] Widmer, H. M. *Anal. Methods & Instrumentation* **1993**, *1*, 60-72.
- [3] Janata, J. *Anal. Chem.* **1992**, *64*, 196R-219R.
- [4] Linder, E.; Toth, K.; Pungor, E. *Dynamic Characteristics of Ion-selective Electrodes* CRC Press, **1988**.
- [5] Koryta, J.; Stulik, K. *Ion-Selective Electrodes*; 2nd edn., Cambridge University Press: Cambridge, Great Britain, **1983**.
- [6] Morf, W. E. *The Principles of Ion-selective Electrodes and of Membrane Transport*; Elsevier Scientific Publishing Company: Amsterdam, Oxford and New York, **1981**.
- [7] Simon, W.; Pretsch, E.; Ammann, D.; Morf, W. E.; Guggi, M.; Bissig, R.; Kessler, M. *Pure. Appl. Chem.* **1975**, *44*, 613.
- [8] Moody, G. J.; Thomas, J. D. R. *Selective Ion-sensitive Electrodes*, Merrow, Watford, Herts.: Great Britain **1971**.
- [9] Janata, J. *Solid State Chemical Sensors*, Academic Press, New York, **1985**.
- [10] Domansky, K.; Janata, J.; Josowicz, M.; Petelenz, D. *Analyst* **1993**, *118*, 335-340.
- [11] Cremer, M. Z., *Biol.* **1906**, *47*, 562.
- [12] Iglehart, M. L.; Buck, R. P.; Pungor, E. *Anal. Chem.* **1988**, *60*, 290.
- [13] Buck, R. P. *J. Phys. Chem.* **1987**, *91*, 2347-2350.
- [14] O'Brien, R. N.; Zhao, B.; Fyles, T. *J. Membrane Sci.* **1984**, *20*, 297-323.
- [15] Thomas, A. P.; Viviani-Nauer, A.; Arvanitis, S.; Morf, W. E.; Simon, W. *Anal. Chem.* **1977**, *49*, 1567-1572.
- [16] Morf, W. E.; Simon, W. *Helvetica Chim. Acta* **1986**, *69*, 1120.

- [17] Shatkay, A. *Anal. Chem.* **1967**, *39*, 1056-1065.
- [18] Bloch, R.; Shatkay, A.; Saroff, H. A. *Biophys. J.* **1967**, *7*, 865-877.
- [19] Mikhelson, K. N. *Sensors and Actuators B* **1994**, *18-19*, 31-37.
- [20] Moody, G. J.; Oke, R. B.; Thomas, D. R. *Analyst* **1970**, *95*, 910.
- [21] Oesch, U.; Simon, W. *Anal. Chem.* **1980**, *52*, 692-700.
- [22] Armstrong, R. D.; Horvai, G. *Electrochimica Acta.* **1990**, *35*, 1-7.
- [23] Li, X. *Transport Behavior of Water and Ions in Polyvinylchloride Based Ion-Selective Membranes* Ph.D. Thesis, University of Alberta, Edmonton, Canada, 1992. Chapter 4.
- [24] Horvai, G.; Graf, E.; Toth, K.; Pungor, E.; Buck, R. P. *Anal. Chem.* **1986**, *58*, 2735-2740.
- [25] Verpoorte, E. *Analysis of The Permeability and Behavior of Dissociable Species in Ion-Selective Membranes* Ph.D. Thesis, University of Alberta, Edmonton, Canada, 1991.
- [26] Harrison, D. J.; Li, X.; Petrovic, S.; In *Biosensors and Chemical Sensors. Optimizing Performance through Polymeric Materials*; Edelman, P.G., Wang, J., Eds.; ACS Symp. Ser. 487; Washington, DC, **1992**, 292-300.
- [27] Chan, A.D.C.; Harrison, D. J. *Anal. Chem.* **1993**, *65*, 32.
- [28] Chan, A. D. C.; Li, X.; Harrison, D. J. *Anal. Chem.* **1992**, *64*, 2512-2517.
- [29] Crank, J. *The Mathematics of Diffusion* Oxford University Press, **1975**.
- [30] Crank, J.; Park, G. S. *Diffusion in Polymers* Academic Press, New York, **1968**.
- [31] Barrie, J. A. *Trans IMarE (C)* **1985**, *97*, 79-85.
- [32] Buck, R. P.; Berube, T. R. *J. Electroanal. Chem.* **1988**, *256*, 239-253.
- [33] Li, X.; Petrovic, S.; Harrison, D. J. *Sensors and Actuators* **1990**, *B1*, 275-280.

- [34] Li, X. *Ph.D. Thesis*, University of Alberta, Edmonton, Canada, 1992, p63-64.
- [35] Li, X. *Ph.D. Thesis*, University of Alberta, Edmonton, Canada, 1992, p98-106.
- [36] Li, X. *Ph.D. Thesis*, University of Alberta, Edmonton, Canada, 1992, p67.
- [37] Li, Z.; Li, X.; Petrovic, S.; Harrison, D. J. *Analytical Methods and Instrumentation* 1993, 1, 30-37.
- [38] Ingle, J. D.; Crouch, S. R. *Spectrochemical Analysis* Prentice Hall, Englewood Cliffs, NJ 1993, p513.
- [39] Zarrin, F.; Risfelt, J. A.; Dovichi, N. J. *Anal. Chem.* 1987, 59, 850.

## **Chapter 2**

# **Modeling of Water Uptake In PVC-Based Ion-Selective Membranes**

## **2.1 INTRODUCTION**

Poly(vinyl chloride)(PVC)-based ion-selective membranes have been used in a wide variety of technological applications, where they are called upon to withstand varying aqueous solution compositions. It is a matter of considerable practical importance, as well as scientific interest to understand the mechanism of water sorption in such membranes and to know how sorbed water affects physical properties and performance of chemical sensors made with those membranes.

The sorption and diffusion of water in polymers has been studied extensively and several general reviews of the role of water in polymers have appeared in the scientific literature [1-6]. However, relatively little attention has been given to the transport behavior of water in PVC based ion selective membranes [7-10]. In those publications, values reported for the diffusion

coefficient,  $D$ , of water in 64 - 70 wt. % plasticized PVC range from  $(0.4 - 2.3) \times 10^{-6} \text{ cm}^2/\text{s}$ , while estimates of the water content vary from 0.15 to 0.38 M. All of these studies assumed a homogeneous distribution of water within the membrane and a constant diffusion coefficient. A major problem with those measurements is that they give only the integrated or average water content across the membranes; the true distribution of water was not obtained.

As part of an effort directed at understanding the role of water in ion-selective membranes, we have undertaken a variety of experimental studies of the behavior of water in PVC-based membranes [11-16]. We have used a spatial imaging spectrometer (SIP) [11-13], which combines digital, quantitative acquisition of light intensity with collection optics that essentially form a microscope, in order to obtain quantitative sample absorbance data (optical density) with spatial resolution (imaging capability). Using this tool, Li and Harrison showed [12] that water uptake in PVC based membranes occurs as a two-stage process, with an initial rapid uptake of water associated with water freely dissolved (miscible) in the membrane matrix. During this step water transport obeys Fick's laws of diffusion and exhibits a diffusion coefficient ranging from 0.9 to  $3 \times 10^{-6} \text{ cm}^2/\text{s}$ , depending on the membrane composition. A second, much slower stage then begins that is associated with the formation of light scattering centers. Using variable temperature nuclear magnetic resonance (NMR) methods Chan and Harrison have shown that these centers are due to the formation of water droplets within the polymer matrix [15]. These centers appear to diffuse into the membrane with a time and water concentration dependent diffusion coefficient. This is not believed to be the actual mechanism, and it has been proposed that dissolved water diffuses through the polymer bulk from droplet nucleation site to nucleation site [12]. The process was modeled mathematically by X. Li as the diffusion of the droplets themselves, which provided an apparent diffusion for the droplets, or light

scattering centers. Results with the SIP also showed that hydrophilic salts added to the membrane have a significant effect on the transport behavior of water in these membranes [12, 13].

In this chapter, we propose a model of water uptake based on a dual-sorption theory [6,17,18] and osmotic pressure arguments, in an attempt to explain the above observed phenomena. A quantitative analysis of both equilibrium water distribution and the kinetics of the water transport process has been applied to the experimental data obtained by Li and Harrison. In addition, experiments using both SIP and UV-Visible spectrophotometer have been carried out to evaluate the theory.

## 2.2 THEORY

### 2.2-1 Equilibrium Water Absorption

It has been proposed that the absorption of substantial amounts of water in polymers occurs by means of osmosis [19,20] - the polymer contains water-soluble inclusions that are not soluble in the polymer itself. The polymer surrounding these inclusions then functions as a semipermeable membrane. A. G. Thomas *et al.* used this assumption to explain water uptake in rubber that contains salt impurities [21-23]. PVC based membranes are also known to contain deliberately added and adventitious salts [24-26]. We have applied the osmotic pressure theory to model the equilibrium uptake of water in PVC membranes.

It is assumed that the absorption of water by membranes is due to the presence of hydrophilic impurities in the membrane. Water diffuses through the membrane phase, in which it is slightly soluble, and forms droplets of saturated

aqueous solution at impurity sites containing water soluble salts. This concentrated solution will have a different osmotic pressure than the external bathing solution in which the membrane is immersed. As a result of this more water may diffuse through the membrane into the impurity droplets. These droplets consequently grow in size and deform the membrane surrounding them. Equilibrium water uptake is reached when the osmotic-pressure difference between the droplet solution and the external solution balances the restraining elastic stresses acting on the droplet. The concept is shown schematically in Fig. 2.1. K. Muniandy *et al.* have developed a mathematical model to describe the role of osmotic pressure effects on water absorptions [22, 23]. This model is outlined below.

If  $\pi_{aq}$  is the osmotic pressure of the external aqueous solution,  $\pi_i$  is the osmotic pressure of the impurity-droplet solution in the membrane and  $p$  is the average elastic pressure associated with the formation of a pocket in the membrane phase, then at equilibrium water uptake:

$$\pi_{aq} = \pi_i - p \quad (2.1)$$

This assumes that the membrane acts as a semi-permeable membrane permitting the passage of water but not of the relevant dissolved impurities.

The osmotic pressures are given by:

$$\pi_{aq} = C_{aq}RT \quad (2.2)$$

$$\pi_i = \frac{C_i^*RT\rho_w}{(C_w - C_i)M_w} \quad (2.3)$$



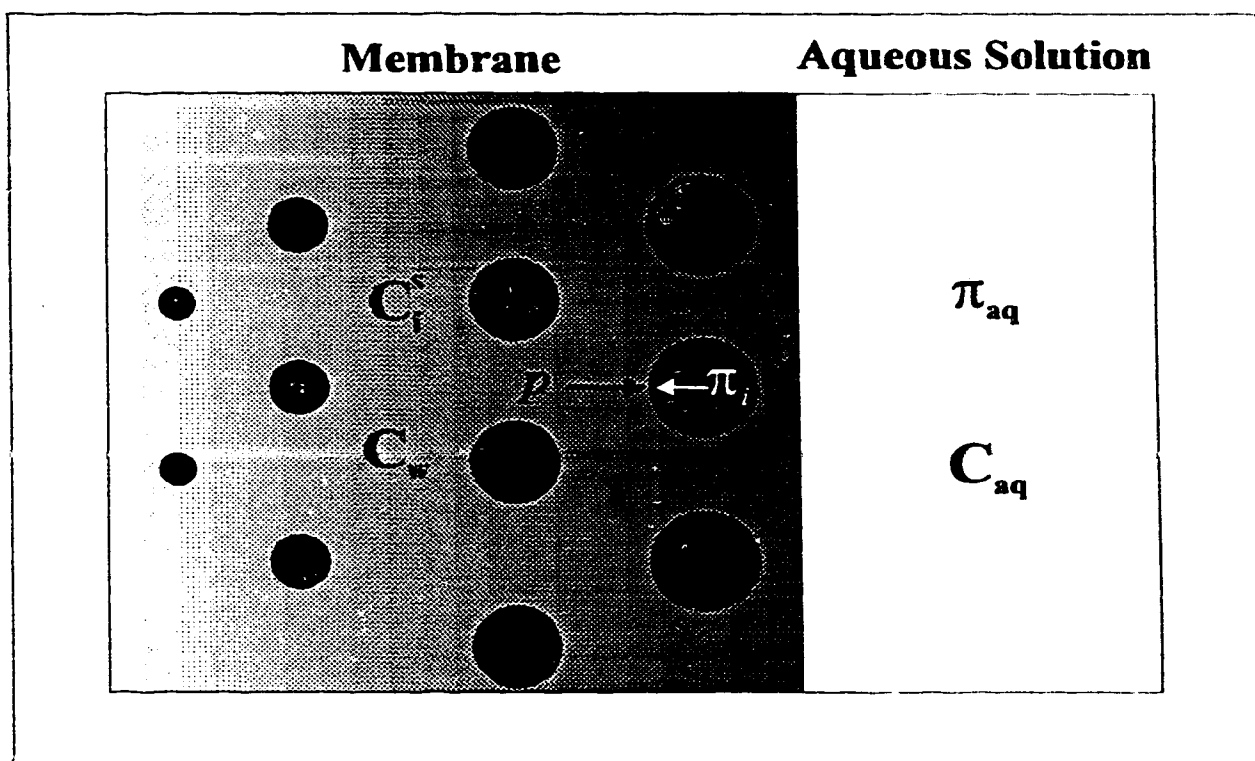


Figure 2-1. Cartoon illustrating different sized water droplets formed inside a membrane. The shading indicates decreasing water content away from the membrane/solution interface, while the decreasing size of droplets represents the gradient of water content within droplets. ( See text for details on symbols )

where  $C_{aq}$  is the molar concentration of the electrolyte in the external aqueous solution and  $C_i^*$  is the average concentration of salt impurity in the membrane.  $C_w$  is the total, or average, molar concentration of water in the membrane. Activity coefficients of significance have been neglected in this analysis. In fact, most of  $C_w$  will be contained in droplets with a concentration of about 55 M. However, here the approximation is made that this excess water can be expressed as its average distribution over the entire membrane volume. In contrast  $C_i$  is the true molar concentration of water in the membrane phase itself.  $\rho_w$  is the density of water.  $M_w$  is the molecular weight of water.

The elastic pressure,  $p$ , is given by equation 2.4 [20, 27], assuming the droplets are spherical:

$$p = \frac{G}{2} \left( 5 - \frac{4}{\kappa} - \frac{1}{\kappa^4} \right) \quad (2.4)$$

where  $G$  is the elastic shear modulus of the membrane,  $\kappa$  is the ratio of the radius of the droplets after it absorbs water, to the radius before it absorbs water, and can be related to the concentrations of impurity and water in a membrane by [22, 23]:

$$\kappa^3 - 1 = \frac{(C_w - C_i^*)\rho_i M_w}{C_i^* \rho_w M_i} \quad (2.5)$$

where  $M_i$  is the molecular weight of impurity in the membrane and  $\rho_i$  is the density of impurity.  $M_i$  must be the suitable average if an electrolyte is the impurity, viz.  $\frac{1}{2}(M_1 + M_2)$  where  $M_1$  and  $M_2$  are the weights of the two ions.

Substituting equations 2.2, 2.3 and 2.4 into equation 2.1 and rearranging yields:

$$C_{aq} = \frac{C_i \rho_w}{(C_w - C_i) M_w} - \frac{G}{2RT} \left( 5 - \frac{4}{\kappa} - \frac{1}{\kappa^3} \right) \quad (2.6)$$

Equation 2.6 represents the condition that has to be satisfied when the membrane attains equilibrium water uptake. At equilibrium absorption,  $C_w \gg C_i$  and  $\kappa \gg 1$ , so equation 2.6 can be rewritten in the form:

$$C_w = \frac{C_i \rho_w / M_w}{(C_{aq} + 5G / 2RT)} \quad (2.7)$$

Equation 2.7 predicts that the amount of equilibrium water uptake by a membrane is proportional to the salt concentration in the membrane and is inversely proportional to the salt concentration in the external solution. It also predicts that the membrane matrix will affect the equilibrium water uptake through the elastic shear modulus.

Effects due to the surface energy of the liquid/rubber interface were neglected in the Thomas model as the sizes of the water droplets, which are usually greater than microns in dimension, are too large for the effects to be significant [23]. It has been shown that water droplets in PVC based ISE membranes range in size from 16 nm to many micrometers [15]. The surface energy will contribute about 1% to the total energy of a droplet which has a radius of 37nm [28]. Therefore, surface effects could be significant in the early stage of droplet formation.

## **2.2-2 Kinetics of Water Absorption**

The kinetics of water absorption in a PVC-based ion-selective membrane can be described by the Dual Sorption Theory [6,17-18] that was originally developed to account for sorption in glassy polymers. In the Dual Sorption Model sorption is visualized as a process in which there are dual modes: either the penetrant molecule is normally dissolved and is free to diffuse or it is immobilized and contributes little to the transport.

As water diffusion progresses, the impurity droplets gradually increase in size as a result of accumulation of water. It can be anticipated that until equilibrium is reached droplets near the surface of a membrane will be generally larger (more dilute solution) than those in the bulk of the membrane. If we assume that the water dissolved in the membrane phase immediately adjacent to the impurity droplets is in local equilibrium with the water in the droplets' solution, then a concentration gradient exists in the membrane phase favoring movement of water into the bulk of the membrane. In the usual statement of Fick's law, this concentration gradient is the driving force.

In formulating the diffusion equation based on the dual mode sorption model, a set of postulates is advanced, as follows:

- (1) Two concurrent modes of water sorption are operative in a microheterogeneous medium.
- (2) The first mode of sorption involves mobile water molecules in the membrane phase.
- (3) The second mode of sorption occurs by immobilization of water molecules at a fixed number of impurity sites within the membrane.
- (4) Local equilibrium between mobile water molecules and immobilized water molecules is always maintained throughout the medium. In

other words, it is assumed that the kinetics of the immobilization process is very rapid compared with the rate of migration of mobile species (i.e., the diffusion process is rate-controlling).

- (5) Water sorbed by the second mode is completely immobilized and therefore does not contribute to the diffusive flux.
- (6) Only diffusion of the mobile water molecules occurs and this is driven by the concentration gradient.
- (7) The true diffusion coefficient (**D**) of water molecules in the membrane phase is a constant, independent of concentration or position in the membrane.

Again, we denote the true molar concentration of water in the membrane phase itself as  $C_1$  and the molar concentration of immobilized water molecules in the membrane as  $C_2$ , respectively. Both  $C_1$  and  $C_2$  have the same physical meanings as ones in X. Li's model (see Chapter 1). Accordingly, the unidirectional flux is given by Fick's law:

$$J = -D \frac{\partial C_1}{\partial x} \quad (2.8)$$

A material balance on a differential element of membrane in the net flow direction yields the one dimensional, non-steady state transport equation:

$$\frac{\partial C_w}{\partial t} = \frac{\partial C_1}{\partial t} + \frac{\partial C_2}{\partial t} = -\frac{\partial J}{\partial x} \quad (2.9)$$

where  $C_w$  denotes the total, or average, molar concentration of water in the membrane and:

$$C_w = C_1 + C_2 \quad (2.10)$$

Substituting equation 2.8 into equation 2.9 with the condition that the diffusion coefficient,  $D$ , is constant results in:

$$\frac{\partial C_1}{\partial t} + \frac{\partial C_2}{\partial t} = D \frac{\partial^2 C_1}{\partial x^2} \quad (2.11)$$

Equation 2.11 is a modification of Fick's second law that accounts for accumulation of water by immobilization at fixed sites within the membrane as well as accumulation by simple dissolution within the membrane phase.

The concentration of water,  $C_1$ , present in the membrane phase is given by means of Raoult's and Henry's laws as [22-23]:

$$C_1 = \frac{s_0(\kappa^3 - 1)}{(\kappa^3 - 1) + M_w \rho_i / M_i \rho_w} \quad (2.12)$$

where  $s_0$  is the maximum molar concentration of water in the membrane phase when it contains no impurities.

Substituting equations 2.5 and 2.10 into equation 2.12 and rearranging yields:

$$C_1 = \frac{s_0 C_2}{C_2 + C_1^s} \quad (2.13)$$

### **Case 1:**

If  $C_2$  is very small at an early stage of water absorption, equation 2.13 becomes:

$$C_1 = \frac{s_0}{C_1^s} C_2 \quad (2.14)$$

Substituting equation 2.14 into equation 2.11 gives:

$$\frac{\partial C_1}{\partial t} = \frac{D}{1 + \frac{C_1^s}{s_0}} \frac{\partial^2 C_1}{\partial x^2} = D_1 \frac{\partial^2 C_1}{\partial x^2} \quad (2.15a)$$

$$\frac{\partial C_2}{\partial t} = \frac{\frac{s_0}{C_1^s} D}{1 + \frac{s_0}{C_1^s}} \frac{\partial^2 C_2}{\partial x^2} = D_2 \frac{\partial^2 C_2}{\partial x^2} \quad (2.15b)$$

where

$D_1$  is the apparent diffusion coefficient of mobile water

$D_2$  is the apparent diffusion coefficient of immobilized water

$$D_1 = D_2 = \frac{D}{1 + C_1^s / s_0} \quad (2.16)$$

It should be pointed out that  $D_1$  in the model presented here has the same definition as that in X. Li's model, while the meanings of  $D_2$  in these two models are not exactly the same. In equation 2.15b  $D_2$  is defined in terms of water concentration while  $D_2$  in X. Li's model was defined in terms of water droplet transport. However, the two definitions, while distinct, are qualitatively similar. Equation 2.16 predicts that both  $D_1$  and  $D_2$  decrease with increasing salt concentration within the membrane at low total water content. This condition

should be met when the concentration of water is too low for light scattering to be observed, as in the initial stage of water uptake in X. Li's model (see chapter one).

**Case 2:**

At later stages of water uptake, equivalent to the second stage process of water uptake in X. Li's model,  $C_2$  can not be ignored. Then equation 2.13 must be substituted into equation 2.9 instead of equation 2.14. By ignoring the change in the true water concentration in the membrane phase, that is, taking  $C_1$  as approximately constant, we get:

$$\frac{\partial C_w}{\partial t} \equiv \frac{\partial C_2}{\partial t} = \frac{\partial}{\partial x} \left[ \frac{s_0 C_1^s}{(C_2 + C_1^s)^2} D \left( \frac{\partial C_2}{\partial x} \right) \right] = \frac{\partial}{\partial x} \left[ D_2 \frac{\partial C_2}{\partial x} \right] \quad (2.17a)$$

with the condition:

$$C_w \approx C_2 \gg C_1 \quad (2.17b)$$

where

$$D_2 = \frac{s_0 C_1^s}{(C_2 + C_1^s)^2} D \quad (2.18)$$



Equation 2.18 predicts that  $D_2$  is approximately inversely proportional to the square of the water concentration in the membrane. When  $C_2$  is large (case 2), equation 2.18 can be written as:

$$D_2 \cong \frac{s_0 C_i^s}{(C_2)^2} D \quad (2.18a)$$

This equation predicts that  $D_2$  increases with the increase of  $C_i^s$  as was observed experimentally previously [12].

### 2.2-3 Mathematical Solutions of The Diffusion Models

#### Case 1:

The analytical solution to equation 2.15a has been given by Crank [29] for the following plan sheet boundary conditions of the sorption experiment:

$$t = 0, 0 \leq x \leq l, \quad C_1 = 0 \quad (2.19)$$

$$t \geq 0, x = 0, \quad \frac{\partial C_1}{\partial x} = 0 \quad (2.20)$$

$$t > 0, x = 0; l, \quad C_1 = C_i^s \quad (2.21)$$

where  $l$  is the thickness of the membrane and  $C_i^s$  is the concentration of dissolved water at the membrane/water interface. The solution in the form of an infinite trigonometric series is:

$$C_1(x, t) = C_1^* \left\{ 1 - \frac{4}{\pi} \sum_{n=1}^{\infty} \frac{1}{(2n-1)} \exp \left[ -\frac{D_1 (2n-1)^2 \pi^2 t}{l^2} \right] \sin \frac{(2n-1)\pi x}{l} \right\} \quad (2.22)$$

In X. Li's model (see Chapter 1) at short times, the value of  $D_1$  comes from equation 1.13 and the meaning of  $C_1^0$  is complicated by the diffusion boundary where the diffusion coefficient undergoes a step change. In the model presented here no step change in the diffusion coefficient is involved. However, the form of the infinite trigonometric series is the same in both models, so the calculated value of  $D_1$  is also the same.

In the above discussion, we have assumed that  $C_1^*$  is constant. However, this approximation requires further consideration. It was found by X. Li [30] that the surface concentration of water is a function of time, based on the increasing amount of light scattering seen at the surface. However, this effect is likely due to changes in the elastic properties of the polymer with time. Such changes would mean different amounts of water could be incorporated in the droplets. The total or maximum amount of dissolved water would be expected to be relatively unchanged, so that the effect on  $C_1$  and  $D_1$  need not be considered when  $C_2$  is small.

### Case 2:

Equation 2.17 is a non-linear partial differential equation. To further complicate the situation, our experimental results show that there is a surface region that develops at later stages of water uptake [12-14], which differs in water content from the membrane bulk. No analytical solutions of the differential

equation are possible. This necessitates the use of numerical techniques that will be discussed in chapter 4.

The analytical approximation methods (see Chapter 1) can also be used to analyze data in the case 2 regime. Equations 1.11 and 1.13 provide good fits to the observed data at any point in time. However, the parameters obtained must be regarded as empirical values, since they must change over time to account for the factors ignored by X. Li's model, including the change in the concentration of water at the membrane/water interface with time. Nevertheless, such parameters have useful predictive power, and also provide the initial parameters for numerical calculations based on the more detailed models described above.

## 2.3 EXPERIMENTAL

### 2.3-1 Sample Preparation:

A number of ion-selective membrane samples were prepared. The following compositions were examined: (1) Potassium-sensitive membrane - 66% bis(2-ethylhexyl)adipate (DOA, Fluka Selectrophore grade), 33% PVC (Polysciences, chromatographic grade), 1% Valinomycin (Aldrich), 0.01%  $\text{KB}(\text{C}_6\text{H}_5)_4$  ( $\text{KBPh}_4$ ), and 0 to 1% anhydrous  $\text{CoCl}_2$  (from  $\text{CoCl}_2 \cdot 6\text{H}_2\text{O}$  Anachemia, purified); (2) Ammonium-sensitive membrane - 64% DOA, 32% PVC, 2.6% nonactin (Sigma), and 1.7% potassium tetrakis(*p*-chlorophenyl)borate ( $\text{KTPClPB}$ , Fluka).

Water was deionized and doubly distilled. The dehydration of  $\text{CoCl}_2 \cdot 6\text{H}_2\text{O}$  was carried out under vacuum ( $< 5 \times 10^{-3}$  mm Hg) at 60 °C for 16 hours (DUO-SEAL (1400) vacuum pump, Welch Scientific Co.). The wt% of  $\text{CoCl}_2$  in the dehydrated material was determined by direct ethylenediaminetetraacetic acid

titration [32] as 99.9%.  $\text{KBPh}_4$  was prepared by precipitation in water from  $\text{KCl}$  and  $\text{NaBPh}_4$ , followed by vacuum drying [32].

Membranes were cast from solutions of components in freshly distilled tetrahydrofuran (THF) (BDH, distilled from potassium) according to the method of Craggs et al. [33] using a glass mould for casting. The mould was 2.5 cm in diameter and 3 cm deep with an optical flat glass bottom and was placed inside a bottle as shown in Figure 2.2. The bottle was placed on a leveled platform to ensure uniform thickness of the membrane casting. Aliquots of solutions were delivered into the mould. Dried Ar passed through a 30 cm drierite column, was introduced to the bottle to ensure the membrane was very dry after the evaporation of THF. The flow rate of Ar was kept very low to allow a slow evaporation of THF. After 48 hours of solvent evaporation, the master membrane was taken out and stored in a vacuum desiccator.

### 2.3-2 SIP Measurements:

A spatial imaging photometer (SIP) was used to measure concentration profiles of water inside membranes. A set up of the SIP is shown in Figure 2.3. The details of the instrumentation were presented elsewhere [11]. It consisted of a He:Ne 632.8 nm laser as light source, a membrane mounted in an optical cell at the object plane of a Pentax lens, and a 512-element photodiode array detector in the image plane, interfaced to a Compaq 286 programmed using ASYST (Macmillan). Master membranes were cut into thin slices and mounted between two glass plates treated with  $\text{ClSi}(\text{CH}_3)_3$  (Petrarch) and bonded together with epoxy to form the optical cell illustrated in Figure 2.3. The membrane surface parallel to the bottom of the casting mould was placed against the glass plates so that the

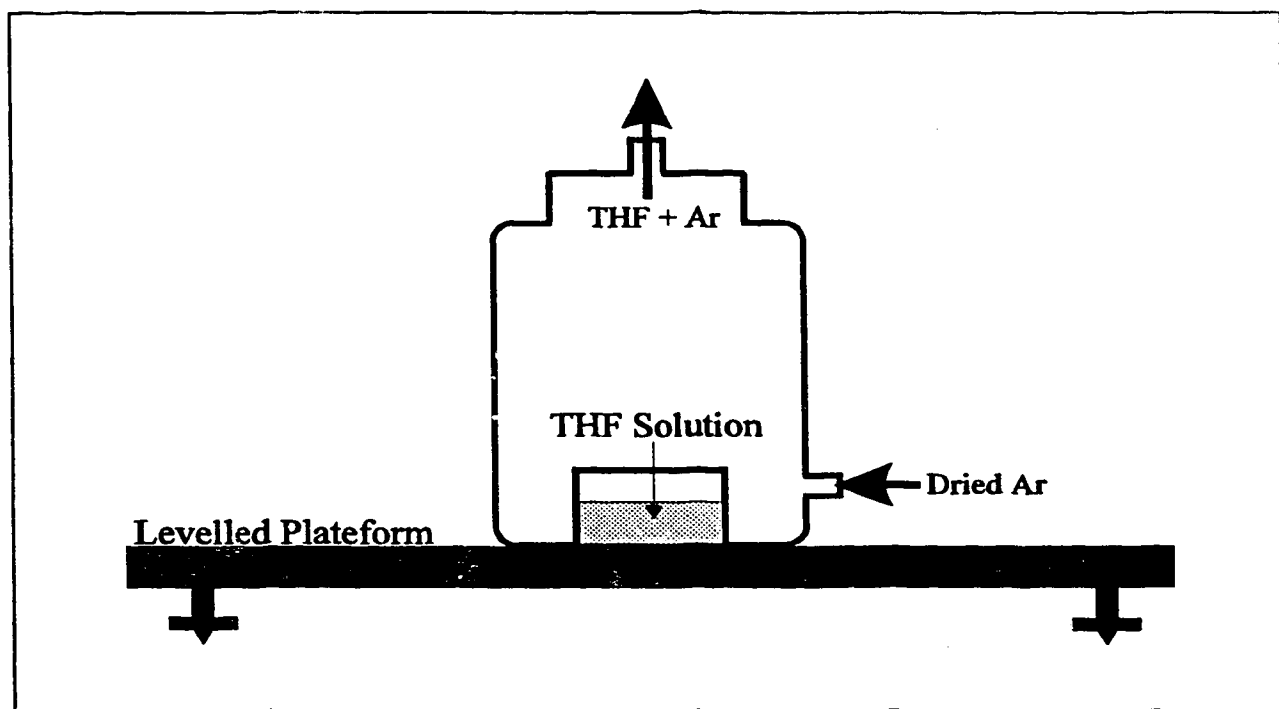


Figure 2-2. The schematic diagram for membrane casting

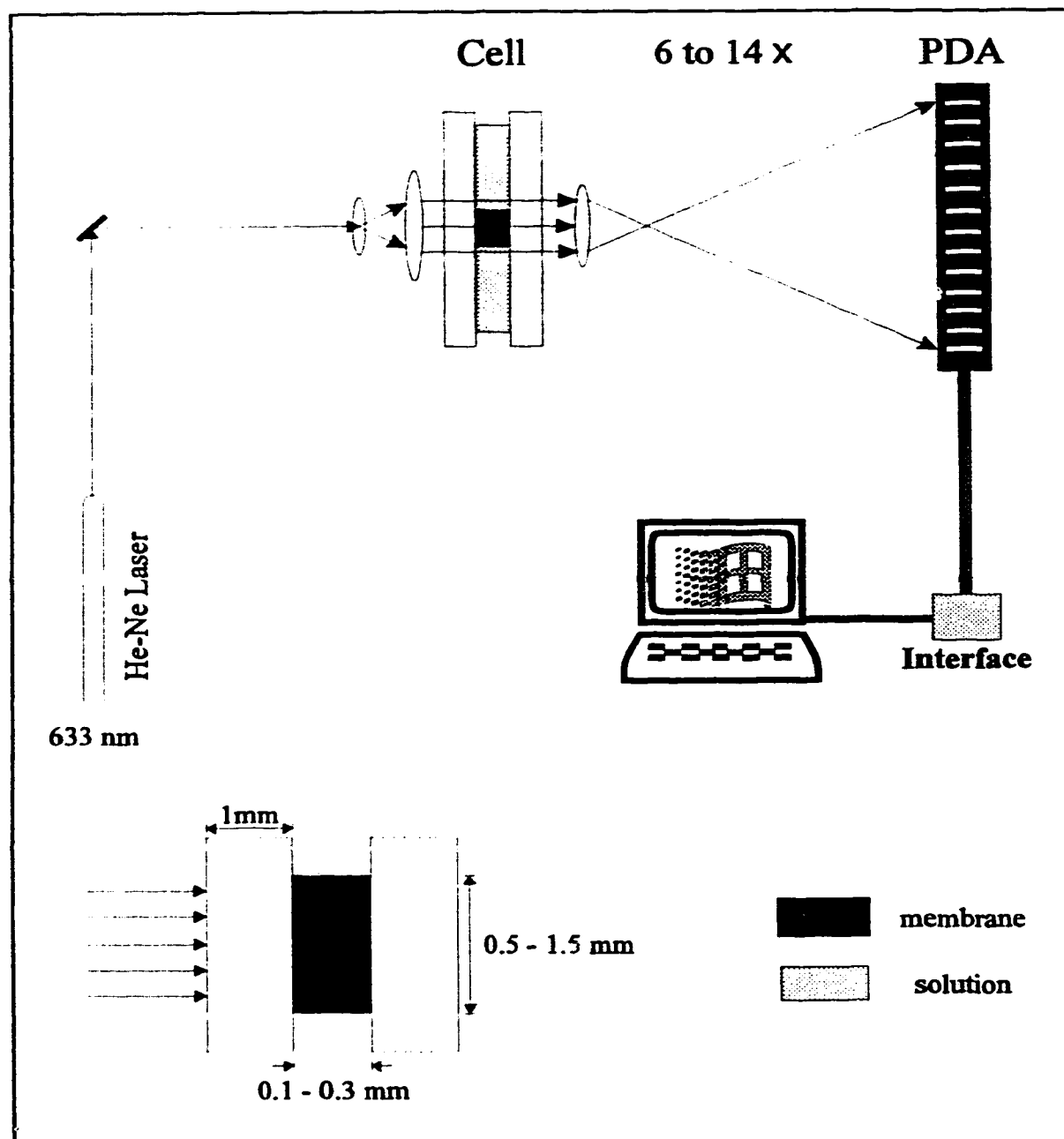


Figure 2-3. Spatial imaging photometer with one laser source. The beam was expanded using cylindrical lenses. The membrane cell dimensions are distorted for clarity in this diagram. The cell is placed in the object plane of a Pentax lens and a 512 element diode array is located in the image plane.

direction of transport of water in the cell was perpendicular to the direction of evaporation of the THF during the casting procedure. However, membranes mounted so that transport was parallel to the direction of evaporation did not exhibit different behavior. Magnifications of 6 to 14 were used in this study, giving nominal spatial resolutions of 2 to 5  $\mu\text{m}$ . The optical path length through the cell was 0.1 - 0.3 mm and was determined by using a micrometer (Mitutoyo Manufacturing Co., Ltd., Tokyo, Japan) with a resolution of 0.01 mm, while the membranes were typically 0.8 - 1.5 mm thick in the direction of water transport ( $90^\circ$  to the optical path). The initial transmitted light was measured within 10 to 15 seconds of introducing water into the cell. To account for source intensity variation over time, the transmittance for each diode,  $T$ , was ratioed to the average intensity of a subset of the diodes which collected light that passed through the aqueous solution in the cell,  $T_0$ . The relative transmittance,  $T/T_0$ , was then measured periodically and the absorbance calculated using the initial curve as the reference intensity.

Potassium-sensitive membranes were examined in this experiment. First water without any salts added was introduced into the optical cells. The transmittance was measured periodically with water kept inside the cells. When the membrane was saturated with water (usually about 24 - 48 hours after water uptake), no more significant intensity changes can be observed. Then, a salt solution was introduced to replace the water inside the cells and the intensity changes with time in the membranes were measured again. After a new equilibrium was established between the membrane and the outside salt solution, the salt solution inside the cell was replaced with either pure water or another salt solution and the transmittance changes were measured again. The experimental data was saved as text files that were imported to an Origin document (Origin 2.88, Microcal) and analyzed on a PC 486.

### 2.3-3 UV-Visible Absorption Studies:

The UV spectra of the membranes were obtained with a Hewlett-Packard 8451A photodiode array spectrometer. One side of a normal 1 cm quartz cell was blocked by black tape leaving a hole (0.25 in. diameter) in the center of the optical path of the spectrometer. A piece of ammonium-sensitive membrane was placed inside the cell to cover the hole. The spectra were obtained by transmission through the membrane bulk parallel to the direction of transport, and so any concentration gradient across the membrane was averaged. The absorbance was measured periodically once the aqueous solution was introduced into the cell, so the changes of the total amount of  $H_2O$  inside the membranes could be obtained after each perturbation. The bathing solutions were then switched and the corresponding absorbance changes were recorded. The references were taken about 5 - 10 seconds after the solutions inside the cell were switched.

### 2.3-4 SIP Data Analysis:

#### Case 1:

To image the penetration of water into the PVC based membranes the inorganic complex  $CoCl_2$  was used as a readily available, water-sensitive dye [11-13]. During casting of the membrane,  $CoCl_2$  is complexed with THF or DOA



(solvent) to form the blue tetrahedral complex  $\text{Co(sol)}_2\text{Cl}_2$ . In the early stage of water uptake, water molecules react with  $\text{Co(sol)}_2\text{Cl}_2$ . At 632.8 nm a decrease of absorbance ( $\Delta A_1$ ) due to the bleaching of the dye will be observed. The relation between  $C_1$  and the absorbance change has been given as [34]:

$$\Delta A_1 = -n_{\text{dw}} \epsilon b C_1 \quad (2.23)$$

where  $n_{\text{dw}}$  is the molar ratio of the bleached dye to the absorbed water ( $n_{\text{dw}} = 1 - 6$ ).

At this stage of water uptake,  $C_2$  is relatively small. Therefore, equation 2.22 can be used to analyze the experimental data. Substituting equation (2.23) into equation 2.22, we have equation 2.24, the absorbance change as a function of distance and time at an early stage when plane-sheet boundary conditions (equations 2.19, 2.20, and 2.21) are applicable:

$$\Delta A_1(x, t) = \Delta A_{1, \text{max}} \left\{ 1 - \frac{4}{\pi} \sum_{n=1}^{\infty} \frac{1}{(2n-1)} \exp \left[ -\frac{D_1 (2n-1)^2 \pi^2 t}{l^2} \right] \sin \frac{(2n-1)\pi x}{l} \right\} \quad (2.24)$$

$D_1$  can be calculated by fitting the experimental data with equation 2.24. By varying the salt concentration  $C_1$  we can obtain a plot of ( $D_1 \sim C_1$ ). The true diffusion coefficient of water molecules ( $D$ ) and the solubility of water ( $s_0$ ) in the membrane phase can then be calculated by fitting this curve with equation 2.15.

**Case 2:**

As water uptake proceeds, light scattering becomes appreciable. An absorbance increase due to the light scattering ( $\Delta A_2$ ) is observed. In X. Li's analysis [12], an assumption has been made that a Beer's law type of relationship holds true for the scattering due to droplets in the membrane, i.e.,  $A_2 \propto C_2$ . This needs a further consideration. At this stage,  $\Delta A_2$  may be related to the average water content due to droplets,  $C_2$ , based on the assumption that water only forms droplets at the sites of salt particles. Therefore, at equilibrium the number of light scattering centers ( $n_{lc}$ ) is equal to the number of salt particles in the membrane.

$$n_{lc} = \frac{\tilde{N} C_i V_{mem}}{\gamma} \quad (2.25)$$

Where:  $\gamma$  is the average aggregation number of ions in the salt particles.  
 $V_{mem}$  is the volume of the membrane in  $\text{cm}^3$ .  
 $\tilde{N}$  is the Avogadro Constant ( $6.022 \times 10^{23} \text{ mol}^{-1}$ ).

The value of  $\gamma$  is unknown. The number of water droplets (which is taken as the same as the number of lighter scattering centers) may also be calculated as:

$$n_{lc} = \frac{C_2 V_{mem} M_w}{V_{droplet} \rho_w} = \frac{C_2 V_{mem} M_w}{\frac{4}{3} \pi r^3 \rho_w} \quad (2.26)$$

Where  $r$  is the radius of the water droplet in  $\text{cm}$ ,  $\rho_w$  is the density of water in  $\text{gram/cm}^3$ .

Combining equation 2.25 and 2.26 gives:

$$\frac{C_2}{C_1^s} = \frac{\frac{4}{3} \pi r^3 \tilde{N} \rho_w}{\gamma M_w} \propto r^3 \quad (2.27)$$

For small particles (  $r \ll \lambda$ ,  $\lambda$  is the wavelength of light), the intensity of transmitted light can be expressed as [35]:

$$I = I_0 e^{-\sigma b} \quad (2.28)$$

where  $b$  is the optical path length and  $\sigma$  is the turbidity, which may be expressed as:

$$\sigma = \frac{8\pi^3}{3} \left( \frac{\alpha}{\epsilon_0} \right)^2 \frac{(n_{lc} / V_{mem})}{\lambda^4} = \frac{8\pi^3 \tilde{N}}{3\gamma} \left( \frac{\alpha}{\epsilon_0} \right)^2 \frac{C_1^s}{\lambda^4} \quad (2.29)$$

where  $\alpha$  is the polarizability of the scattering center and is proportional to the volume of a water droplet [35]. Therefore, for a membrane with fixed salt sites, the absorbance due to light scattering ( $A_2$ ) by water droplets is given by:

$$A_2 = -\log \frac{I}{I_0} = \frac{8\pi^3 \tilde{N}}{3\gamma} \left( \frac{\alpha}{\epsilon_0} \right)^2 \frac{C_1^s}{\lambda^4} b \propto r^6 \quad (2.30)$$

Combining 2.27 and 2.30 gives:

$$A_2 \propto (C_2)^2 \quad \text{or} \quad C_2 \propto \sqrt{A_2} \quad (2.31)$$

The relation of equation 2.31 can also be predict by Mie scattering theory [36-37]. Dovichi *et al.* have shown [38] that the light scattering intensity for particles smaller than 100 nm is proportional to particle size raised to the sixth power. Using this square root relation 2.31, equations 1.17 and 1.18 are modified to:

$$\sqrt{\Delta A_2^b(x, t)} = \sqrt{\Delta A_b^0} \left\{ 1 - \frac{4}{\pi} \sum_{n=1}^{\infty} \frac{1}{(2n-1)} \exp \left[ -\frac{D_2^b (2n-1)^2 \pi^2 t}{l^2} \right] \sin \frac{(2n-1)\pi x}{l} \right\} \quad (2.32)$$

$$\sqrt{\Delta A_2^s(x, t)} = \sqrt{\Delta A_{2, \max}(x, t)} \left[ 1 - \frac{1}{\operatorname{erf} \frac{x_k}{2\sqrt{D_2^s t}}} \operatorname{erf} \frac{x}{2\sqrt{D_2^s t}} \right] \quad (2.33)$$

Chan and Harrison have shown [15] that the droplets formed inside PVC-based ion-selective membranes range in size from 16 nm to many micrometers. Larger particles (  $r > 100 \text{ nm}$  ) will display a weaker light scattering intensity dependence upon particle size [38]. Both theoretical calculation and experimental data show that particles of more than 300-nm radius show a very weak dependence of the scattering cross-section on size [38]. Therefore, equation 2.31 might not be applicable to the most water-rich regions of the membrane where water droplets could have sizes on the scale of micrometers.

## 2.4 RESULTS AND DISCUSSION

### 2.4-1 Equilibrium Water Uptake:

Equation 2.7 can be used to calculate the average equilibrium amount of water ( $C_w$ ) absorbed by PVC membranes. However, values of the elastic shear modulus ( $G$ ) are unknown for PVC-based ion-selective electrode membranes. The contribution of the elastic pressure ( $p$ ) to the balance of osmotic pressure is about 10% in rubbers [21] and should be much higher than it is in heavily plasticized PVC membranes. If  $p$  is neglected, equation 2.7 becomes:

$$C_w \approx \frac{C_i^s \rho_w}{C_{aq} M_w} \propto \frac{C_i^s}{C_{aq}} \quad (2-34)$$

X. Li's thesis and reference 12 describe the influence of the amount of salt within a membrane ( $C_i^s$ ) on the water distribution characteristics in PVC/DOA membranes, determined using the SIP method. The results shown in Figure 2.4 compare the absorbance profiles in membranes containing varying amounts of  $\text{CoCl}_2$  after a 24 hour exposure to water. In Figure 2.4 the water is penetrating from the left edge and the magnification is increased so that only a portion of the membrane is visible. The data clearly demonstrate that the higher the salt concentration in the membrane, the higher the water uptake, as would be predicted by equation 2-34.

Further tests of the proposed osmosis model have been made by examining the effect of the salt concentration in the external solution ( $C_{aq}$ ) on the final equilibrium water uptake in PVC-based ion-selective membranes, using both the SIP and a conventional UV-Vis absorbance spectrometer.

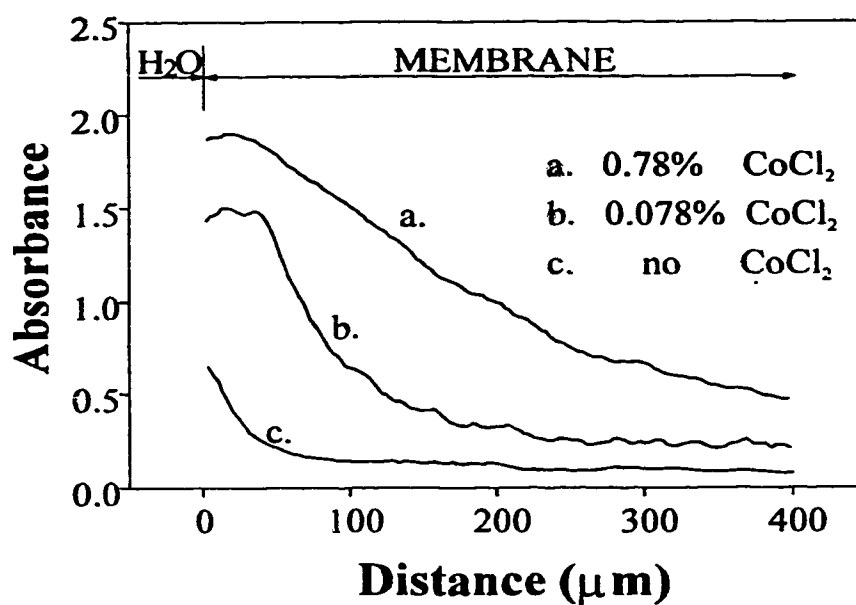


Figure 2.4 Absorbance profiles in membrane containing varying wt.% CoCl<sub>2</sub> after 24 hour's exposure to water (water on left side only). (a) 0.78% CoCl<sub>2</sub> (b) 0.078% CoCl<sub>2</sub> (c) No CoCl<sub>2</sub> (adapted from X. Li, Ph. D. Thesis, 1992, p95)

Figure 2.5 shows a plot of the absorbance due to light scattering centers as a function of distance from the membrane/water interface and the electrolyte strength of the aqueous phase. This is a typical potassium-selective membrane, composed of DOA and PVC as a matrix, with about 1% valinomycin and 0.01%  $\text{KBPh}_4$  added to give selectivity and reduce anion interference, respectively. It can be seen that as the aqueous phase is changed from pure water to 0.1 M  $\text{NaNO}_2$  and then back to pure water the absorbance decreases, and is then returned to its initial value. This is consistent with equation 2-34 and indicates osmotic pressure control of water droplet formation inside the membrane. The absorbance changes with time during the second step and third steps of Figure 2.5 are shown in Figure 2.5a. The reversibility of the process indicates it is a thermodynamic effect, and is not due to irreversible changes in the polymer or membrane structure with water uptake. However, the process is very slow.

We have also used a UV-Vis spectrometer to study the effect of the external aqueous solution on light scattering in an ammonium-sensitive membrane. It has a composition of 64% DOA, 32% PVC, 2.6% nonactin (Sigma), and 1.7%  $\text{KTpClPB}$  which has been used for ammonium ion selective optical sensors [39].

Figure 2.6 is a typical spectrum of the membrane soaked with water as a function of time. It shows that further absorbance changes became very slow after about 48 hours soaking. The equilibrium absorption of water was reached at about 72 hours and the absorbance change was 0.75 at 400 nm. At 98 hour of water soaking, the water inside the cell was replaced by a 0.1M  $\text{NH}_4\text{Cl}$  solution. The absorbance of the membrane decreased with time (Figure 2.7(a)), indicating a decrease in light scattering and by inference that water migrated out of the membrane. After 24 hour, the solution inside the cell was switched back to water. An increasing absorbance with time was observed (Figure 2.7(b)). This is consistent with the SIP results observed in Figures 2.5 and 2.5a.

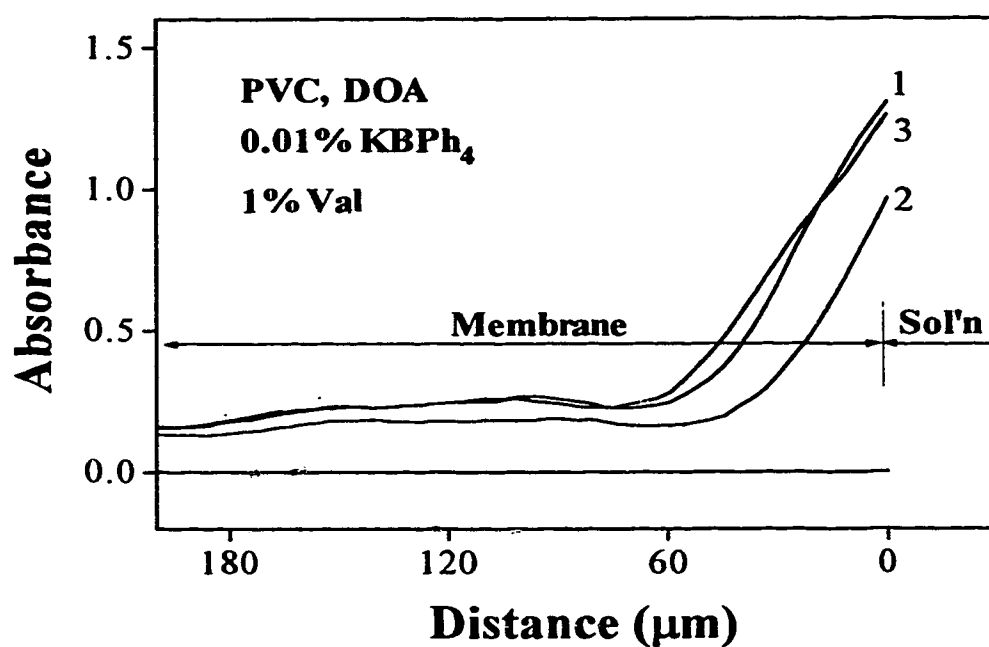


Figure 2.5 Absorbance due to light scattering with distance from the membrane/water edge after (1) 12 days in water, (2) plus a further 24 hr in 0.1 M  $\text{NaNO}_2$ , (3) then a further 24 hr. in water for a total of 14 days in solution.



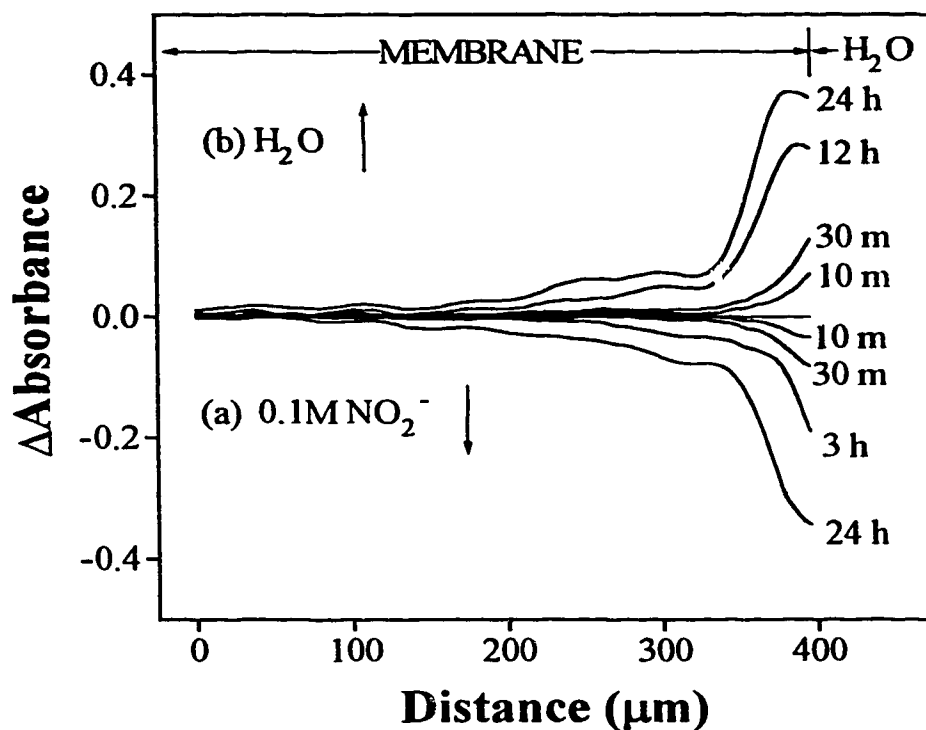


Figure 2.5a. Absorbance changes ( $\Delta A$ ) with time in the membrane: (a)\* The membrane was saturated with pure water for 12 days, then placed in 0.1M  $\text{NaNO}_2$ ; (b)<sup>†</sup> After soaking the membrane in 0.1M  $\text{NaNO}_2$  for 24 hr., it was then returned to pure water.

\*  $\Delta A$  was calculated by taking the transmitted light intensity after 12 days of soaking in water as the reference data.

<sup>†</sup>  $\Delta A$  was calculated by taking the transmitted light intensity after a further 24 hours in 0.1M  $\text{NaNO}_2$  as the reference data.

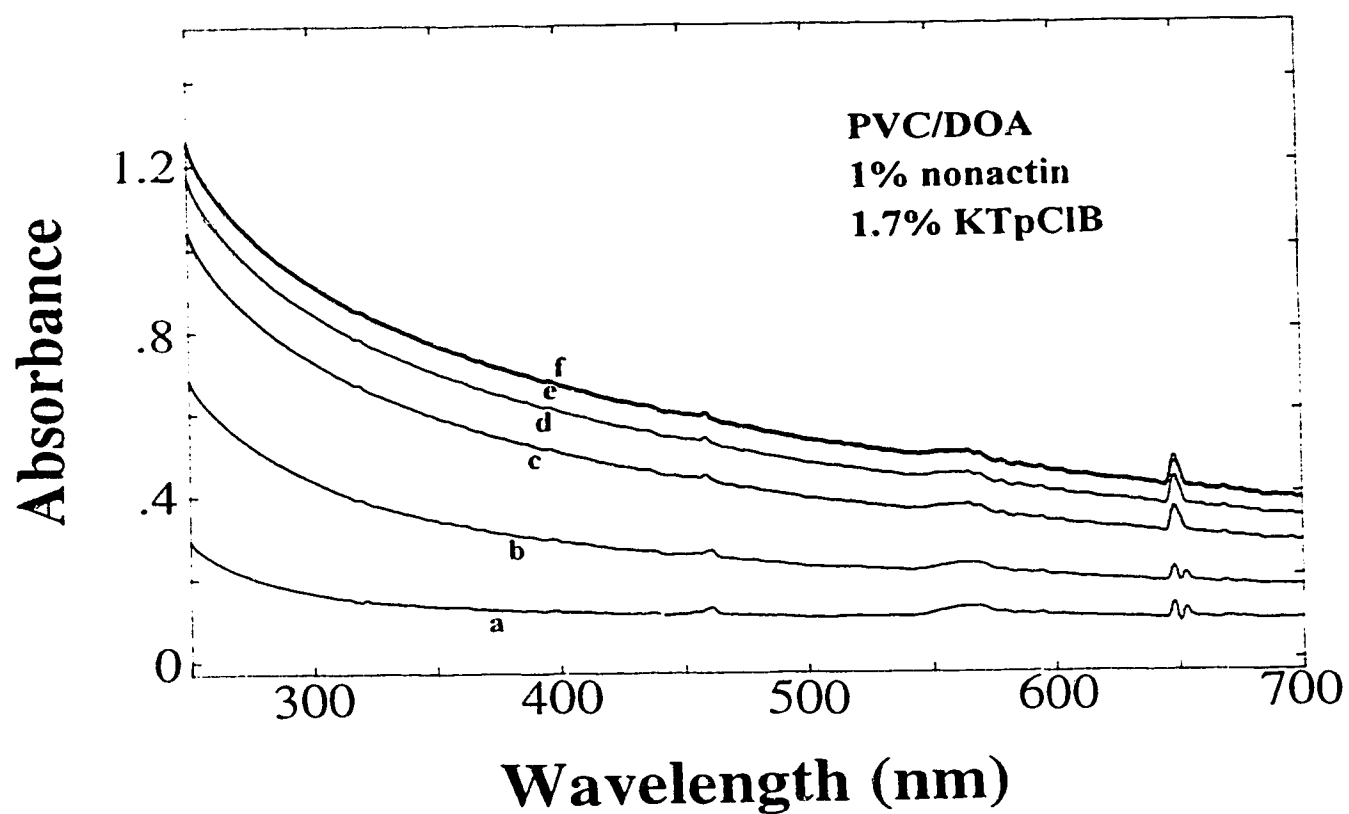


Figure 2.6 Absorbance due to light scattering in an ammonium-selective membrane as a function of time between 250 and 700 nm. (a) 1 hour; (b) 6 hours; (c) 24 hours; (d) 48 hours; (e) 72 hours; (f) 98 hours.

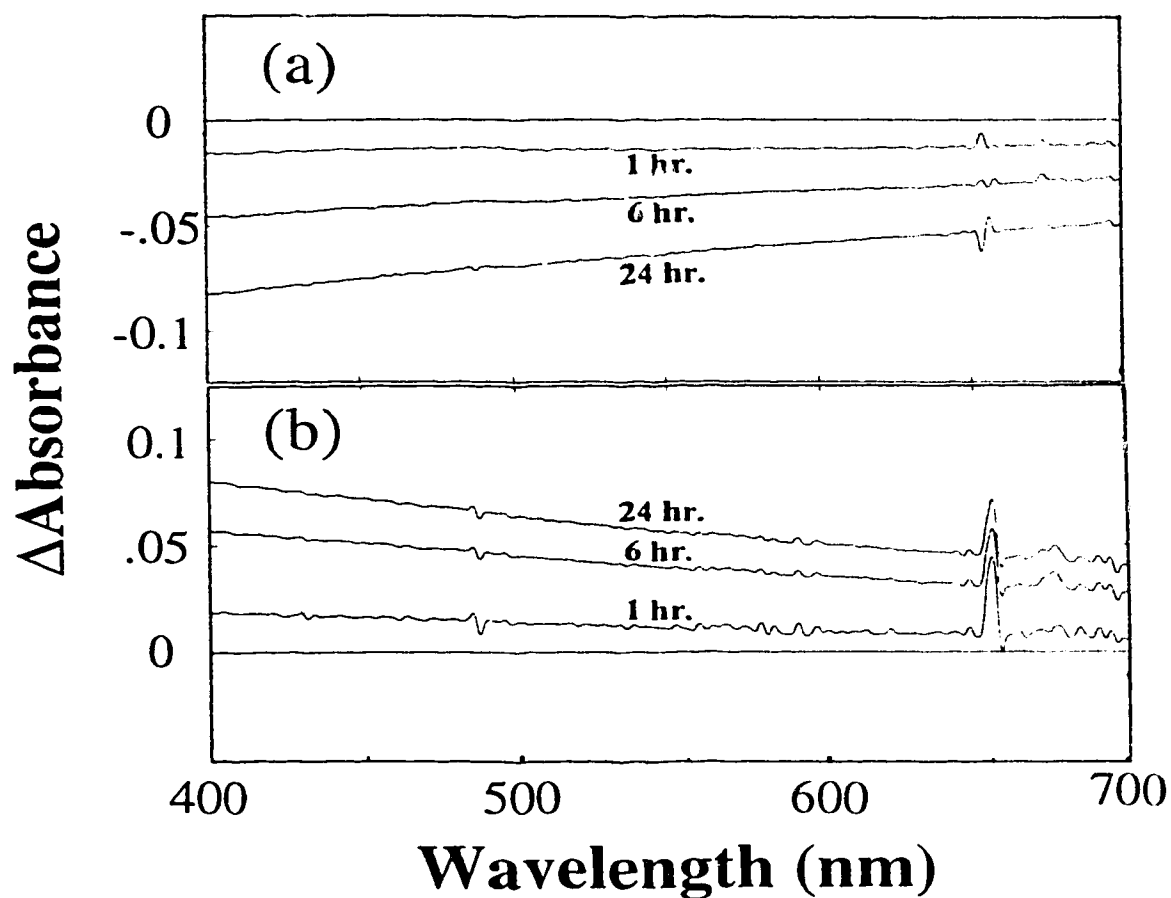


Figure 2.7 Effects of the ionic strength of external aq. solutions on the light scattering in a PVC/DOA/1%Nonactin/1.7%KTPClB membrane.

- (a) The membrane soaked with pure water for 98 hours, then replace water by 0.1M  $\text{NH}_4\text{Cl}$ .
- (b) The membrane soaked with 0.1M  $\text{NH}_4\text{Cl}$  for 24 hours, then replace aq. solution by pure water.

To further test the osmotic effect on water uptake in membranes, we have measured the variation in absorbance with the salt concentration of aqueous solution. Figure 2.8 illustrates the total absorbance change for several steps of soaking with different bathing solutions. The absorbance change was measured at 400 nm for the comparison. The figure shows in step 4 that the water content in the membrane decreased again after the external solution was switched to 0.1 M  $\text{NH}_4\text{Cl}$ . In step 5, the bathing solution was replaced by a 0.001 M  $\text{NH}_4\text{Cl}$  solution after the membrane was soaked with the 0.1 M  $\text{NH}_4\text{Cl}$  solution for just 2 hours. The absorbance then increased over the next 2 hours. In step 6, the bathing solution was then switched to a 0.01 M  $\text{NH}_4\text{Cl}$  solution and measured after 2 hours. The absorbance of the membrane still increased during this 2 hour period, instead of decreasing as might be expected from the concentration change mode. This indicates that water re-absorption in step 5 had not reached the equilibrium point for either a 0.001M or a 0.01M  $\text{NH}_4\text{Cl}$  solution.

The above experimental results provide strong evidence that osmotic pressure is the main driving force for water uptake in PVC based ion-selective membranes.

#### **2.4-2 Kinetics of Water Uptake:**

X. Li measured [39] the apparent diffusion coefficients of dissolved water ( $D_1$ ) in the PVC/DOA membranes containing varying amounts of  $\text{CoCl}_2$  using the SIP. The values of  $D_1$  obtained are listed in Table 2.1. The plot of  $D_1$  vs.  $C_i^*$  is shown in Figure 2.9. It shows that  $D_1$  decreases with the increase of  $C_i^*$  as predicted by equation 2.16. By fitting the plot with equation 2.16, the values of

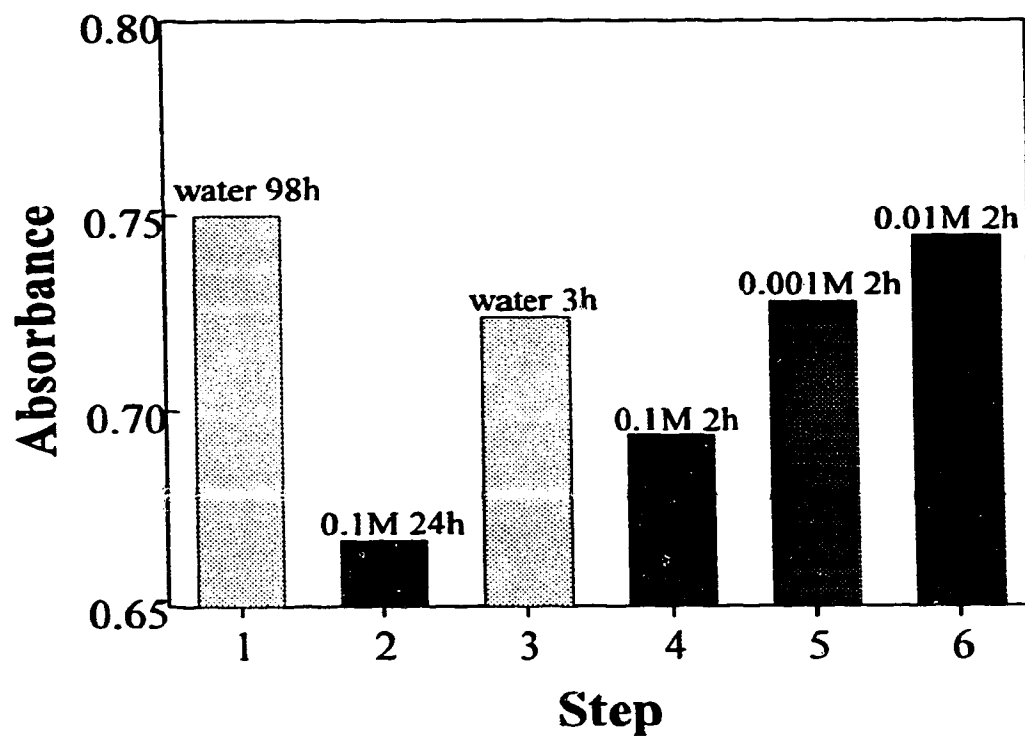


**Figure 2.8** Total absorbance changes for six consecutive steps

Step 1: soaked with water for 98 hours

Step 2: soaked with 0.1 M  $\text{NH}_4\text{Cl}$  for 24 hours

Step 3: soaked with water for 24 hours

Step 4: soaked with 0.1 M  $\text{NH}_4\text{Cl}$  for 2 hours

Step 5: soaked with 0.001 M  $\text{NH}_4\text{Cl}$  for 2 hours

Step 6: soaked with 0.01 M  $\text{NH}_4\text{Cl}$  for 2 hours

**Table 2.1** The diffusion coefficient of water as a function of  $C_i'$   
 (Adapted from X. Li's thesis, 1992, p77 & p87).

<b>Salt Concentration (<math>C_i'</math>)</b>	<b><math>D_1^*</math> (<math>\times 10^{-7} \text{cm}^2/\text{s}</math>)</b>	<b><math>D_2</math> (24 hour)** (<math>\times 10^{-9} \text{cm}^2/\text{s}</math>)</b>
25.4	9.9	1.0
31.1	9.5	3.0
45.8	7.8	3.5
86.6	5.7	7.6
107	4.7	10
209	3.2	14
311	1.8	16

\* Values were calculated by fitting the SIP data with equation 1.15.

\*\* Values were calculated by fitting the SIP data with equation 1.16.

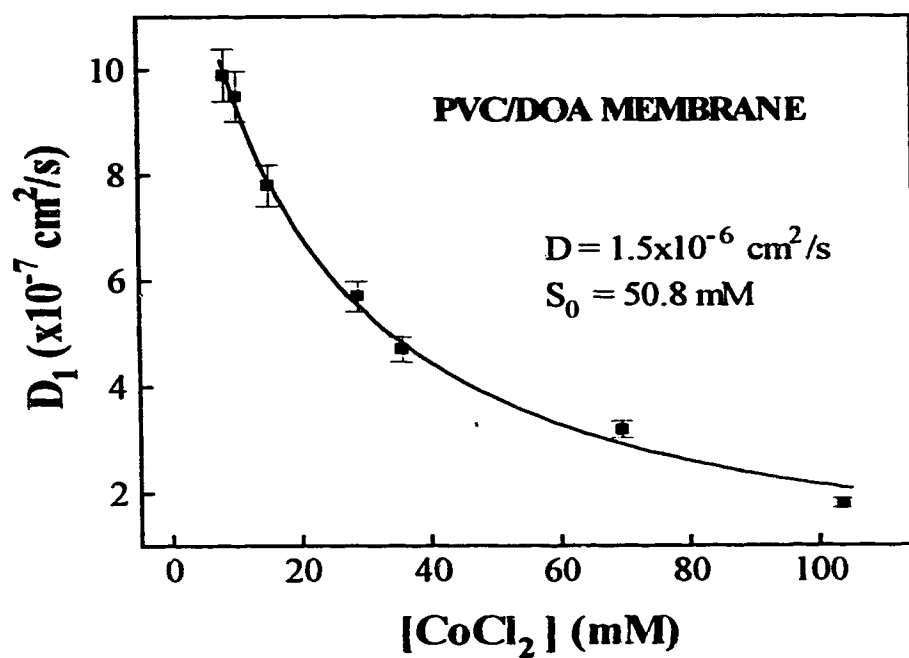


**Figure 2.9** The apparent diffusion coefficient of water as a function of  $\text{CoCl}_2$  concentration at the early stage. The solid line is the fit to equation 2.16 with  $D = (1.5 \pm 0.1) \times 10^{-6} \text{ cm}^2/\text{s}$  and  $s_0 = (50.8 \pm 5.1) \text{ mM}$ .

the true diffusion coefficient,  $D$ , and the solubility of water,  $s_0$ , in PVC/DOA membranes were then calculated as  $(1.5 \pm 0.1) \times 10^{-6} \text{ cm}^2/\text{s}$  and  $(50.8 \pm 5.1) \text{ mM}$  respectively.

The obtained values of the apparent diffusion coefficient of water droplets ( $D_2$ ) for a long period of time (24 hours) of water uptake [40] are also listed in Table 2.1. The dependence of  $D_2$  on the concentration of  $\text{CoCl}_2$  in a membrane is shown in Figure 2.10. It can be seen that  $D_2$  increases with the increase of  $C_i^*$ . This is in agreement with equation 2.18a. It should be pointed that X. Li's data analysis gave the values of  $D_2$  which can be taken as the apparent diffusion coefficient of droplets while  $D_2$  in equation 2.18a represents the apparent diffusion coefficient of water immobilized in droplets. Values are not the same, but the trends will be.

X. Li and Harrison also examined the blank membranes prepared from PVC and DOA alone [40]. A highly hydrated surface layer was observed and the simplified two stage uptake model was used to analyze the data. Apparent diffusion coefficients were obtained by fitting the data at the surface regions using equation 1.17 and the bulk region using equation 1.18. Their results show that both  $D_2^s$  and  $D_2^b$  decreased with the increasing water concentration as would be predicted by equation 2.18. Detailed analysis of the data will be discussed in Chapter 5.

## 2.5 CONCLUSIONS

The model formulated in this chapter, which makes use of dual-sorption theory and the concept of osmotic pressure as the driving force for diffusion, satisfactorily predicts the trends for water transport and equilibrium uptake in PVC based ion-selective electrode membranes.



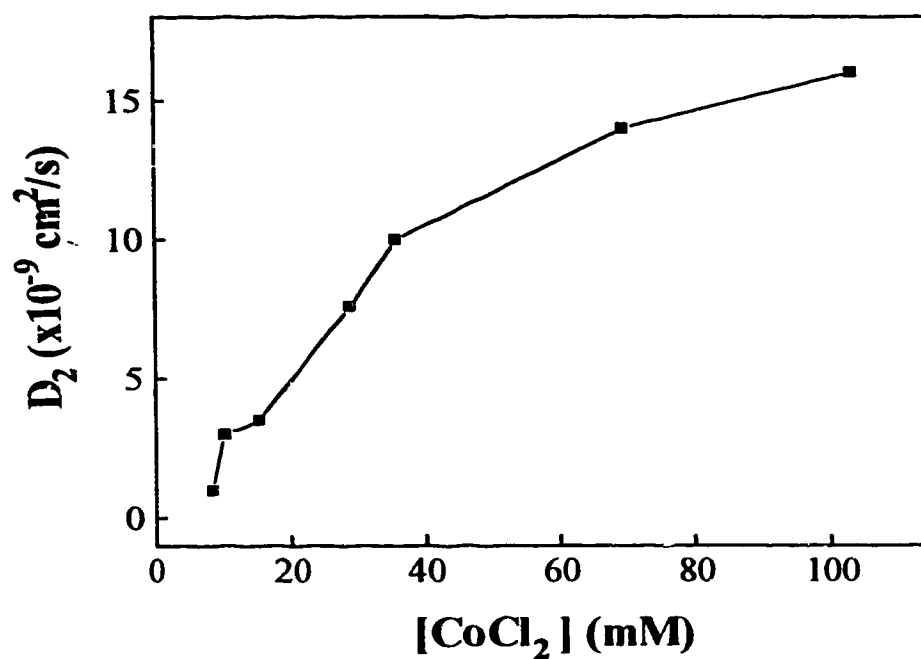


Figure 2.10 Diffusion coefficient vs. concentration of  $\text{CoCl}_2$  (mM) in membrane for 24 hours associated with light scattering (Adapted from X. Li's thesis, 1992, p93)

The formation of water droplets within PVC based membranes is governed by the same principle that controls water uptake in rubber. In rubber it has been shown that the formation of droplets is associated with the presence of hydrophilic salts within the polymer phase that act as nucleation sites for the droplets. Since the water droplets solvate or dissolve the ionic sites in the polymer phase, an osmotic pressure equilibrium between the droplets and the solution is set up. The experimental evidence presented here shows that water in PVC based membranes exhibits the expected trends for a system controlled by osmotic pressure effects. Solvation of the salt and charged sites within PVC based membranes, and dilution of the salt solution within the droplets, acts as the driving force for the continued water uptake once the freely miscible limit for water has been reached. One consequence of this is that the light scattering in a membrane will be a function of the ionic strength in the external aqueous phase. For ISE membranes this will not present a problem. However, for optical sensors based on the plasticized PVC matrix the variation in light scattering with ionic strength could lead to some variability between measurements in samples and standard solutions. Matrix matching might be required if the maximum precision and accuracy was desired.

The dual-sorption theory was used to study the water transport process in PVC based membrane. The proposed model relates the measured apparent diffusion coefficients of water droplets to the true diffusion coefficient of water in a membrane. It also implies that the apparent diffusion coefficient,  $D_2$ , of water depends on water and impurity contents in membranes, in agreement with published results.  $D_2$  decreases as water in the membrane increases. Adding salt to the membrane phase decreases the initial rate of water transport while  $D_2$  for later stages increases as salt content in the membrane increases. The true diffusion coefficient ( $D$ ) and solubility of water ( $s_0$ ) in PVC/DOA membrane were found to be  $(1.5 \pm 0.1) \times 10^{-6} \text{ cm}^2/\text{s}$  and  $(50.8 \pm 5.1) \text{ mM}$ , respectively.

## 2.6 REFERENCES

1. Barrie, J. A. In *Diffusion in Polymers*, Edited by Crank, J. and Park, G. S., Academic Press: London and New York, 1968, Chapter 8.
2. Water Structure at the Water/Polymer Interface, ed. H. H. G. Jellinek, Plenum Press, New York, 1972.
3. Water in Polymers, *ACS Symposium Series, No. 127*, Edited by Rowland, S. P., 1980.
4. Machin, D.; Rogers, C. E. *CRC Critical Reviews in Macromolecular Science*, CRC Press, Cleveland, 1972.
5. Meares, P. *Philos. Trans. R. Soc. London, Ser. B.* 1977, 278, 113-116.
6. Barrie, J. A. *Trans. Inst. Mar. Eng. (C)* 1985, 97, 79-85.
7. Thoma, A. P.; Viviani-Nauer, A.; Arvantis, S.; Morf, W. E.; Simon, W. *Anal. Chem.* 1977, 49, 1567-1672.
8. Marian, S.; Jagur-Grozinski, J.; Kedem, O.; Vodis, D. *Biophys. J.* 1970, 10, 901-910.
9. Armstrong, R. D.; Handyside, T. M.; Johnson, B. W. *Corrosion Sci.* 1990, 30, 569-574.
10. Oesch, U. *Ph. D. Thesis*, ETH, Zurich, Switzerland, 1979.
11. Li, X.; Petrovic, S.; Harrison, D. J. *Sensors and Actuators* 1990, B1, 275-280.
12. Harrison, D. J.; Li, X.; Petrovic, S.; In *Biosensors and Chemical Sensors. Optimizing Performance through Polymeric Materials*; Edelman, P.G., Wang, J., Eds.; ACS Symp. Ser. 487; Washington, DC, 1992, 292-300.
13. Li, Z.; Li, X.; Petrovic, S.; Harrison, D. J. *Analytical Methods and Instrumentation* 1993, 1, 30-37.
14. Chan, A.D.C.; Li, X.; Harrison, D. J. *Anal. Chem.* 1992, 64, 2512-2517.

15. Chan, A.D.C.; Harrison, D. J. *Anal. Chem.* **1993**, *65*, 32.
16. Chan, A.D.C.; Harrison, D. J. Submitted to *Anal. Chem.*
17. Vieth, W. R.; Sladek, K. J. *J. Colloid Sci.* **1965**, *20*, 1014.
18. Vieth, W. R.; Howell, J. M.; Hsieh, J. H. *J. Membrane Sci.* **1976**, *1*, 177.
19. Briggs, G. J.; Edwards, D. C.; Storey, E. B. *Proc. Fourth Rubber Technology Conference*, London, May 22, 1962, p. 362.
20. Fedors, R. F. *Polymer*, **1980**, *21*, 207-212.
21. Southern, E.; Thomas, A. G. *Water in Polymer*, ACS symposium series 127, ACS Washington, D.C., 1980, 375-386.
22. Muniandy, K.; Thomas, A. G. *Trans. Inst. Mar. Eng.(C)* **1985**, *97*, 87-94.
23. Thomas, A. G.; Muniandy, K. *Polymer* **1987**, *28*, 408-415.
24. Morf, W. E.; Simon, W. *Helv. Chim. Acta* **1986**, *69*, 1120-1131.
25. Harrison, D. J. *J. Electroanal. Chem.* **1990**, *278*, 193.
26. Armstrong, R. D.; Horvai, G. *Electrochim. Acta* **1990**, *35*, 1-7.
27. Gent, A. N.; Lindley, P. B. *Proc. Roy. Soc. A* **1958**, *249*, 195.
28. Castellan, G. W. *Physical Chemistry*, 3rd ed., 1983, 408-409.
29. Crank, J. *The Mathematics of Diffusion*, 2nd ed.; Clarendon Press: Oxford, U.K., 1975, 47-48.
30. Li, X. *Ph.D. Thesis*, University of Alberta, Edmonton, Canada, 1992, p64.
31. Schwarzenbach, G.; Flaschka, H. *Complexometric Titrations*, Methuen, London, 1969, [translated by H. M. N. Irving].
32. Bassett, J.; Denney, R. C.; Jeffery, G. H.; Mendham, J. *Vogel's Textbook of Quantitative Inorganic Analysis*, 4th edn, Longman, London, 1978.
33. Craggs, A.; Moody, G. J.; Thomas, J. D. R. *J. Chem. Educ.* **1974**, *51*, 541.
34. Li, X. *Ph.D. Thesis*, University of Alberta, Edmonton, Canada, 1992, p62.
35. Castellan, G. W. *Physical Chemistry*, 3rd ed., 1983, 934-935.

36. Wickramasinghe, N. C. *Light Scattering Functions for Small Particles*, AdamHilger, London, 1973, Chapter 3.
37. Born, M.; Wolfe, E. *Principles of Optics*, 5th ed., Pergamon, Oxford, 1975, 633-664.
38. Zarrin, F.; Risfelt, J. A.; Dovichi, N. J. *Anal. Chem.* 1987, 59, 850-854.
39. Seiler, K.; Morf, W. E.; Rusterholz, B.; Simon, W. *Analytical Science*, 1989, 5, 557-561.
40. Li, X. *Ph.D. Thesis*, University of Alberta, Edmonton, Canada, 1992, Chapter 4.

## **Chapter 3**

### **Water Distribution In PVC Based Ion-Selective Membrane And Effects of Polymer Matrices and Membrane Additives**

#### **3.1 INTRODUCTION**

In Chapter 2 we developed a mathematical model to describe the transport process of water in poly(vinyl chloride) (PVC) based ion-selective electrode membranes. Some experimental results using a spatial imaging photometer and a conventional UV-Visible spectrometer were presented in order to evaluate the proposed theories. The optical studies [1-3] of water transport were focused primarily on membranes consisting of 33 wt.% PVC, and 66 wt.% bis-(2-ethylhexyl)adipate (DOA), which acts as a plasticizer (organic solvent) and provides the environment for the electrical reaction of the ion-selective membranes. DOA has a low dielectric constant of four [4] and this leads to a DOA/PVC membrane with a dielectric constant of 8 and a preference for monovalent over divalent cations [5]. For example, a PVC/DOA membrane has been used in the potassium-selective membrane electrode, which is a valuable tool

for physiologists because the transport of neural signals appears to involve movement of potassium ion across nerve membranes [6].

Another liquid ion-selective membrane electrode also of great value for physiological studies is that for calcium ion, which plays an important role in such processes as nerve conduction, bone formation, cardiac expansion and contraction, *etc.* [7]. A high dielectric constant plasticizer, *e.g.*, *o*-nitrophenyl octyl ether (NPOE) is generally used in calcium-selective membranes for the selection of calcium ion over monovalent cations [8]. NPOE has a dielectric constant of 21, and the plasticized PVC has a dielectric constant of 14. It is important to determine the transport behavior of water in PVC/NPOE membranes and whether there is a non-uniform distribution of water, so as to evaluate the generality of the theories we have proposed for PVC based ion-selective electrode membranes.

One important aspect in designing neutral carrier based ion-selective membranes is to add ions to ensure an electrically neutral membrane. Neutral-carrier-based membrane electrodes are found to have improved characteristics when lipophilic anions such as tetraphenylborate ( $\text{BPh}_4^-$ ) in the form of potassium or sodium salts are incorporated [9-15]. This lipophilic anion and others of the same general type (*e.g.*, tetrakis(4-chlorophenyl) borate) provide the necessary charged sites to reduce interferences by lipophilic anions in the sample (*via* co-ion exclusion). The presence of mobile cation-exchange sites in cation-selective membranes based on neutral-carriers has also proved to be beneficial in many other respects. The additives lower the electrical membrane resistance as well as the activation barrier for the cation-exchange reaction at the membrane-solution interface. They also reduce the response time and give rise to significant changes in the selectivity. Our previous optical work has shown that the nature and concentration of the additives strongly affect the behavior of water in ISE

membranes [1]. The natural extension is to examine the effects of these lipophilic anions on water transport and distribution in PVC based ISE membranes.

In this Chapter, a study of water distribution in PVC/NPOE ion-selective electrode membranes using a spatial imaging photometer is presented. As well, the effects of lipophilic salt  $\text{KBPh}_4$ , which is added to PVC/DOA membranes, are investigated.

## 3.2 EXPERIMENTAL

Ion-selective membranes were cast from solutions of distilled tetrahydrofuran (THF) according to the method described in Chapter 2. Two sets of ion-selective membrane samples were examined: (1) Calcium-sensitive membrane - about 66 wt.% NPOE (Fluka, Selectophore grade), and 33 wt.% PVC (Polysciences, chromatographic grade), and several other additives such as 1 wt.% (-) - (R,R) - N,N' - bis[11 - ethoxycarbonyl]undecyl] - N,N',4,5 - tetramethyl - 3,6-dioxaoctanediamide (ETH 1001, Fluka, Selectophore grade); 0.1 wt.%  $\text{KBPh}_4$  (prepared by precipitation in water from KCl and  $\text{NaBPh}_4$ , followed by vacuum drying [16]); 0 to 1 wt.% dehydrated  $\text{CoCl}_2 \cdot 6\text{H}_2\text{O}$  (Anachemia, purified) dried under vacuum at 60 °C for 16 hours (99.9% by ethylenediaminetetraacetic acid titration [17]); (2) Potassium-sensitive membrane - about 66 wt.% DOA (Fluka Selectophore grade); 33 wt.% PVC; 1 wt.% Valinomycin (Aldrich); 0.15 wt.% dehydrated  $\text{CoCl}_2 \cdot 6\text{H}_2\text{O}$ ; 0 - 0.5 wt.%  $\text{KBPh}_4$ .

The membrane cells used with the spatial imaging photometer, the instrument design and the experimental procedures have been previously described in Chapter 2.



### 3.3 RESULTS AND DISCUSSIONS

#### 3.3-1 Water Transport and Distribution in PVC/NPOE Membranes

A spatial imaging photometer (SIP) has been used to determine the spatial distribution of water within the PVC/NPOE membranes during the process of water uptake. The initial rapid uptake process can be monitored by the bleaching of an added, water sensitive dye, dehydrated  $\text{CoCl}_2 \cdot 6\text{H}_2\text{O}$ , while the later stages of water uptake can be monitored directly by the increase in absorbance due to formation of light scattering centers (see Chapters 1 and 2).

Figure 3.1 shows experimental curves for the absorbance change due to the uptake of water in PVC/NPOE membrane containing 0.15 wt.%  $\text{CoCl}_2$  during the first 30 minutes. The water enters from the left side of the membrane and evaporates from the right side. Bleaching of the dye upon reaction with water leads to a decrease in absorbance which is visible in the membrane bulk. An increase in absorbance near the membrane edge has been identified as the growth of water droplets which act as light scattering centers [2, 18]. Those light scattering centers penetrate very slowly into the membrane, as has been observed in PVC/DOA membranes (see Chapter 1, Figure 1.4). The experimental data can be analyzed using either the *two-stage uptake* or *dual-sorption* models (see discussions in Chapter 2) at this stage of water uptake. The smooth lines in Figure 3.1 are fits to equation 1.15:

$$\Delta A_1(x, t) = \Delta A_{1, \max}(x, t) \left[ 1 - \text{erf} \frac{x}{2\sqrt{D_1 t}} \right] \quad (1.15)$$

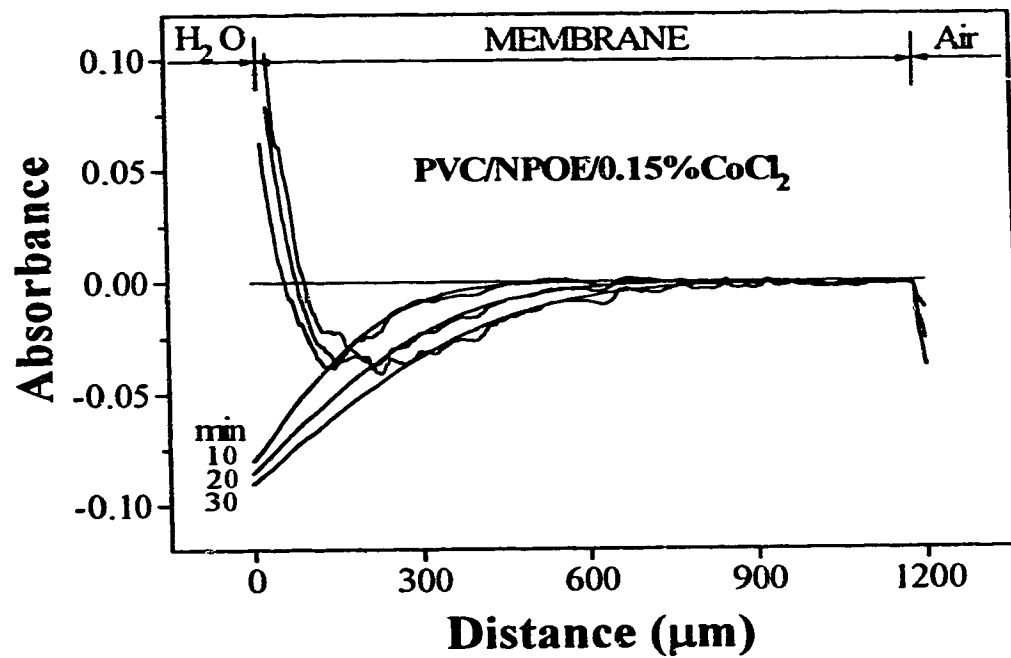


Figure 3.1 Absorbance profile inside PVC/NPOE membrane during first 30 minutes. Water enters from the left and evaporates at the right edge. Smooth lines are fits to equation 1.15 for dye bleaching.

in the bulk region of the membrane for the semi-finite initial-boundary conditions. The apparent diffusion coefficient of dissolved water,  $D_1$ , was then obtained. A series of diffusion experiments with membranes of various concentrations of  $\text{CoCl}_2$  have been carried out. The results are listed in Table 3.1. The standard deviations of the calculated parameters are also given in the table. These are usually less than 6%, indicating the modeling curves describe the experimental data reasonably well.

Figure 3.2 shows the diffusion coefficient  $D_1$  as a function of concentration of salt ( $C_1^s$ ) in the PVC/NPOE membranes. It can be seen that the rate of diffusion decreases about threefold as the doping with  $\text{CoCl}_2$  increases from 0.08 wt.% to 1.17 wt.%. This is in agreement with equation 2.16 of the dual-sorption model:

$$D_1 = \frac{D}{1 + C_1^s / s_0} \quad (2.16)$$

where  $D$  is the true diffusion coefficient of water molecule and  $s_0$  is the solubility of water in PVC/NPOE membrane. The smooth line in Figure 3.2 is a fit to equation 2.16 and the calculated values of  $D$  and  $s_0$  are  $(4.3 \pm 0.2) \times 10^{-7} \text{ cm}^2/\text{s}$  and  $(81.7 \pm 7.2) \text{ mM}$ , respectively. The results demonstrate that water has a larger solubility in PVC/NPOE membrane than in PVC/DOA membrane ( $s_0 = 50.8 \text{ mM}$ ), while the diffusion rate of water molecules is slower in PVC/NPOE membrane than in PVC/DOA membrane ( $D = 1.6 \times 10^{-6} \text{ cm}^2/\text{s}$ ). This may result from the higher polarities of NPOE and PVC/NPOE membrane. Differences in viscosity of the membrane matrix also play a role in determining the diffusion coefficient.

Figure 3.3 is an expanded plot of absorbance profiles inside a PVC/NPOE membrane containing 0.15 wt.%  $\text{CoCl}_2$ . It shows the apparent absorbance increase

**Table 3.1** The apparent diffusion coefficients of dissolved water,  $D_1$ , as a function of  $\text{CoCl}_2$  concentration in the early stages of water uptake in PVC/NPOE membranes.

$\text{CoCl}_2$ (wt.%)	$D_1^*$ ( $10^{-7} \text{ cm}^2/\text{s}$ )	$\sigma_{D_1}$ ( $10^{-8}$ )	$\sigma_{D_1} / D_1$ (%)
0.08	3.12	1.55	5.0
0.15	2.90	0.93	3.2
0.33	2.05	0.12	5.9
0.50	1.61	0.31	1.9
0.67	1.22	0.37	3.1

\* Values were calculated by fitting the SIP data with equation 1.15.

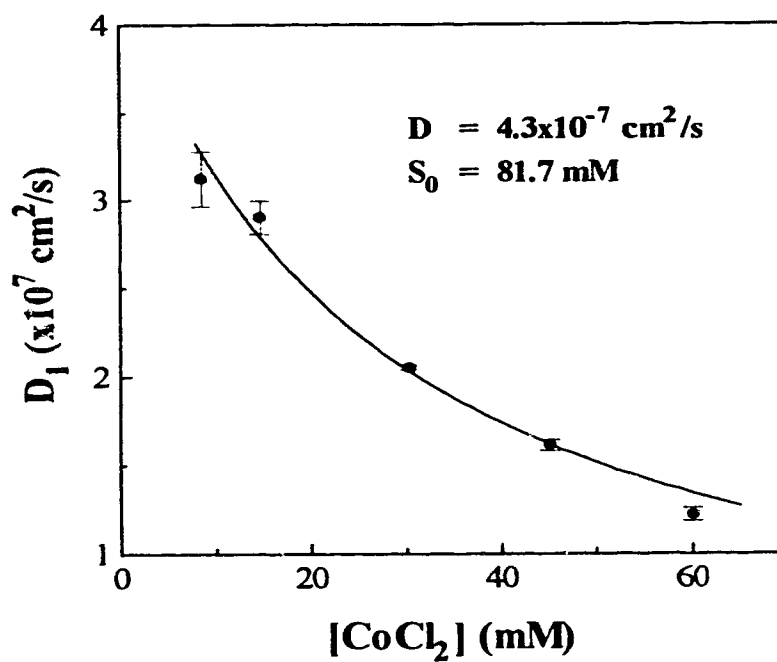


Figure 3.2 Diffusion coefficient vs. concentration of  $\text{CoCl}_2$  (mM) in PVC/NPOE membranes for the early stage of water uptake (in the bulk region).

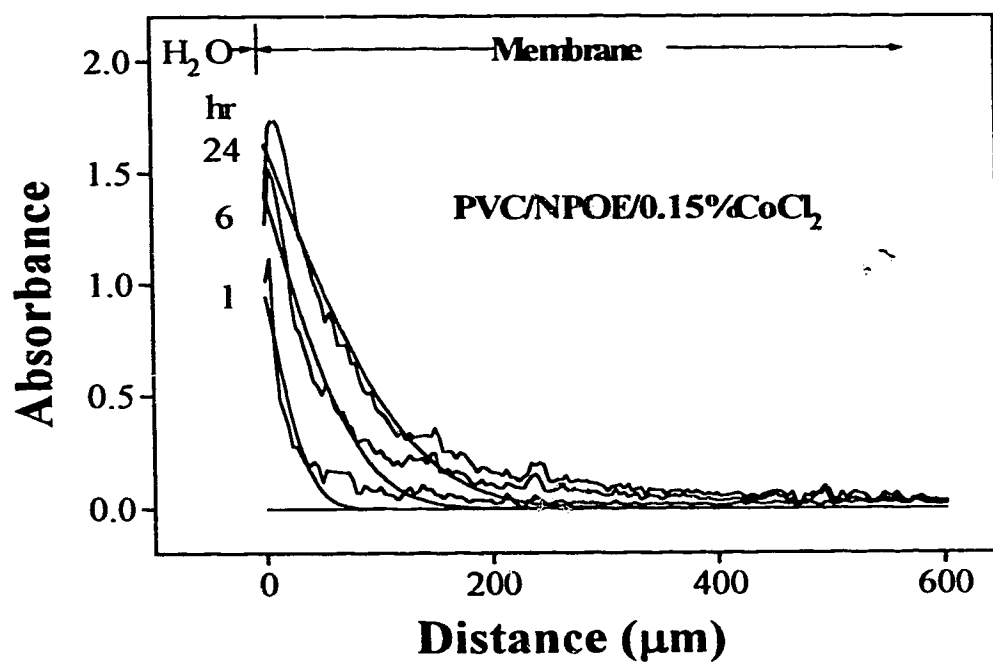


Figure 3.3 The expanded plot of the absorbance profiles in a PVC/NPOE membrane containing 0.15 wt.% CoCl<sub>2</sub> during the later stages of water uptake (water on left side only).

due to light scattering effects at the later stages of water uptake. The smooth lines are theoretical fits to the data at the near surface region according to the simplified diffusion model (equation 1.16):

$$\Delta A_2(x, t) = \Delta A_{2, \max}(x, t) \left[ 1 - \frac{1}{\operatorname{erf} \frac{x_k}{2\sqrt{D_2 t}}} \operatorname{erf} \frac{x}{2\sqrt{D_2 t}} \right] \quad (1.16)$$

Table 3.2 lists the calculated diffusion coefficients of light scattering centers,  $D_2$ , and the maximum absorbance (corresponding to the concentration of water at the water/membrane interface) 24 hours after the membrane is contacted with water. The plot of  $D_2$  as a function of the concentration of  $\text{CoCl}_2$  is shown in Figure 3.4, which demonstrates that  $D_2$  increases with increasing concentration of  $\text{CoCl}_2$  inside PVC/NPOE membranes. This is consistent with the dual-sorption model (equation 2.18a):

$$D_2 \cong \frac{s_0 C_i^s}{(C_2)^2} D \quad (2.18a)$$

where  $C_2$  denotes the average concentration of water in the membrane that resides in the droplets. As we discussed previously in Chapter 2, equation 1.16 is derived using assumptions of constant  $D_2$  and surface concentrations that are apparently poor approximations for the later stages of water uptake. This means that the magnitudes of  $D_2$  calculated here may not be accurate, but they should reflect the real trends in  $D_2$  with the concentration of  $\text{CoCl}_2$  inside those PVC/NPOE membranes.

Table 3.2 The apparent diffusion coefficients of light scattering centers ( $D_2$ ) and maximum absorbance of water at the water/membrane interface ( $\Delta A_{2,\max}$ ) as a function of  $\text{CoCl}_2$  concentration at 24 hours of water uptake in PVC/NPOE membranes.

$\text{CoCl}_2$ (wt.%)	$D_2^*$ ( $10^{-9} \text{ cm}^2/\text{s}$ )	$\Delta A_{2,\max}^*$
0.00	0.17	0.96
0.08	1.45	1.45
0.15	2.23	1.42
0.33	6.85	1.73
0.50	9.78	2.05
0.67	12.0	1.96

\* Values were calculated by fitting the SIP data with equation 1.16.



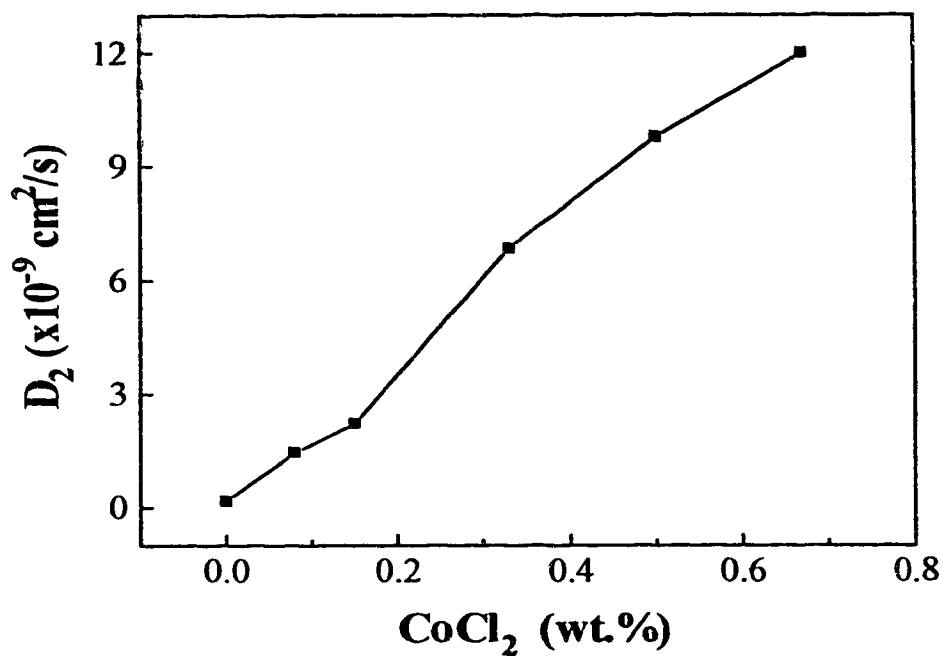


Figure 3.4 Apparent diffusion coefficient  $D_2$  vs. concentration of  $\text{CoCl}_2$  (wt.%) in the PVC/NPOE membrane for 24 hours of water uptake.

Figure 3.5 compares the observed absorbance profiles in PVC/NPOE membranes containing 0.00, 0.15, and 0.50 wt.%  $\text{CoCl}_2$  after 24 hour exposure to water. It can be seen that the membrane with a higher  $\text{CoCl}_2$  concentration absorbs more water than a membrane with less salt added, as would be predicted by the equilibrium water uptake model presented in Chapter 2. It is also noteworthy in Figure 3.5 that a nearly linear gradient of water is observed after 24 hours for the membrane with high salt content (curve a), as would be expected at steady state when one side of the membrane is exposed to air, while a surface layer is developed in the membranes with low salt content (curves b and c). This is consistent with the observations for PVC/DOA membranes [3]. The water-rich surface region can be seen more clearly in Figure 3.6, which shows the absorbance-distance curves of water in a PVC/NPOE membrane with no  $\text{CoCl}_2$  added after the membrane was in contact with water up to 24 hours. It can be seen that there is indeed a distinct, highly hydrated surface layer extending about  $60\text{ }\mu\text{m}$  into the membrane, whereas the bulk of the membrane remains relatively dry. The comparison of this hydrated surface layer with observations of similar regions in other PVC based membrane systems will be discussed in detail in Chapter 5.

### **3.3-2 Effects of $\text{KBPh}_4$ on Water Transport and Distribution in PVC/DOA Membranes**

The effect of adding the lipophilic salt  $\text{KBPh}_4$  to PVC/DOA membranes on the apparent diffusion rate of water has been investigated using the SIP method. Membranes containing 0.05 wt.%, 0.10 wt.%, and 0.50 wt.%  $\text{KBPh}_4$  have been examined. About 0.15 wt.% of  $\text{CoCl}_2$  was also added to each membrane, as the indicator dye for the determination of the diffusion rate of water in the initial stage

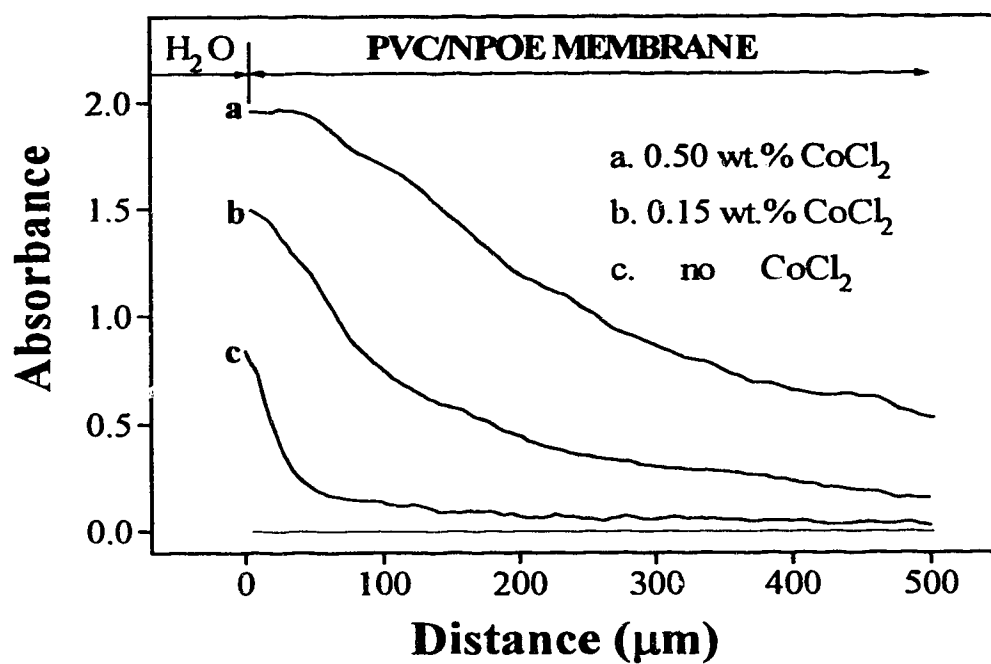


Figure 3.5 Absorbance profiles in membrane containing varying %  $\text{CoCl}_2$  after 24 hours exposure to water (water on left side only). (a) 0.50%  $\text{CoCl}_2$  ( $l = 1267\mu\text{m}$ ); (b) 0.15%  $\text{CoCl}_2$  ( $l = 1238\mu\text{m}$ ); (c) no  $\text{CoCl}_2$  ( $l = 1194\mu\text{m}$ ).

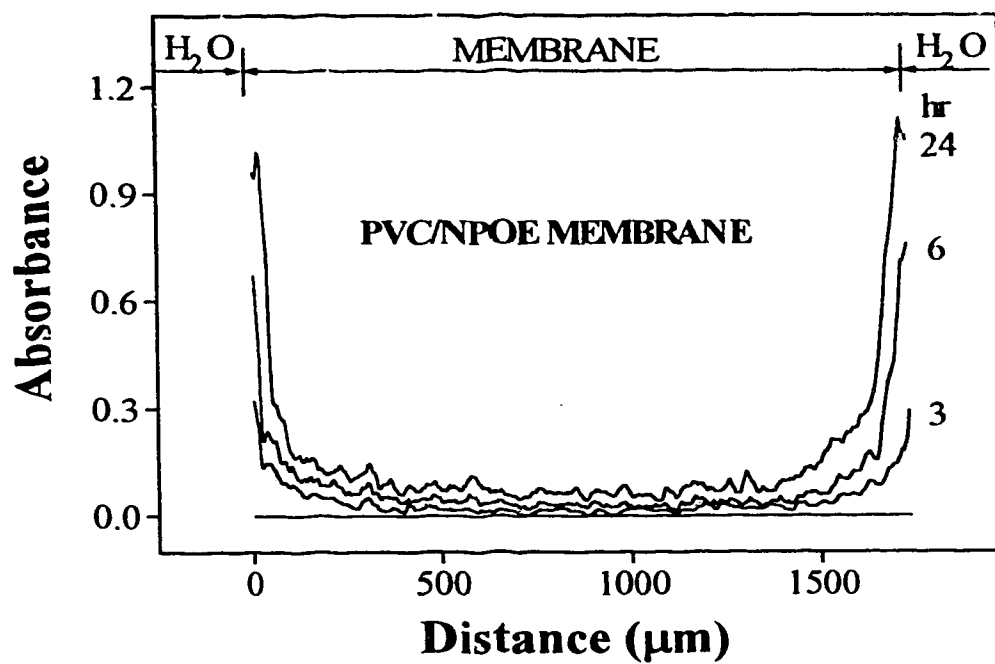


Figure 3.6 Absorbance profiles of a PVC/NPOE membrane (with no added dye) after the membrane was soaked in water for 24 hours.

of uptake,  $D_1$ . SIP data were analyzed using equation 1.15 to obtain  $D_1$  and equation 1.16 to obtain  $D_2$ , as described in the preceding section. Table 3.3 summarizes the calculated results for  $D_1$  and Figure 3.7 shows a plot of the effect of concentration of  $\text{KBPh}_4$  on  $D_1$ . It can be seen that there is a decrease of  $D_1$  with increasing concentration of  $\text{KBPh}_4$ . Qualitatively, this decrease is consistent with the dual-sorption model and observations for hydrophilic salt  $\text{CoCl}_2$ .

Table 3.4 gives the calculated apparent diffusion coefficient of water,  $D_2$ , after the first 24 hours of water uptake. Figure 3.8 shows the plot of  $D_2$  as a function of  $\text{KBPh}_4$  concentration in PVC/DOA membranes. In Figure 3.8, it can be seen that as the concentration of tetraphenylborate increases the apparent rate of diffusion of the light scattering centers increases. Although the precision of the measurements is poor (about  $\pm 18\%$ ), the general trend is demonstrated and is in agreement with the observations for hydrophilic salt  $\text{CoCl}_2$  in both PVC/DOA and PVC/NPOE membranes.

## 3.4 SUMMARY AND CONCLUSIONS

### 3.4-1 Summary

The behavior of water inside ion-selective membranes formulated from PVC plasticized with 66% (wt/wt) NPOE has been studied by using the SIP. The uptake and transport effects for water observed, and the dependence on impurity salt in the PVC/NPOE membrane are consistent with the previous observations with PVC/DOA membranes. A water-rich surface region develops in the PVC/NPOE membranes with very low salt content, while a uniform distribution of water across the membrane arises after long equilibration times with high salt

**Table 3.3** The apparent diffusion coefficients of water in the early stage of water uptake,  $D_1$ , as a function of  $\text{KBPh}_4$  concentration in PVC/DOA membranes.

$\text{KBPh}_4$ (wt.%)	$D_1^*$ ( $10^{-7} \text{ cm}^2/\text{s}$ )	$\sigma_{D_1}$ ( $10^{-8}$ )	$\sigma_{D_1} / D_1$ (%)
0.05	6.05	4.29	4.28
0.10	4.93	4.66	3.75
0.50	3.49	3.81	3.29

\* Values were calculated by fitting the SIP data with equation 1.15.

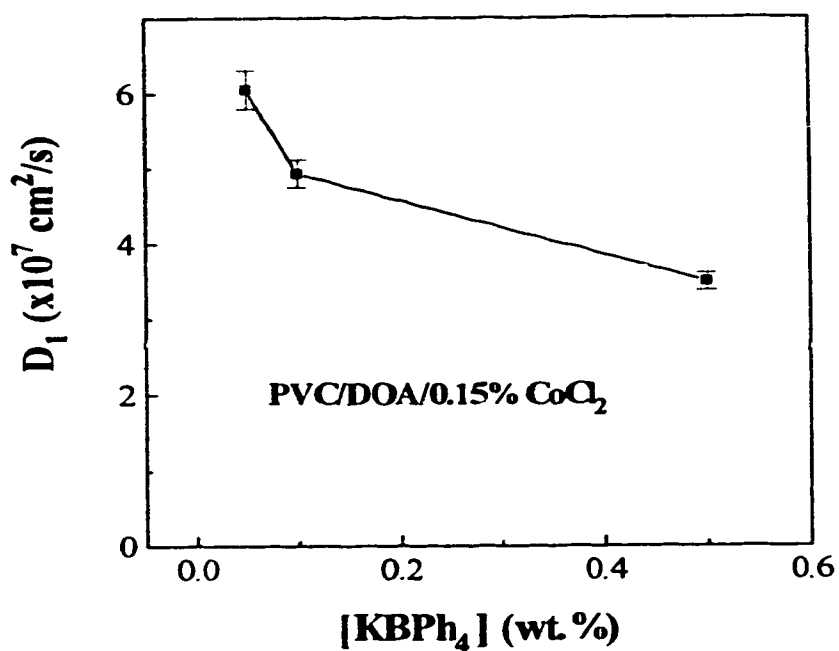


Figure 3.7 Plot of the effect of added  $\text{KBPh}_4$  concentration on the initial diffusion coefficient for water uptake in a PVC/DOA membrane with 0.15 wt.%  $\text{CoCl}_2$  added as an indicator dye.

**Table 3.4** The apparent diffusion coefficients of water at 24 hours of water uptake,  $D_2$ , as a function of  $\text{KBPh}_4$  concentration in PVC/DOA membranes.

$\text{KBPh}_4$ (wt.%)	$D_2^*$ ( $10^{-9} \text{ cm}^2/\text{s}$ )	$\sigma_{D_2}$ ( $10^{-8}$ )	$\sigma_{D_2} / D_2$ (%)
0.05	2.24	0.40	17.8
0.10	2.82	0.35	12.4
0.50	3.96	0.60	15.2

\* Values were calculated by fitting the SIP data with equation 1.16.



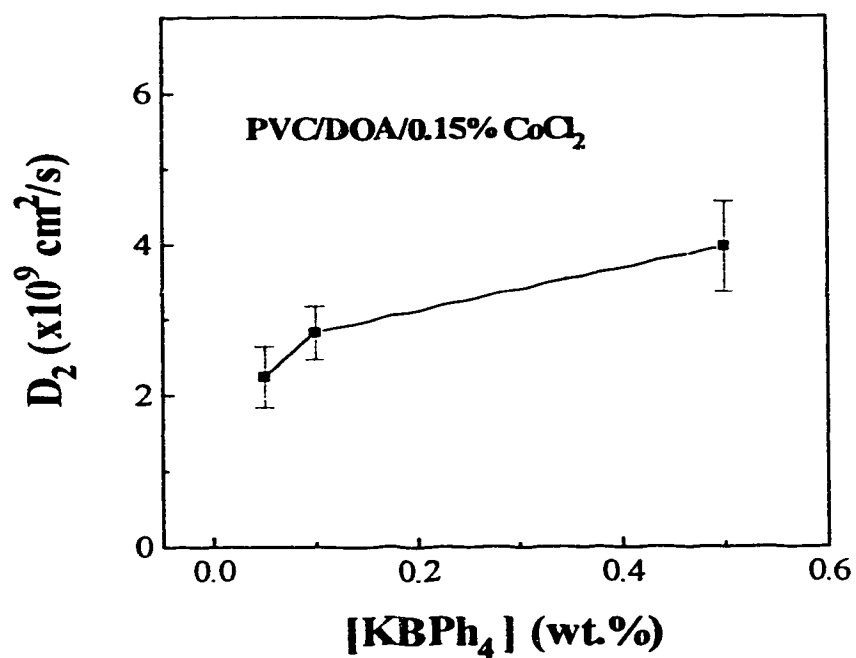


Figure 3.8 Apparent diffusion coefficient vs. concentration of  $\text{KBPh}_4$  (wt.%) in  $\text{PVC/DOA}$  membrane for the 24 hour water uptake associated with light scattering.

content, as reported for the PVC/DOA membranes. The initial rate of water uptake decreases as the concentration of hydrophilic salt  $\text{CoCl}_2$  increases while the apparent diffusion rate of light scattering centers at later stages of uptake increases; this is also observed in PVC/DOA membranes. The experimental data has been analyzed using dual-sorption model and the true diffusion coefficient and solubility of water molecules in PVC/NPOE membranes were founded as  $(4.3 \pm 0.2) \times 10^{-7} \text{ cm}^2/\text{s}$  and  $(81.7 \pm 7.2) \text{ mM}$ , respectively.

The effect of lipophilic salt,  $\text{KBPh}_4$ , on the behavior of water in PVC/DOA based ISE membranes have been studied. The results obtained demonstrate that  $\text{KBPh}_4$  affects the transport of water in the same way as hydrophilic salt although the latter has much stronger effects. Consequently, adding lipophilic salt to ISE membranes, one would expect to increase the water content in the membranes while decreasing the rate of water uptake.

### 3.4-2 Conclusions

The experimental evidence presented in this chapter provides further strong support to the dual-sorption and osmotic-uptake models we have proposed for PVC based ion-selective electrode membranes in Chapter two. The effect of the dye  $\text{CoCl}_2$  on the water distribution was similar for both PVC/DOA and PVC/NPOE membranes. This confirms that the osmotic pressure is the main driving force for the water uptake in the membrane, as DOA and NPOE are very different plasticizers. The effect of lipophilic salt,  $\text{KBPh}_4$ , on the rate of water uptake in a membrane is consistent with the dual-sorption model, as observed for the hydrophilic salt,  $\text{CoCl}_2$ . This demonstrates the generality of the theory.

### 3.5 REFERENCES

- [1] Li, X. *Transport Behavior of Water and Ions in Polyvinylchloride Based Ion-Selective Membranes* Ph. D. Thesis, University of Alberta, Edmonton, Canada, 1992. Ch. 4.
- [2] Chan, A. D. C.; Li, X.; Harrison, D. J. *Anal. Chem.* **1992**, *64*, 2512-2517.
- [3] Harrison, D. J.; Li, X.; Petrovic, S.; In *Biosensors and Chemical Sensors. Optimizing Performance Through Polymeric Materials*; Edelman, P.G., Wang, J., Eds.; ACS Symp. Ser. 487; Washington, DC, 1992, 292-300.
- [4] Verpoort, E. M. J. *Analysis of Permeability and Behavior of Dissociable Species in Ion-Selective Membranes*, Thesis, The University of Alberta, Edmonton, Canada, 1990.
- [5] Morf, W. E. *The Principles of Ion-selective Electrodes and of Membrane Transport* Elsevier Scientific Publishing Company: Amsterdam, Oxford and New York, 1981, p291.
- [6] Arnow, L. E. *Introduction to Physiological and Pathological Chemistry* The C. V. Mosby Company, Saint Louis, 1972.
- [7] Williams, R. J. P. *The Regulation of Intracellular Calcium* Cambridge University Press, England, 1976.
- [8] Armstrong, R.D.; Horvai, G. *Electrochim. Acta*, **1990**, *35*, 1-7.
- [9] Oehme, M.; Simon, W. *Anal. Chem. Acta* **1976**, *86*, 21.
- [10] Armstrong, R. D.; Covington, A. K.; Evans, G. P. *J. Electroanal. Chem.* **1983**, *159*, 33.
- [11] Ammann, D.; Pretsch, E.; Simon, W.; Lindner, E.; Bezegh, A.; Pungor, E. *Anal. Chim. Acta* **1985**, *171*, 119.

- [12] Pretsch, E.; Wegmann, D.; Ammann, D.; Bezegh, A.; Dinten, O.; Laubi, M. W.; Morf, W. E.; Oesch, U.; Sugahara, K.; Weiss, H.; Simon, W. *Recent Advances in the Theory and Application of Ion-Selective Electrodes in Physiology and Medicine* Springer-Verlag, Berlin, 1985.
- [13] Morf, W. E.; Simon, W. *Helv. Chim. Acta* **1986**, *69*, 1120
- [14] Lindner, E.; Graf, E.; Niegiesz, Z.; Toth, K.; Pungor, E.; Buck, R. P. *Anal. Chem.* **1988**, *60*, 295.
- [15] Eugster, R.; Gehrig, P. M.; Morf, W. E.; Spichiger, U. E.; Simon, W. *Anal. Chem.* **1991**, *63*, 2285.
- [16] Bassett, J.; Denney, R. C.; Jeffery, G. H.; Mendham, J. *Volgel's Textbook of Quantitative Inorganic Analysis* 4th edn, Longman, London, 1978.
- [17] Schwarzenbach, G.; Flaschka, H. *Complexometric Titrations*, Methuen, Londong, 1969, [translated by H. M. N. H. Irving].
- [18] Chan, A. D. C.; Harrison, D. J. *Anal. Chem.* **1993**, *65*, 32.

## **Chapter 4**

### **Numerical Analysis of Water Transport In Poly(vinyl chloride) Based Ion-Selective Electrode Membranes**

#### **4.1 INTRODUCTION**

In the preceding chapter we have used the dual-sorption theory [1-2] to describe the transport process of water in poly(vinyl chloride) (PVC) based ion-selective membranes. Two concurrent mechanisms of sorption were suggested: ordinary dissolution and "droplet-forming". The theory assumes that most of the absorbed water is in the form of droplets around the impurity particles, but that the diffusion is controlled by the water truly in solution in the membrane matrix. A mathematical model has been formulated in terms of Fick's second law. The governing diffusion equation in the membranes is given as

$$\frac{\partial C_1}{\partial t} + \frac{\partial C_2}{\partial t} = D \frac{\partial^2 C_1}{\partial x^2} \quad (2.11)$$

Only at low water content, when the concentration of immobilized water ( $C_2$ ) is directly proportional to the concentration of free moving water ( $C_1$ ) can equation (2.11) be solved analytically. A number of analytical solutions (equations 1.31-1.35, and 2.22) have been given, most of them in the form of infinite series. They are, for the most part, restricted to the simplest case of very low water concentration presented in membranes. Obviously, this assumption of a linear adsorption isotherm is not applicable at most stages of water uptake, due to the nonlinear relation between the two different states of water (equation 2.13) in the membranes. The usefulness of these solutions is further restricted to problems for which the boundary conditions can be satisfied [3]. This not only eliminates all problems with boundary conditions that can not be expressed in terms of equations, but also many for which the boundary conditions are too difficult to satisfy even though the equations for the boundary conditions are known. In such cases, approximation methods are the only means of solution, either analytical or numerical in character. Xizhong Li *et al.* have used analytical approximation methods that have provided extremely useful information concerning the character of water transport behavior in PVC based ion selective membranes [4].

Solution of the diffusion equations that more closely model experimental and practical situations is made possible by methods of numerical analysis [5]. A numerical treatment of the problem would be more satisfactory than using analytical approximations. The advent of the high speed digital computer has made numerical analysis a relatively easy task for the scientist and engineer [6]. Of the numerical approximation methods available for solving differential equations, those employing finite-differences are more frequently used and more universally applicable than any other. Numerical methods have been extensively used in the study of matter transport between plasticized PVC and various liquids [7-10].

In this chapter, we develop a finite-difference equation for simulation of the water transport process in PVC based, ion-selective electrode membranes. The algorithm was developed by the explicit-finite-difference method, which has the advantages of flexibility and programming simplicity compared to the implicit-finite-difference method. Data from measurements of the early stage of water uptake in membranes have been used for input into the calculations. The calculated results have been compared with experimental ones obtained using the Spatial Imaging Photometer (SIP) for PVC/DOA membranes containing the water sensitive dye  $\text{CoCl}_2$ . Some of the analyzed data was obtained by X. Li [4].

## **4.2 THEORETICAL**

The numerical technique most often used in solving diffusion equations is that of finite differences, although other methods such as finite elements have been used. The basis of numerical analysis by finite difference is to take the differential equations describing the system in question and approximate them as a series of finite difference equations which can be solved by simple arithmetic. In this section, we first provide a graphical description of the physical processes occurring during transport of water in membranes, which leads to a numerical expression of the problem, followed by a mathematical derivation of the explicit-finite-difference scheme.

### **4.2-1 Graphical Description of The System [3]**

The physical system considered here consists of a plane sheet of PVC based ion-selective electrode membrane immersed in water. The membrane thickness ( $l$ )

is small compared to its length or width to insure one-dimensional diffusion. Concurrent diffusion of plasticizer or any additives such as ion carriers, etc., is assumed negligible.

The diffusion process can be easier to view pictorially and is illustrated in Figure 4.1. We divide the sheet of membrane into layers each of thickness ( $h$ ) and denote by ( $C_{w,I}$ ,  $C_{w,II}$ ,  $C_{w,III}$ ) the total concentrations of water at three neighboring interfaces (I, II, III). The dotted lines at R and S denote the mid sections of the two adjacent layers. As discussed in Chapter 2, there are two states of water presented in the membrane: mobile water with concentration denoted by  $C_1$  and immobilized water with concentration denoted by  $C_2$ .

According to equation 2.8 (Fick's first law), the rate of transfer of water through a unit area is proportional to the gradient of concentration of mobile water ( $C_{1,II} - C_{1,I}$ ) and the constant of proportionality is the diffusion coefficient ( $D$ ) of a water molecule in the membrane. Thus, in a short time ( $\tau$ ), the amount of water that entered the shaded layer in Figure 4.1 through a unit area of the surface, R, is given approximately by:

$$q_R = -\frac{D\tau(C_{1,II} - C_{1,I})}{h} \quad (4.1)$$

In the same time, the amount flowing out through the face at S is approximately:

$$q_S = -\frac{D\tau(C_{1,III} - C_{1,II})}{h} \quad (4.2)$$



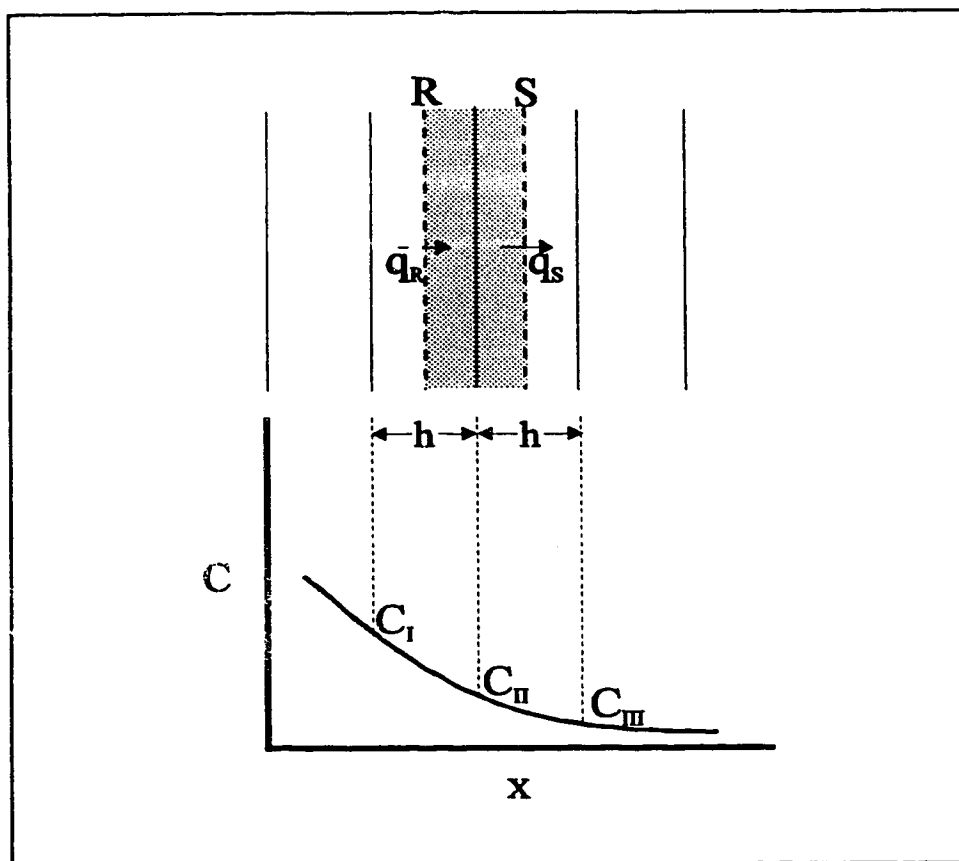


Figure 4.1 Schematic of one-dimensional diffusion process in membrane.

The net amount of water accumulated in the shaded element in time  $\tau$  is given by:

$$q_R - q_S = -\frac{D\tau}{h}(C_{1,II} - C_{1,I} - C_{1,III} + C_{1,II}) = \frac{D\tau}{h}(C_{1,I} - 2C_{1,II} + C_{1,III}) \quad (4.3)$$

If we now take  $C_{w,II}$  to represent the average concentration in the narrow shaded element, the net gain of water by the element can be written approximately as:

$$(C'_{w,II} - C_{w,II}) \times h \quad (4.3a)$$

where  $C'_{w,II}$  is the concentration at the end of the interval  $\tau$ . Equating this with equation 4.3 we have:

$$C'_{w,II} - C_{w,II} = \frac{D\tau}{h^2}(C_{1,I} - 2C_{1,II} + C_{1,III}) \quad (4.4)$$

Rearrange equation 4.4:

$$C'_{w,II} = \frac{D\tau}{h^2}(C_{1,I} - 2C_{1,II} + C_{1,III}) + C_{w,II} \quad (4.5)$$

This relationship enables us to calculate by simple arithmetic the concentration of water at a point at time  $(t + \tau)$  if we know the concentration  $C_{w,I}$ ,  $C_{w,II}$ ,  $C_{w,III}$  at the time  $t$ . We can apply equation 4.5 successively at each point of

the sheet and advance the equation in time steps  $\tau$ . A computer can carry out this repetitive arithmetic easily and quickly.

So far, we have used no calculus nor have we directly referred to the partial differential equation (equation 2.11) that expresses Fick's second law. Since we have made certain approximations, it is very important to know how accurate the numerical calculation is. A more mathematical derivation of equation 4.5 will be given in the following section.

#### 4.2-2 Finite-Difference Solution: Explicit Method [3,10]

We recall the diffusion equation 2.11 and divide the membrane sheet into equal finite slices of thickness ( $h$ ) in the direction of water transport by concentration-time reference planes ( $i, n$ ) as in Figure 4.2. The process of transport can then be represented in 3-dimensional space with axes of time expressed in units of ( $n\tau$ ), where  $n$  is an integer, position in units of ( $ih$ ), where  $i$  is an integer, and concentration. Figure 4.2 shows one of the time versus distance planes in this 3-D space, where concentrations at any point on the plane are represented by symbols describing their coordinates relative to the time-distance plane, e.g.,  $C_i^n$  is the concentration at time ( $n\tau$ ) and position ( $ih$ ).

Finite increments of space ( $h$ ) and time ( $\tau$ ) are considered in numerical analysis. The time at which an event occurs, as well as the place, are defined as follows

$$\text{time} \quad t = n \cdot \tau$$

$$\text{place} \quad x = i \cdot h$$

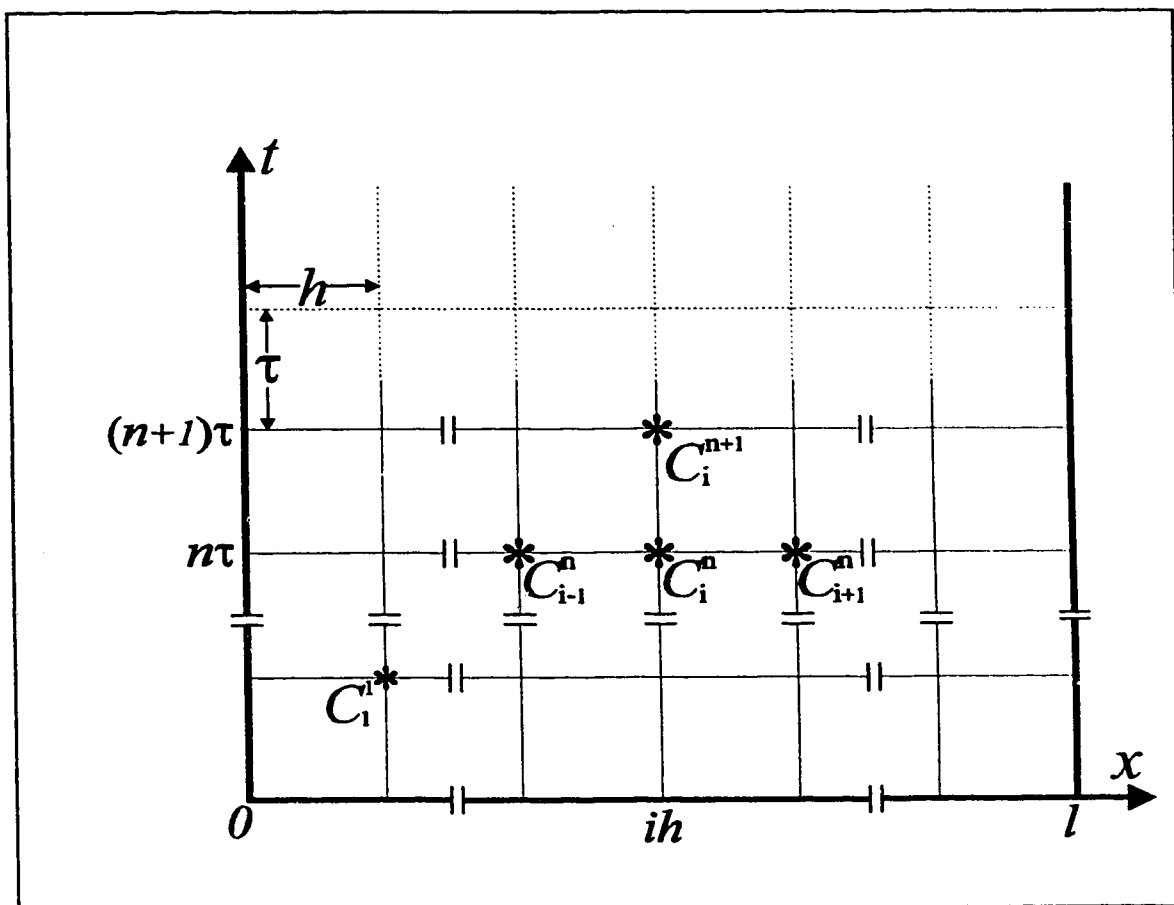


Figure 4.2 Space-time diagram for numerical analysis. Concentration of diffusing substance for various places and times.

At time  $t$ , defined by integer  $n$ , the concentrations for each location in the membrane are indexed as follows:  $C_{i-1}^n$ ,  $C_i^n$ ,  $C_{i+1}^n$ . After the elapse of time  $\tau$ , the time is  $(n + 1)\tau$ . The concentrations for each place in the membrane are indexed in the same way:  $C_{i-1}^{n+1}$ ,  $C_i^{n+1}$ ,  $C_{i+1}^{n+1}$ .

By using Taylor's series with  $t$  as a variable and position constant, it is possible to obtain the concentration at the following time and at position  $n$ :

$$C_i^{n+1} = C_i^n + \left( \frac{\partial C}{\partial t} \right)_{n,i} dt + \frac{1}{2} \left( \frac{\partial^2 C}{\partial t^2} \right)_{n,i} (dt)^2 + \dots \quad (4.6)$$

The following equation can be written by rearranging equation 4.6:

$$\left( \frac{\partial C}{\partial t} \right)_{n,i} = \frac{C_i^{n+1} - C_i^n}{dt} + 0(dt) = \frac{C_i^{n+1} - C_i^n}{\tau} + 0 \times \tau \quad (4.7)$$

where  $(0 \times \tau)$  signifies that the leading term to have been neglected is of the order of  $\tau$  when we have divided both sides of equation 4.6 by  $dt$  to get equation 4.7.

Similarly, by applying Taylor's series with position as a variable and keeping time constant, the following is obtained:

$$C_{i+1}^n = C_i^n + \left( \frac{\partial C}{\partial x} \right)_{n,i} dx + \frac{1}{2} \left( \frac{\partial^2 C}{\partial x^2} \right)_{n,i} (dx)^2 + \dots \quad (4.8)$$

$$C_{i-1}^n = C_i^n - \left( \frac{\partial C}{\partial x} \right)_{n,i} dx + \frac{1}{2} \left( \frac{\partial^2 C}{\partial x^2} \right)_{n,i} (dx)^2 + \dots \quad (4.9)$$

On adding we find:

$$\left( \frac{\partial^2 C}{\partial x^2} \right)_{n,i} = \frac{C_{i+1}^n - 2C_i^n + C_{i-1}^n}{(dx)^2} + 0(dx)^2 = \frac{C_{i+1}^n - 2C_i^n + C_{i-1}^n}{h^2} + 0 \times h^2 \quad (4.10)$$

By substituting equations 4.7 and 4.10 in equation 2.11 and neglecting the error terms  $0 \times h^2$  we find after slight re-arrangement:

$$(C_{1,i}^{n+1} - C_{1,i}^n) + (C_{2,i}^{n+1} - C_{2,i}^n) = \frac{D\tau}{h^2} (C_{1,i+1}^n - 2C_{1,i}^n + C_{1,i-1}^n) \quad (4.11)$$

where subscripts 1 and 2 denote free water and immobilized water respectively.

Equation 4.11 can be seen to be the finite difference equivalent of equation 2.11. By rearranging equation 4.11, the basic equation is found:

$$C_{1,i}^{n+1} + C_{2,i}^{n+1} = \frac{D\tau}{h^2} (C_{1,i+1}^n - 2C_{1,i}^n + C_{1,i-1}^n) + C_{1,i}^n + C_{2,i}^n \quad (4.12)$$

Substituting equation 2.13 in equation 4.12 and replacing  $s_0$  and  $C_i^*$  with  $a$  and  $b$  respectively, gives:

$$\frac{aC_{2,i}^{n+1}}{C_{2,i}^{n+1} + b} + C_{2,i}^{n+1} = \phi_i^n \quad (4.13)$$

where  $\phi_i^n$  is simply used to represent the right hand side of equation 4.12 with the substitution of equation 2.13 as:

$$\phi_i^n = \frac{D\tau}{h^2} \left[ \frac{aC_{2,i+1}^n}{C_{2,i+1}^n + b} - \frac{2aC_{2,i}^n}{C_{2,i}^n + b} + \frac{aC_{2,i-1}^n}{C_{2,i-1}^n + b} \right] + \frac{aC_{2,i}^n}{C_{2,i}^n + b} + C_{2,i}^n \quad (4.14)$$

Rearranging equation 4.13:

$$(C_{2,i}^{n+1})^2 + (a + b - \phi_i^n)C_{2,i}^{n+1} - b\phi_i^n = 0 \quad (4.15)$$

Equation 4.15 has two solutions given by:

$$C_{2,i}^{n+1} = \frac{-(a + b - \phi_i^n) \pm \sqrt{(a + b - \phi_i^n)^2 + 4b\phi_i^n}}{2} \quad (4.16)$$

Since  $b\phi_i^n > 0$ , we have:

$$\sqrt{(a + b - \phi_i^n)^2 + 4b\phi_i^n} > (a + b - \phi_i^n) \quad (4.16a)$$

Therefore, we can take the root:

$$C_{2,i}^{n+1} = \frac{-(a + b - \phi_i^n) + \sqrt{(a + b - \phi_i^n)^2 + 4b\phi_i^n}}{2} \quad (4.16b)$$

as the solution we are looking for.

The values of the coefficients  $a$  and  $b$  depend on the membrane considered. The initial value of  $\phi_i^n$  is determined from the initial-boundary conditions. Then,  $C_{2,i}^{n+1}$  can be calculated from equation 4.16b and the profiles of concentration of water with time can be obtained. The wt.% of water absorbed by the membrane at time  $t$  can be easily obtained by integrating  $C_w$  over the entire concentration profile with the distance ( $x$ ) as the integration variable.

$$\text{Water (wt\%)} = \frac{\rho_{H_2O} \times \int_0^l C_w dx}{\rho_{\text{membrane}} \times l} \quad (4.17)$$

where  $\rho_{\text{membrane}}$  is the density of the membrane.

The finite-difference method presented above is approximate in the sense that derivatives *at a point* are approximated by difference quotients *over a small interval*, i.e.,  $\partial C / \partial x$  is replaced by  $\delta C / \delta x$  where  $\delta x$  is small, but the solutions are not approximate in the sense of being crude estimates. The experimental data are invariably subject to errors of measurement, besides which, all arithmetical work is limited to a finite number of significant figures and contains rounding errors, so even analytical solutions provide only approximate numerical answers. Finite-difference methods generally give solutions that are either as accurate as the data warrant or as accurate as is necessary for the technical purposes for which the solutions are required. In both cases a finite-difference solution is as satisfactory as one calculated from an analytical formula, providing the model employed is satisfactory.



## **4.3 EXPERIMENTAL**

### **4.3-1 Sample Preparation and Measurements**

Membranes were prepared from poly(vinyl chloride) (PVC) (Polysciences, chromatographic grade), bis(2-ethylhexyl) adipate (DOA) (Fluka),  $\text{CoCl}_2$ , as described in Chapter 2. Reagents were used as received, and were either reagent or Selectophore grade. The membrane cells used with the spatial imaging photometer, and the instrument design and use have been previously described in Chapter 1 and Chapter 2.

The equilibrium water concentration,  $C_{eq}$ , in the membrane was measured by the desorption method described elsewhere [11]. The model membrane consisted of 33 wt% PVC and 66 wt% DOA and contained 0.15 wt% of  $\text{CoCl}_2$ . The dimension of the dried membrane was approximately 3.45 cm in diameter (as measured with vernier calipers) and 0.83 mm thick (as measured with a Mitutoyo micrometer). For the desorption measurement, this membrane was soaked in pure water for 6 - 14 days to ensure the equilibrium absorption of water. Surplus water was blotted off the membrane surface with a tissue just prior to the desorption measurement. The weighing of the sample was performed with a Mettler H80 electronic analytical balance.

### **4.3-2 Calculation of Profiles of Concentration of Water Transferred**

The profiles of concentration of water developed through the membranes were obtained by using the above-described method with finite differences and experimental data from our previous work. This explicit method allows the use of

a microcomputer. Digital simulations were carried out on an IBM compatible personal computer (486DX). FORTRAN programs based on the algorithm of the previous section were written using professional FORTRAN (see Appendix).

Figure 4.3 shows scheme I for numerical computing, which does not consider the surface region phenomena. The initial values of the concentration of immobilized water (usually zeros) are first assigned as  $C_{2,i}^0$ , and then  $C_{2,i}^1$  is calculated according to equation (4.16b). At each iteration, values of  $C_2$  at two boundaries ( $x = 0, l$ ) are always given by the boundary conditions instead of equation 4.16b.

## 4.4 RESULTS AND DISCUSSIONS

### 4.4-1 Stability of Method

In deriving the finite-difference equation 4.11 we have neglected higher-order terms in the Taylor series. These will constitute a truncation error in the numerical calculation. We have assumed that this explicit finite-difference method provides a reasonable approximation to the true solution of the partial differential equation 2.11. The investigation of this assumption is very important in determining the reliability of the numerical results.

The explicit finite difference method is an unstable method, which can be used only if the following stability criterion is satisfied [5,12-13]:

$$\frac{D\tau}{h^2} \leq 0.5 \quad (4.18)$$

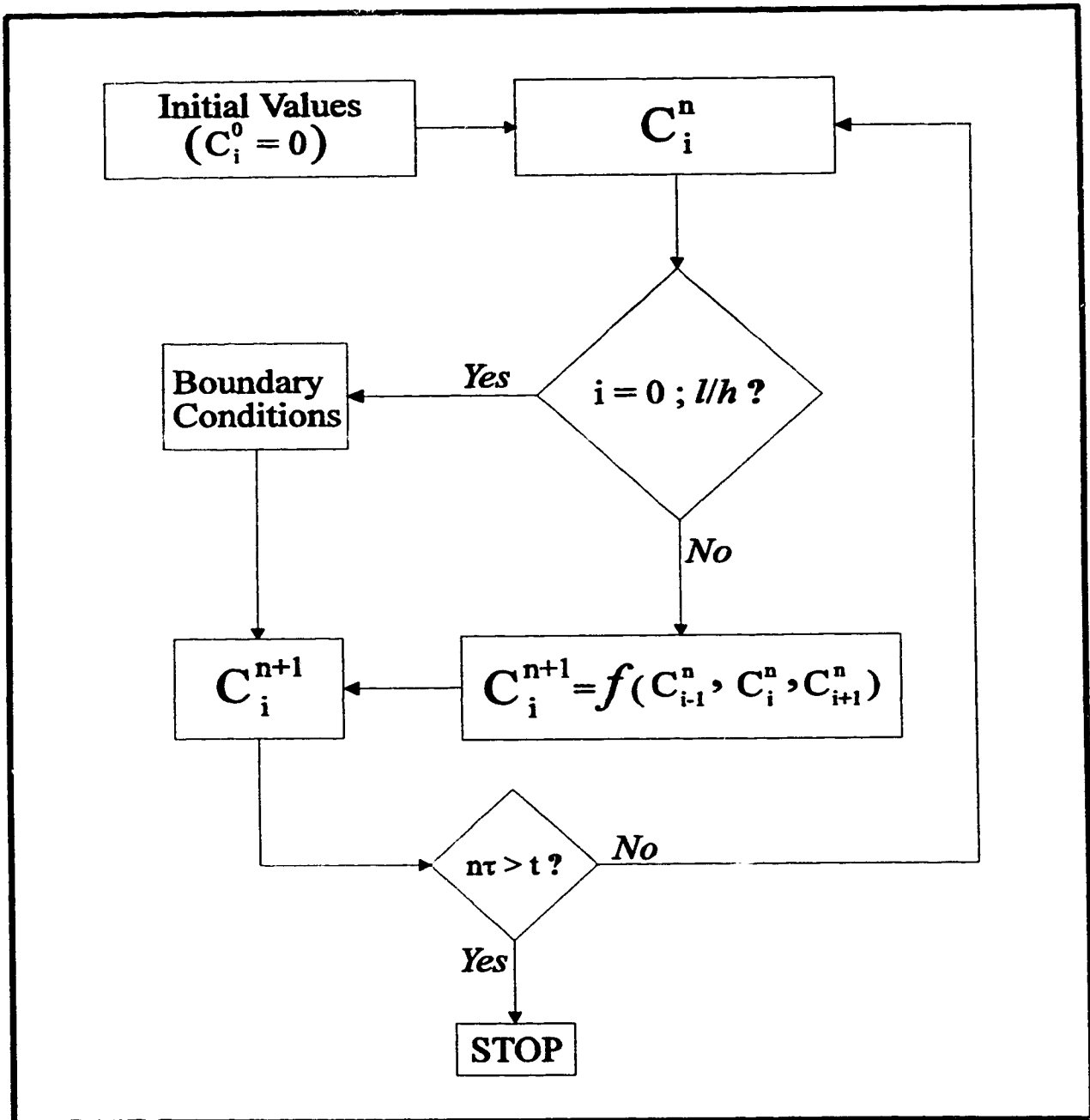


Figure 4.3 Scheme I of computation

or

$$\tau \leq \frac{0.5 \times \left(\frac{l}{n}\right)^2}{D} \quad (4.18a)$$

where:  $l$  is the thickness of membrane in the direction of transport.  
 $n$  is the number of slices the membrane is divided into.

The physical interpretation of the restriction of equation (4.18a) is that the maximum allowed time step ( $\tau_{\max}$ ) is, up to a numerical factor, the diffusion time across a cell of width  $h$ . More generally, the diffusion time  $t$  across a spatial scale of size  $l$  is of the order:

$$t \sim \frac{l^2}{D} \quad (4.19)$$

If we are limited to timesteps satisfying equation 4.18a, we will need to evolve through about  $(l/h)^2$  steps before things start to happen on the scale of interest. This number of steps is usually prohibitive if  $l \gg h$ . For a PVC/DOA membrane, the diffusion coefficient of water molecules has been estimated as  $1.5 \times 10^{-6}$  cm<sup>2</sup>/s (see Chapter 2) while the thickness of the membranes studied is usually about 1000  $\mu$ m. If 100 calculation points are chosen, the corresponding maximum allowed computing timestep  $\tau$  is about 0.33 second. With the computing scheme we have described above, most simulations in compliance with the stability criterion of equation 4.18a can be carried out in a few minutes.

The numerical analysis program may be checked for its compatibility by comparing its output against an analytical solution under the approximate

conditions. At short times, before the water concentration is too high, water transport will be describe by *Case I*, and a solution in the form of equation 2.22:

$$C_1(x,t) = C_1^s \left\{ 1 - \frac{4}{\pi} \sum_{n=1}^{\infty} \frac{1}{(2n-1)} \exp \left[ -\frac{D_1(2n-1)^2 \pi^2 t}{l^2} \right] \sin \frac{(2n-1)\pi x}{l} \right\} \quad (2.22)$$

will be accurate. Consequently, the numerical solution should give results that match the analytical solution at short enough times. Such a comparison is made in Figure 4.4 after 600 seconds has elapsed. The diffusion coefficient used for the analytical solution,  $D_1$ , was  $2.2 \times 10^{-7}$  cm<sup>2</sup>/s, which is equal to the effective diffusion coefficient calculated from equation 2.16:

$$D_1 = \frac{D}{1 + C_1^s / s_0} \quad (2.16)$$

for the true diffusion coefficient,  $D$ , salt concentration and water solubility used in the numerical calculation (see figure caption). A FORTRAN program has been written to evaluate equation 2.22 (see Appendix B) and a constant water concentration of water at the boundaries,  $C_1^s$ , was assumed. Both numerical and analytical results in Figure 4.4 were normalized to the maximum concentration at the boundaries for a convenient comparison. It can be seen that agreement is excellent. The result indicates that the computing scheme and program are operating correctly.

As a further check of the convergence of the difference scheme we have also compared the numerical results (Scheme I) of different sizes of grid as shown in Figure 4.5. Water concentrations at the membrane/water interface  $C_2^s$  were

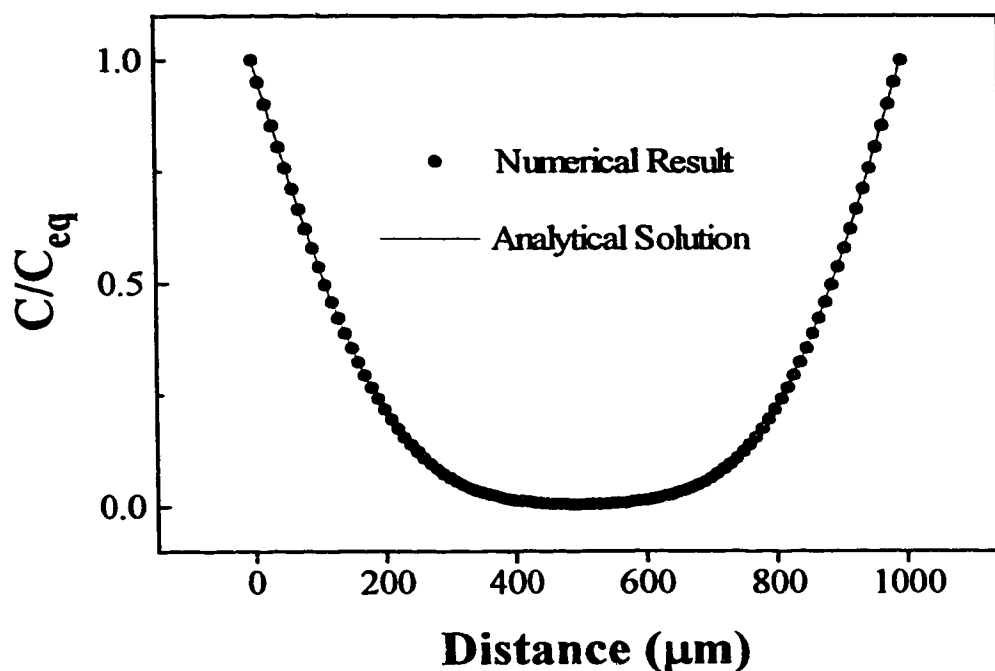


Figure 4.4 Comparison of numerical and analytical results ( $l = 1000 \mu\text{m}$ ,  $t = 600 \text{ sec.}$ )

- numerical simulation was calculated using the Scheme I and shown by the dots. ( $D = 2.2 \times 10^{-7} \text{ cm}^2/\text{s}$ ;  $a = s_0 = 51 \text{ mM}$ ;  $b = C_1^s = 0 \text{ mM}$  )
- analytical solution was calculated using equation (2.16) and shown by the curves. ( $D_1 = 2.2 \times 10^{-7} \text{ cm}^2/\text{s}$ )

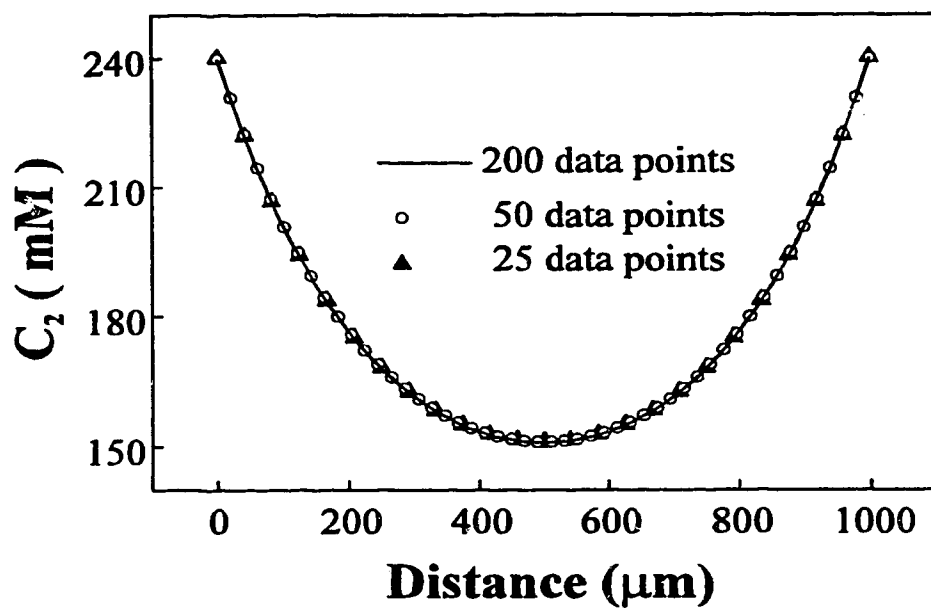


Figure 4.5 Numerical simulations with different sizes of the grid. ( $l = 1000$   $\mu\text{m}$ ;  $t = 24$  hour;  $D = 1.4 \times 10^{-6}$   $\text{cm}^2/\text{s}$ ;  $a = 51$  mM;  $b = 274$  mM,  $C_2^s = 240$  mM)

taken as constant. The plot shows that all three values of  $h$  (determined by the data points) give virtually identical results, and the relative errors are less than 0.48%. It can be expected that the smaller the grid the more accurate the result, but at the same time the computation time will be increased substantially. With the accuracy of simulations thus established we can confidently carry out the numerical simulation of the transport process of water in PVC based ion-selective membranes.

#### 4.4-2 Parameters for The Computations

The numerical solution scheme requires the input of several parameters that are characteristic of a particular membrane system. These values are

- $D$ : the true diffusion coefficient of water molecules in the membrane phase.
- $s_0$ : the solubility of water in the membrane phase.
- $C_i^s$ : the salt concentration in the membrane.
- $C_{eq}$ : the saturated concentration of water in the membrane.

The values of  $D$  and  $s_0$  calculated for PVC/DOA membranes have been given as  $1.5 \times 10^{-6}$  cm<sup>2</sup>/s and 50.8 mM, respectively, in Chapter 2.  $C_{eq}$  may be obtained from the desorption experiment described by A. D. C. Chan *et al.* [11]. Using this method, we have measured the amount of water sorbed by membranes containing 0.15 wt% CoCl<sub>2</sub> to be approximately 5.4 wt%. Desorption data are summarized in Table 4.1 for two measurements on one membrane sample. Since the membrane was very thin (about 0.83 mm) and had been soaked in pure water



Table 4.1 Summary of water desorption data from a PVC/DOA/0.15%CoCl<sub>2</sub> membrane.

Parameters	Test #1	Test #2
Thickness	0.84 mm	0.82 mm
Diameter	~ 3.45 cm	~ 3.45 cm
Soaking time	6 days	14 days
Wet weight	0.9781 g	0.9691 g
Dry Weight	0.9306 g	0.9177 g
Water Absorbed	0.0475 g (5.1%)	0.0514 g (5.6%)

for about 10 days, an equilibrium water uptake and a uniform distribution of water in the membrane may be assumed. Using the density of PVC/DOA membrane of  $1.08 \text{ g/cm}^3$  obtained by Chan [14], the equilibrium average water concentration was calculated as 3.04 M.

In addition to these four parameters, the boundary conditions are also of importance in the digital simulations. Xizhong Li *et al.* have shown that the water concentration at the surface changes with time [15] and it can be modeled by an exponential equation with an additional parameter,  $\beta$ , introduced:

$$C^s = C_{eq}^s [1 - \exp(-\beta t)] \quad (4.20)$$

where  $C_{eq}^s$  is the equilibrium concentration at the surface.

If we assume no surface region was formed (which is the case for membranes containing substantial amounts of  $\text{CoCl}_2$ ),  $C_{eq}^s$  may be approximately represented by  $C_{eq}$  in a membrane of uniform distribution of water. In order to generate a formula which can be used in the simulation scheme, the absorbance changes at the membrane surface ( $\Delta A_{surf}$ ) were first summarized, and then the ratios of  $C^s/C_{eq}^s$  were calculated by assuming the square root relationship of equation 2.31 and plotted against time. The curves were then fitted with equation (4.20) to obtain the value of  $\beta$ . Table 4.2 and Figure 4.6 shows an example for a PVC/DOA membrane with 0.15 wt%  $\text{CoCl}_2$  added. The value of  $\beta$  was estimated as 0.27.

With those parameters available, the profiles of water concentration in a membrane can be simulated for various boundary conditions. In the next section, we present some results for membranes containing  $\text{CoCl}_2$ . The numerical

Table 4.2 Changes of  $C^s$  in the PVC/DOA/0.15%CoCl<sub>2</sub> membranes as a function of time.

Time	$\Delta A_{\text{surf}}^*$	$\Delta A_{\text{surf}}/\Delta A_{\text{eq}}^{**}$	$C^s/C_{\text{eq}}^s$ <sup>+</sup>
1 h	0.296	0.207	0.455
3 h	0.641	0.448	0.669
6 h	1.03	0.721	0.849
12 h	1.23	0.860	0.927
24 h	1.33	0.929	0.963
48 h	1.42	0.992	0.996

\*  $\Delta A_{\text{surf}}$  is the absorbance change at the surface.

\*\* The value of  $\Delta A_{\text{eq}}$  was taken as the  $\Delta A_{\text{surf}}$  at 120 hours soaking.

+  $C^s/C_{\text{eq}}^s = \sqrt{\Delta A_{\text{surf}} / \Delta A_{\text{eq}}}$ .

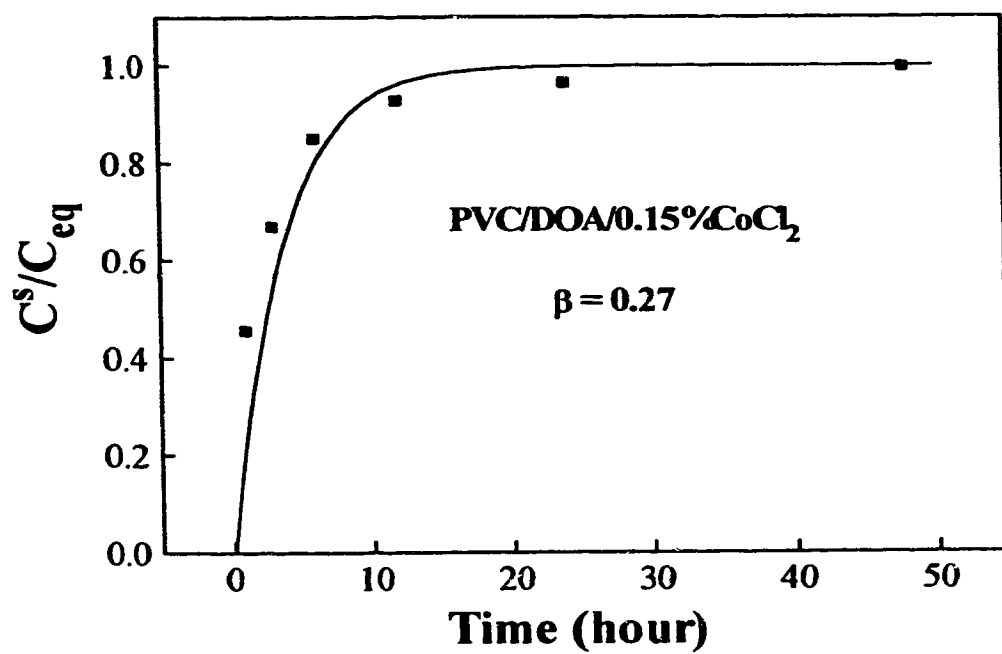


Figure 4.6. The plot of  $C^s/C_{eq}^s$  as a function of time

simulation for blank PVC/DOA membranes is more complicated due to the presence of the water-rich surface region and will be discussed in Chapter 6.

#### 4.4-3 Results of Numerical Simulations

Figure 4.7 shows the typical calculated concentration profiles of water developed across a PVC/DOA membrane doped with 0.15% wt  $\text{CoCl}_2$  after the membrane was contacted with water from both sides. Computing scheme I was used, and the surface region was ignored in the simulation. Parameters used in the calculation are listed in Table 4.3. These parameters were obtained from independent experiments as outlined in the previous section. Figure 4.8 shows the concentration profiles of water calculated using the simple Fick's law diffusion model with the same diffusive parameters as in Figure 4.7. The curves in Figures 4.7 and 4.8 are expressed as normalized concentration,  $C/C_{eq}$ , vs. distance  $x$  for different times.

Comparison of Figures 4.7 and 4.8 shows very different concentration profiles as a function of time, even though both figures used the same value of diffusion coefficient ( $1.5 \times 10^{-6} \text{cm}^2/\text{s}$ ). Figure 4.8 shows the profiles expected for a simple Fick's law diffusion process (equation 1.13), whereas Figure 4.7 uses the case 2 model for transport with the formation of water droplets (equations 2.11 and 2.13), and a changing surface concentration with time (equation 4.20). The two sets of data are quite different, and it is clear that different values of diffusion coefficient would be obtained at each time if the curves in Figure 4.7 were fit according to a simple Fick's law expression. In fact the values of diffusion coefficient would decrease over the course of time in Figure 4.7, as was observed by X. Li using his model [4].

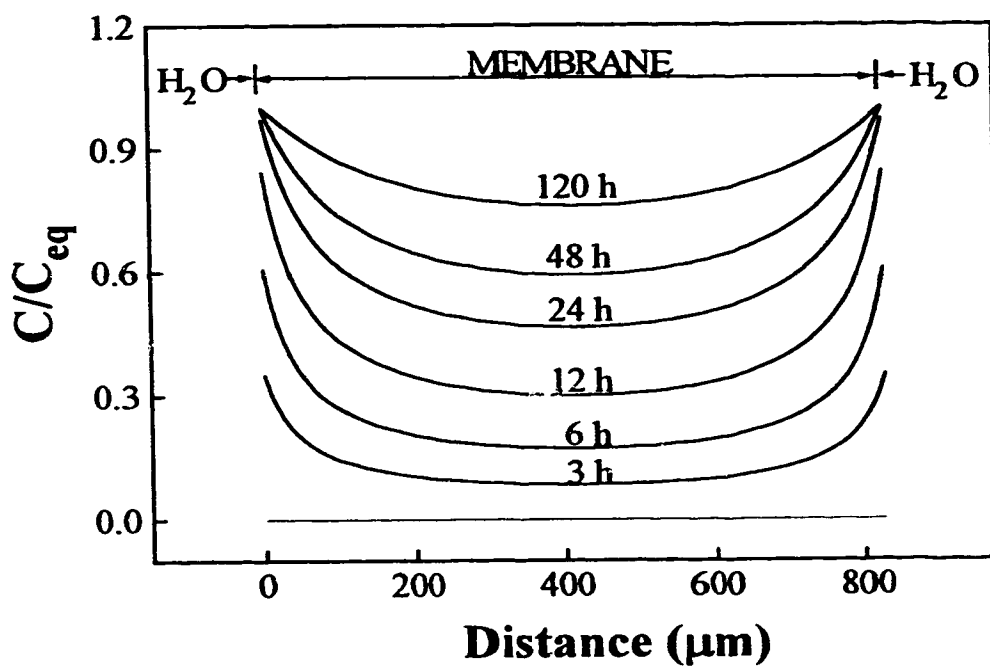


Figure 4.7 Profiles of concentration of water developed through the thickness of membrane sheet calculated at various times.

Table 4.3 Parameters of Numerical Calculation ( Scheme I )

$D = 1.5 \times 10^{-6} \text{ cm}^2/\text{s}$	
$\beta = 0.27$	$s_0 = 50.8 \text{ mM}$
$C_i^s = 45.8 \text{ mM}$	$C_2^{eq} = 2.99 \text{ M}^*$
$h = 8.27 \text{ } \mu\text{m}$	$\tau = 0.34 \text{ second}$

\*  $C_2^{eq}$  is the equilibrium concentration of water in droplets and given as  $(C_2^{eq} = C_{eq} - s_0)$ .

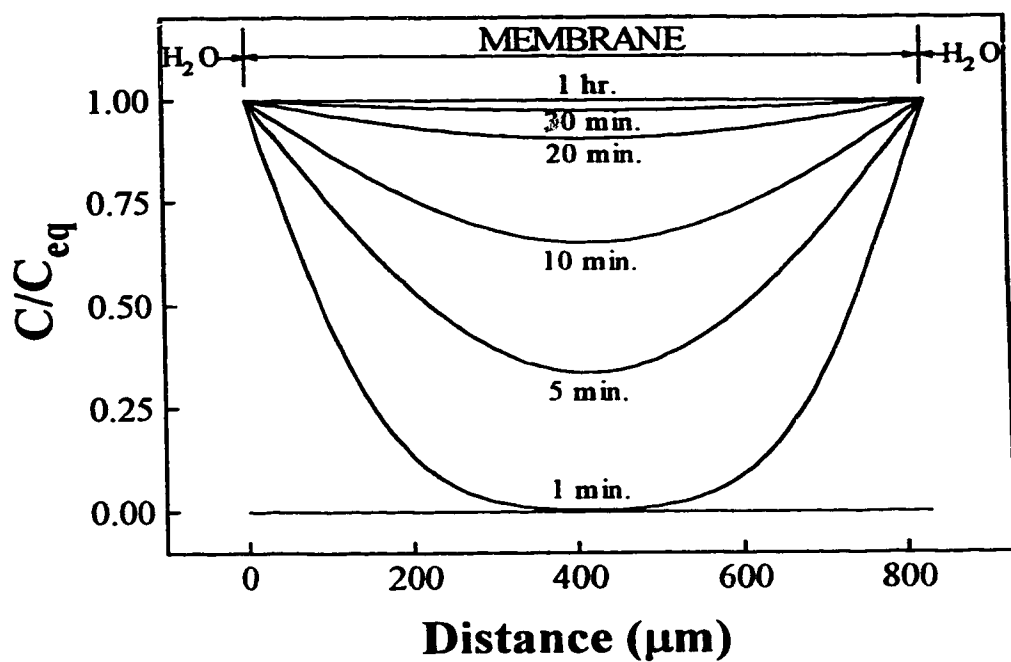


Figure 4.8 Profiles of concentration of water across the membrane calculated using the model of simple Fick's law diffusion process ( $D_I = 7.9 \times 10^{-7} \text{ cm}^2/\text{s}$ ).



Figure 4.9 compares the calculated result with the experimental one observed with a spatial imaging photometer (SIP). The measured absorbance changes ( $\Delta A$ ) were ratioed to the maximum absorbance change at the boundary and the square root was then taken, to obtain the corresponding values of  $C/C_{eq}$  according to equation 2.31. It is important to recognize in Figure 4.9 that there is no fitting parameter involved in the calculated curves. The parameters used, those in Table 4.3, were obtained independently and are the average of a number of experiments. Given this treatment, the agreement in Figure 4.9 between theory and experiment is powerful evidence in support of the dual-sorption model. The agreement is not perfectly quantitative, although this seems to arise from the asymmetry of water content frequently observed during the later stages of water uptake. That is, the two sides are never quite identical in the maximum absorbance attained at the edges. Figure 4.10 shows that the match to the experimental data is very good when just the bottom half of the membrane data is examined.

It should be pointed out that the comparison in Figures 4.9 (and 4.10) is subject to the accuracy of equation 2.31, which is not applicable to droplets with radius greater than 100 nm. Unfortunately, we do not have any resource to measure the distribution of water droplet sizes across the membrane. Nevertheless, the result of the comparison shows that the numerical method gives a reasonable simulation of the water transport process in PVC/DOA membranes.

One of the advantages of the numerical approach is that various kinds of boundary conditions can be easily incorporated into the simulations provided the equations of boundary conditions can be given. Figure 4.11, obtained by Xizhong Li [16], shows the absorbance-distance curves for water in a membrane cell in which one side was blocked to water transport using Hg, after the membrane was contacted with water for 24 hours. Hg blocks water transport just as a solid contact would, and so provides a convenient model for solid contact ion sensors. As

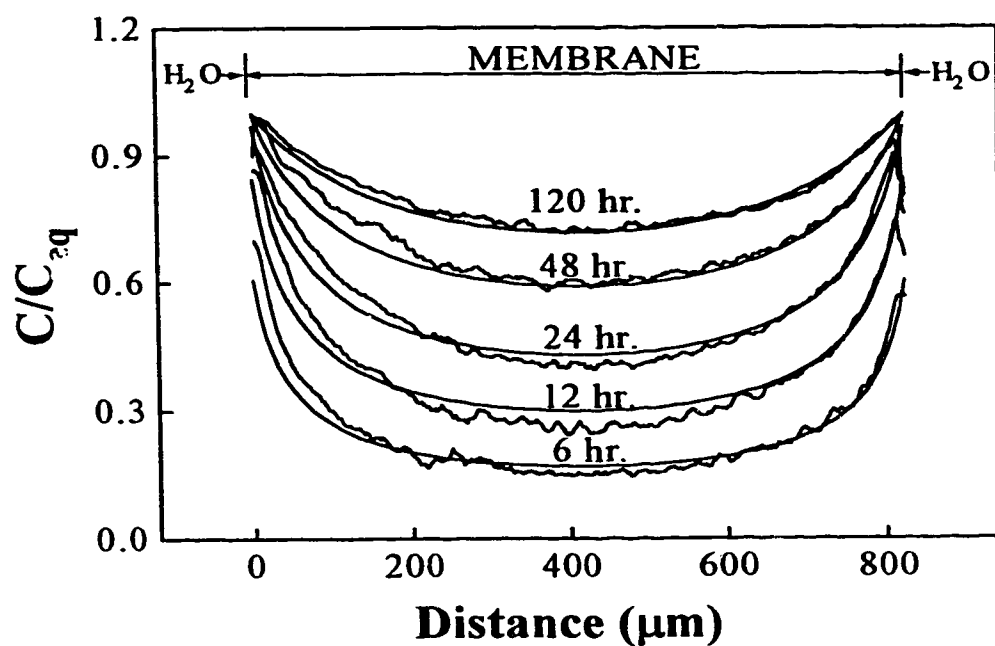


Figure 4.9 Comparison of the concentration-distance curves for a membrane after water contacted on both sides. Dark smooth curves are the numerical results. (The parameters of the calculation are given in Table 4.3)

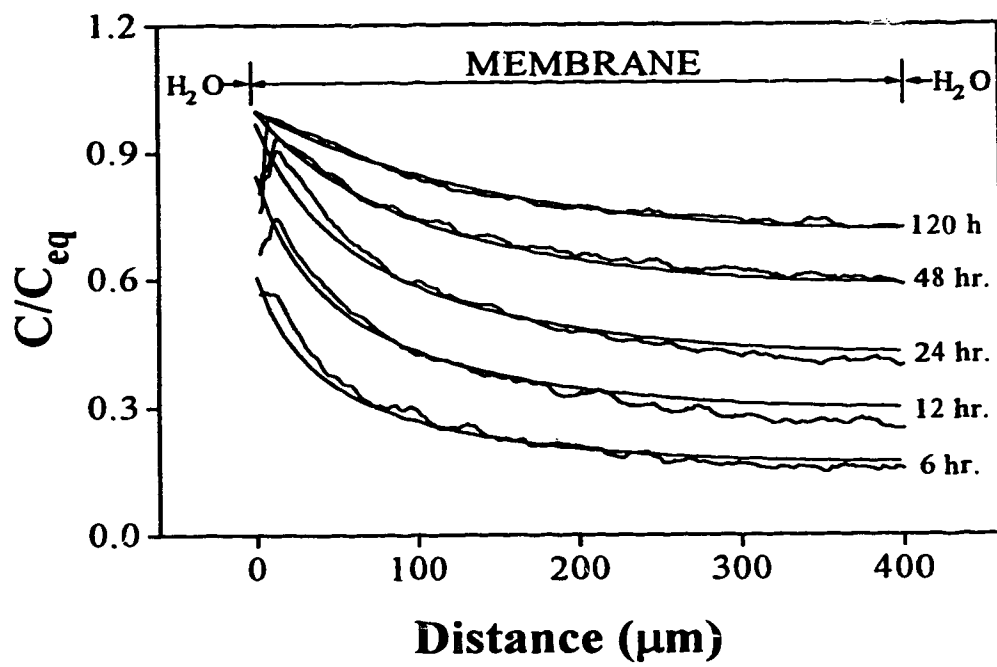


Figure 4.10 Comparison of the numerical results and experimental data (extracted from Figure 4.9).

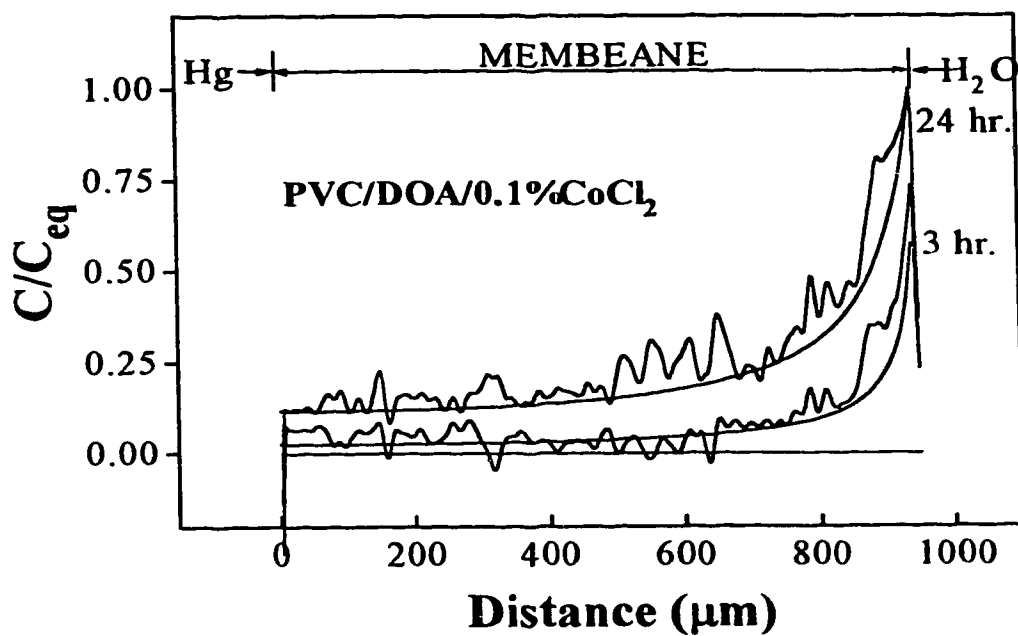


Figure 4.11 Comparison of the concentration-distance curves for a Hg blocked membrane cell after the membrane was contacted with water. Dark smooth curves are the numerical results. (Experimental results are adapted from Xizhong Li's data)

mentioned in reference 16, the obtained data is poor due to the difficulties in handling the Hg, but the result does give the general profiles of water in the transport process. While the analytically approximate solutions (equations 1.10-1.18) given by the simplified transport model are no longer applicable to this case once the water reaches the Hg, numerical simulation is possible by simply assigning the following boundary conditions to computing scheme I:

$$x = 0; C^s = C_{eq}^s [1 - \exp(-\beta t)] \quad (\text{Water contacted side}) \quad (4.21)$$

$$x = l; \frac{\partial^2 C_1}{\partial x^2} = 0 \quad (\text{Hg blocked side}) \quad (4.22)$$

The corresponding difference equation at the boundary ( $x = l$ ) is:

$$(C_{1,j}^{n+1} - C_{1,j}^n) + (C_{2,j}^{n+1} - C_{2,j}^n) = \frac{D\tau}{h^2} (C_{1,j-1}^n - C_{1,j}^n) \quad (4.23)$$

where  $j$  denotes the index of point  $x = l$ . Following the procedure in section 4.2-2 gives the equations to calculate the water concentration at this boundary point ( $C_{2,j}^{n+1}$ ) as:

$$C_{2,j}^{n+1} = \frac{-(a + b - \phi_j^n) + \sqrt{(a + b - \phi_j^n)^2 + 4b\phi_j^n}}{2} \quad (4.24)$$

where:

$$\phi_j^n = \frac{D\tau}{h^2} \left[ \frac{aC_{2,j-1}^n}{C_{2,j-1}^n + b} - \frac{2aC_{2,j}^n}{C_{2,j}^n + b} \right] + \frac{aC_{2,j}^n}{C_{2,j}^n + b} + C_{2,j}^n \quad (4.25)$$

The numerical simulation for the Hg blocked sorption experiment is also shown in Figure 4.11. The parameters used in the calculation are listed in Table 4.4. The value of  $C_{eq}$  for the membrane was estimated using the one for the PVC/DOA/0.15%CoCl<sub>2</sub> membrane (3.04 M) and equation 2-34. If the same aqueous solutions were used in the experiments, equation 2-34 can be rearranged as:

$$C_w \propto C_i^* \quad (4.26)$$

The value of  $C_{eq}$  for the PVC/DOA/0.1%CoCl<sub>2</sub> membrane was then calculated as 2.06 M. Again, the behavior of water transport has been well simulated by the numerical method.

## 4.5 CONCLUSIONS

The numerical analysis technique has been shown to give theoretical results for water transport behavior that are in good agreement with previous theoretical treatments and experimental results. The computing scheme developed is stable as long as the stability criterion (equation 4.18a) is satisfied. The digital simulation approach has the advantage of being directly applicable to situations involving more complex boundary conditions and different coupled stages of water uptake in

Table 4.4 Parameters of Numerical Calculation ( Scheme I ) for Hg blocked experiment

$D = 1.5 \times 10^{-6} \text{ cm}^2/\text{s}$	
$\beta = 0.27$	$s_0 = 50.8 \text{ mM}$
$C_i^s = 31.1 \text{ mM}$	$C_2^{eq} = 2.01 \text{ M}^*$
$h = 9.49 \text{ } \mu\text{m}$	$\tau = 0.34 \text{ second}$

\*  $C_2^{eq}$  is the equilibrium concentration of water in droplets and given as  $(C_2^{eq} = C_{eq} - s_0)$ .

PVC based ion-selective electrode membranes. The good match between the simulation and the experimental data can be taken as the further confirmation of the dual-sorption model of water transport in PVC based ion-selective electrode membranes. With this numerical tool, we can directly simulate the transport process of water in the application of ion-selective membranes. A precisely quantitative simulation will require very accurate parameters needed in calculation. Further work will be required to validate the values of those parameters estimated from previous experimental data, *e.g.*, using pulsed field gradient spin-echo  $^1\text{H}$  NMR [17] to measure the diffusion coefficient of water molecules inside membranes.



## 4.6 REFERENCES

- [1] Vieth, W. R.; Sladek, K. J. *J. Colloid Sci.* **1965**, *20*, 1014-.
- [2] Vieth, W. R.; Howell, J. M.; Hsieh, J. H. *J. Membrane Sci.* **1976**, *1*, 177.
- [3] Crank, J. *The Mathematics of Diffusion* 2nd ed., Oxford University Press, London, 1975, Chapter 11.
- [4] Li, X. *Transport Behavior of Water and Ions in Polyvinylchloride Based Ion-Selective Membranes* Ph. D. Thesis, University of Alberta, Edmonton, Canada, 1992, Chapter 4.
- [5] Crank, J. *The Mathematics of Diffusion* 2nd ed., Oxford University Press, London, 1975, Chapter 8.
- [6] Press, W. H.; Flannery, B. P.; Teukolsky, S. A.; Vetterling, W. T. *Numerical Recipes in FORTRAN: The Art of Scientific Computing*, the 2nd ed., 1992, Chapter 19.
- [7] Taverdet, J. L.; Vergnaud, J. M. *J. Appl. Polym. Sci.* **1984**, *29*, 3391-3400.
- [8] Taverdet, J. L.; Vergnaud, J. M. *J. Appl. Polym. Sci.* **1986**, *31*, 111-122.
- [9] Aboutaybi, A.; Bouzon, J.; Vergnaud, J. M. *Europ. Polym. J.* **1990**, *26*, 285-291.
- [10] Vergnaud, J. M. *Liquid Transport Processes in Polymeric Materials*, Prentice-Hall, Englewood Cliffs, NJ, 1991, Chapter 4.
- [11] Chan, A. D. C.; Li, X.; Harrison, D. J. *Anal. Chem.* **1992**, *64*, 2512-2517.
- [12] Mitchell, A. R.; Griffiths, D. F. *The Finite Difference Method in Partial Differential Equations*, Wiley, New York, 1980.
- [13] Strikwerda, J. C. *Finite Difference Schemes and Partial Differential Equations*, Pacific Grove, Calif., 1989.

- [14] Chan, A. D. C. *Analysis of Electrical and Physical Properties of Ion-Selective Liquid Membranes* Ph. D. Thesis, Edmonton, Canada, 1992, p257.
- [15] Li, X. *Transport Behavior of Water and Ions in Polyvinylchloride Based Ion-Selective Membranes* Ph. D. Thesis, University of Alberta, Edmonton, Canada, 1992, pp.
- [16] Li, X. *Transport Behavior of Water and Ions in Polyvinylchloride Based Ion-Selective Membranes* Ph. D. Thesis, University of Alberta, Edmonton, Canada, 1992, p110.
- [17] Zawodzinski, T.; Neeman, M.; Sillerud, L. O.; Gottesfeld, S. *J. Phys. Chem.* **1991**, *95*, 6040-6044.

## **Chapter 5**

# **Water-Rich Surface Region In Poly(vinyl chloride) Based Ion-Selective Electrode Membranes And The Effect of Additives\***

## **5.1 INTRODUCTION**

In the previous chapters, we have discussed the distribution of water in poly(vinyl chloride) (PVC) based ion-selective electrode membranes. A mathematical model has been proposed to describe the transport process of water in those membranes. In this chapter as well as the following ones, we will discuss the water-rich region near the surface of PVC based membranes in greater detail.

A number of workers have suggested that there is a difference between the surface and bulk regions of ion-selective membranes that are based on plasticized PVC [1-4]. The impedance studies of Tóth *et al.* [1] provided some evidence for a surface region, although their data did not identify the nature of such a region.

---

\* A version of this chapter has been published as:

Li, Z.; Li, X.; Petrovic, S.; Harrison, D. J. *Anal. Methods & Instrumentation* 1993, 1, 30-37.

Surface-sensitive infra-red studies by Tóth *et al.* [2] have also suggested that the water content at the surface of a membrane is greater than that in the bulk, although the implications of that work with respect to the behavior of water were not discussed. Using both optical and classical mass desorption techniques, Harrison *et al.* [3,4] have shown that the surface region of plasticized PVC can be highly enriched in water relative to the bulk. Their experiments with a spatial imaging photometer (SIP) and the studies of the desorption of water from a water-soaked membrane show that the water distribution within the membrane does not necessarily become uniform, even after many days of soaking. Instead, a water-rich surface region develops, in which there is a much greater extent of light scattering than in the bulk. The thickness of this region depends on the nature and concentration of additives present in the membrane [4] and it is the role of the additives on the distribution of water which is the subject of the work reported in this chapter.

We have examined the factors that affect this surface region by varying the concentration and hydrophilicity of the additives, as well as the plasticized polymer matrix. The data presented here indicate that increasing either the hydrophilicity or the concentration of the additives will increase the thickness of the water-rich surface region. In fact, a uniform distribution can be obtained by adding high concentrations of hydrophilic salts to the membrane matrix. The additives also affect the apparent diffusion coefficient of the water which forms the light scattering centers [4,5]; however, this effect is more complex and a detailed analysis has been given in Chapter 2.

## 5.2 EXPERIMENTAL

### 5.2-1 Sample Preparation:

Ion-selective membranes were cast from solutions of distilled tetrahydrofuran (THF) according to the method of Craggs *et al.* [6] using glass or Teflon form for casting. Membranes were about 66 wt. % bis(2-ethylhexyl) adipate (DOA, Fluka Selectophore grade) or *o*-nitrophenyl octylether (NPOE, Fluka, Selectophore grade), and 33% PVC (Polysciences, chromatographic grade) with various additives at 0 - 1 wt. %. Valinomycin (Aldrich) was used as received.  $\text{CoCl}_2$  (Anachemia, reagent grade) was dried under vacuum at 60 °C for 16 hours (99.9% by ethylenediaminetetraacetic acid titration [7]). Bromo(pyridine)-(5,10,15,20-tetraphenylporphyrinato) cobaltate [ $\text{CoTPP}(\text{py})\text{Br}$ ] was prepared as described elsewhere [8] as was 2,6-diphenyl-4-(2,4,6-triphenyl-N-pyridinio) phenolate (ET-30) [9,10].  $\text{KB}(\text{C}_6\text{H}_5)_4$  ( $\text{KBPh}_4$ ) was prepared by precipitation in water from KCl and  $\text{NaBPh}_4$ , followed by vacuum drying [11]. 0.6 wt. % OH-substituted PVC (PVC-OH) was prepared from 1.7 wt. % substituted PVC-COOH (Aldrich) as previously described [12].

### 5.2-2 Instrumentation:

The SIP has been described in Chapter 1 in detail and is shown in Figure 5.1. A pulsed  $\text{N}_2$  dye laser (Laser Photonics LN120C, Orlando, FL, USA), was used for membranes containing the ET-30 dye, as well as the 544 nm He:Ne laser (Melles Griot). A 633 nm He:Ne laser (Melles Griot) was used with the other membranes. In all experiments, water was present on both sides of the membrane.

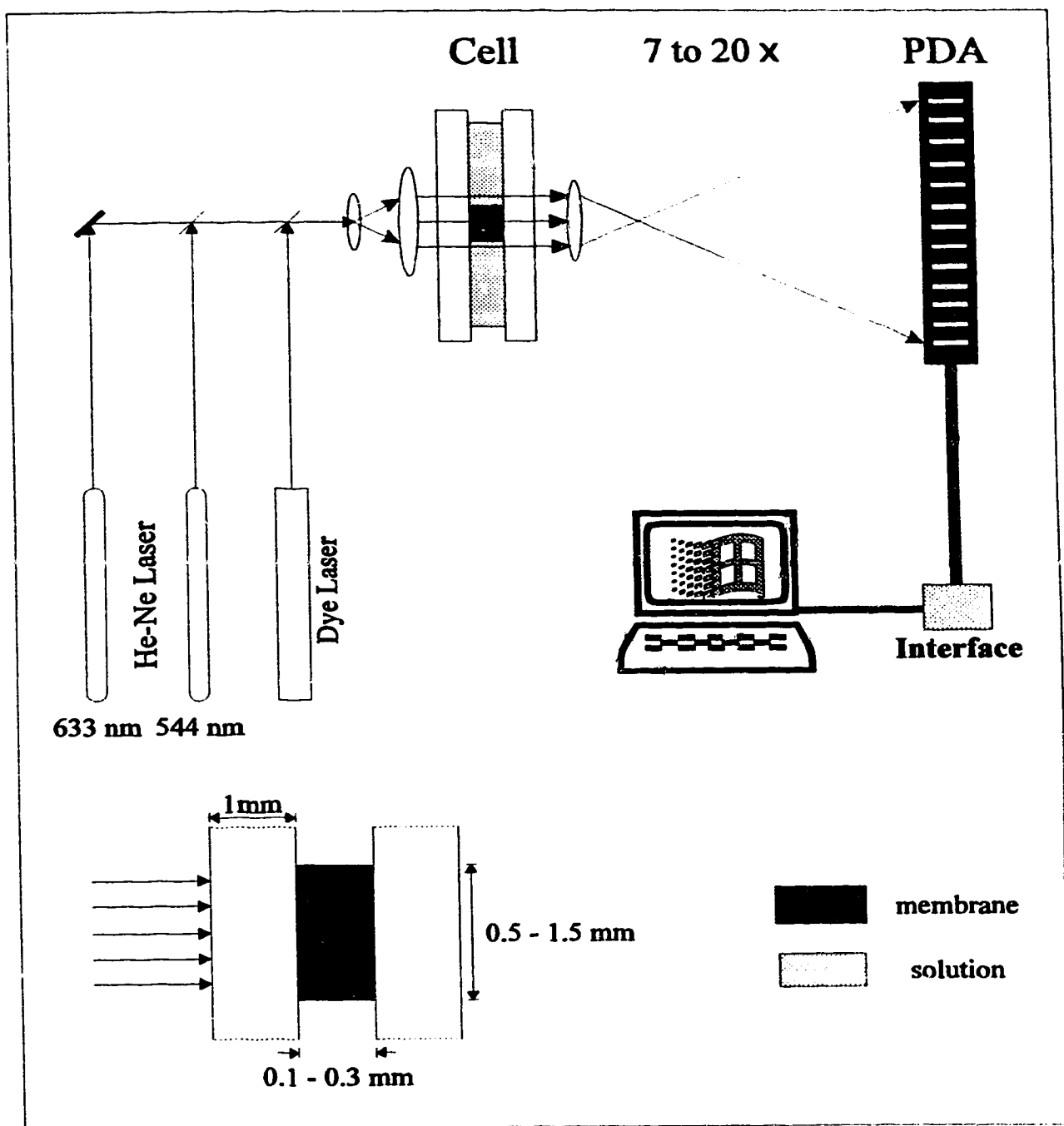


Figure 5.1 Spatial imaging photometer with three laser sources.

This gives a more accurate estimate of the thickness of the water-rich surface region than Harrison *et al.* have made previously [4], as the effect of water evaporation from the membrane-air interface is not able to influence the approach to steady state at the membrane-water interface.

### 5.3 RESULTS AND DISCUSSIONS

Additives in the membrane, and their concentrations, affect the distribution of light scattering centers as it develops over time. We studied four additives, several of which are water-sensitive dyes, to determine the factors that control the influence of an additive on the behavior of water in PVC based membranes. In order of decreasing hydrophilicity these included  $\text{CoCl}_2$ , ET-30 (see Figure 5.2 for the structure),  $\text{CoTPP}(\text{py})\text{Br}$  (see Figure 5.3 for the structure) and valinomycin with 0.01%  $\text{KBPh}_4$ . The first two compounds are water-sensitive dyes used to image the first stage of water uptake, and their affinity for water might be expected to perturb the membranes to a greater extent. The latter two additives are ion carriers added to impart  $\text{NO}_2^-$  or  $\text{K}^+$  selectivity, respectively [13,14]. DOA plasticized membranes without additives were also examined. In addition, the effect of the polarity of the membrane matrix was studied for two systems. We examined the more polar polymer, 0.6 wt. % OH-substituted PVC plasticized with DOA. In addition, the more polar plasticizer NPOE was used at 66 wt. % with PVC. The influence of the various components on water distribution was significant in most instances, particularly in the near-surface region.

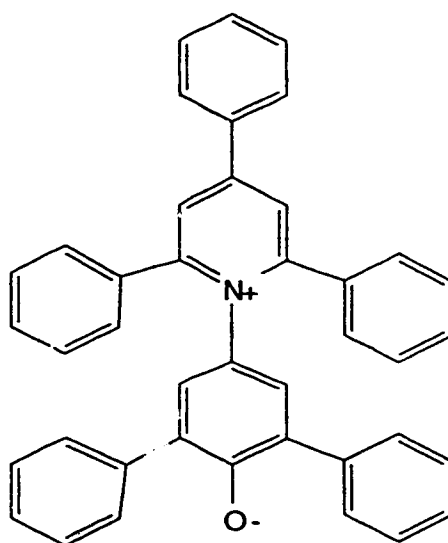


Figure 5.2 The structure of ET-30



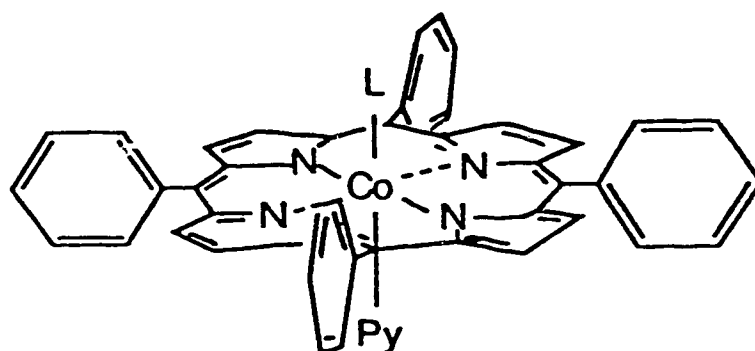
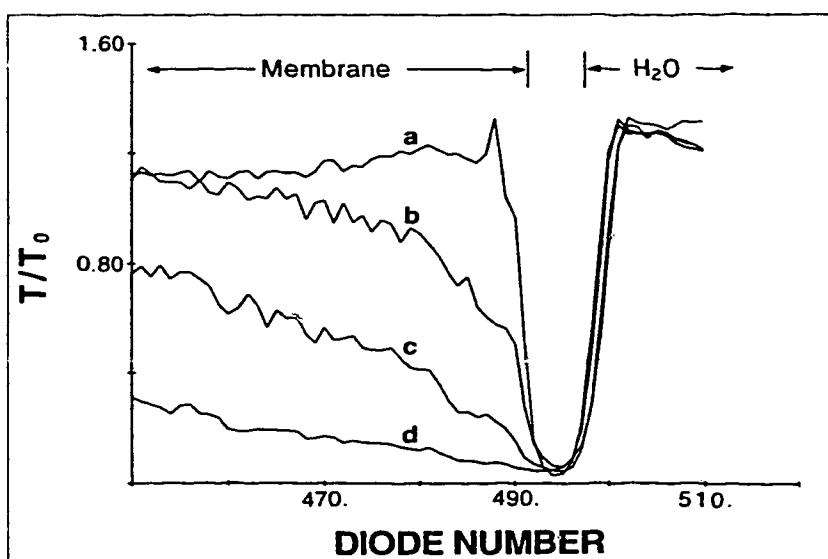


Figure 5.3 The structure of Bromo(pyridine)-(5,10,15,20-tetraphenylporphyrinato) cobaltate, [CoTPP(py)Br], where the Br ligand is symbolized by L.

### 5.3-1 Instrument and Edge Stability

The SIP studies provide evidence for a surface region that differs from the bulk [3-5,8]. However, it is important that the solution-membrane interface is well defined in these studies. Swelling effects or thermal drift in the cell position relative to the diodes must not contribute to apparent changes in absorbance at the edges. As the intensity change at the edge is dramatic, such shifts in the boundary could result in significant absorption artifacts. The transmittance of the cell at the interface must be monitored closely to identify this effect. Figure 5.4 shows the relative transmittance,  $T/T_0$ , at the interface as a function of time after the introduction of water to the cell, for a membrane with 0.15 wt. %  $\text{CoCl}_2$ . The relative transmittance was calculated with respect to the intensity of light that passed through the aqueous solution in the cell, so a value of  $T/T_0$  that is greater than unity simply means that the source intensity varied in space across the cell. From left to right Figure 5.4 shows the relative transmittance through the membrane bulk, the dark region at the membrane solution interface arising from the discontinuity in refractive indices, and the relative transmittance through the aqueous solution. The image is expanded so that the other membrane edge on the left side and the aqueous solution used to obtain the reference intensity are not shown.

Figure 5.4 shows that the membrane-solution edge is stable to within one diode ( $3\text{ }\mu\text{m}$  at 8.5:1 magnification) over 24 hours. The membrane edge is identified as the point on the rising transmittance curve that is at 25% of the maximum transmitted light, in accordance with diffraction theory for a knife edge [15]. As both membrane edges are usually imaged it is possible to determine whether a shift in the cell position relative to the diodes, as opposed to swelling of the polymer, accounts for any observed edge shift.  $\text{CoCl}_2$  is the most hydrophilic



**Figure 5.4** Relative transmittance,  $T/T_0$ , versus diode number (one diode =  $3\ \mu\text{m}$ ) as a function of time that both membrane faces were exposed to water, a) initially, b) 1 h, c) 5 h, d) 23 h. The PVC/DOA membrane contained 0.15 wt. %  $\text{CoCl}_2$ . Only one membrane/solution interface is shown.

additive studied and would be expected to cause the greatest swelling of the membrane. However, for all the additives examined the edges were usually stable to within one or two diodes. Furthermore, when it is clear that a change in the cell position is responsible for the shift, it is possible to shift the index of the diode numbers to realign the images. At worst, this effect may introduce an uncertainty of 2 - 6  $\mu\text{m}$  in the analysis of the width of the surface region. For studies of processes in the bulk membrane the distances are sufficiently large that the error is not significant.

### 5.3-2 Standard Membrane Compositions

A typical  $\text{K}^+$  -selective membrane is composed of DOA and PVC as a matrix, with about 1 wt. % valinomycin and 0.01 wt. %  $\text{KBPh}_4$  added to give selectivity and reduce anion interference, respectively [14,16]. Figure 5.5 shows the development of light scattering centers in such a membrane over an extended period. Although water droplets eventually form throughout the membrane, it is clear that there is a near-surface region that differs considerably in water content from the bulk membrane. It is striking that this surface region is essentially stabilized after about 24 hours, and remains well defined even after 12 days of soaking. The presence of a water-rich surface region is also supported by mass desorption studies of membranes during drying [3]. This water-rich region is approximately 50  $\mu\text{m}$  thick. This estimate of thickness is obtained by linear extrapolation of the absorbance curve. It corresponds approximately to estimating a thickness equal to  $\sqrt{\pi Dt}$ , which is essentially a Nernst layer approximation for diffusion. The thickness varies from membrane to membrane so that the overall precision, including any errors due to shifting of the edges, is about  $\pm 20\%$ .

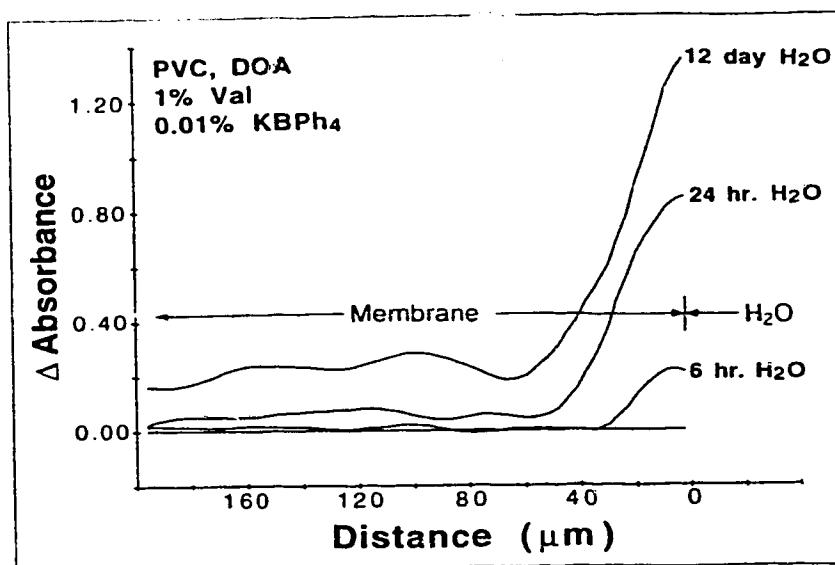


Figure 5.5 Absorbance due to light scattering in a PVC/DOA membrane with 1% valinomycin, 0.01%  $\text{KPh}_4$  as a function of time exposed to water. Only one membrane/solution interface is shown.

The surface region is of considerable thickness compared with that of a standard ion-selective electrode membrane. Free standing ion-selective electrode membranes are typically 100 - 200  $\mu\text{m}$  thick [16], so that this region would be present across one-half to all of a typical sensor. PVC based membranes coated on solids such as the gate of an ion-selective field effect transistor, or the optical window of an optically based ion sensor, are often less than 50  $\mu\text{m}$  thick [17,18]. For such sensors the water-rich region would encompass the entire system, and could lead to slight differences in performance relative to the standard ion-selective electrode configuration. In both instances the surface region described here comprises a significant, but not necessarily complete, volume of a membrane in a typical sensor.

X. Li examined blank membranes prepared from PVC and DOA alone to evaluate the influence of the membrane matrix on water distribution internally [19]. We note that it has been clearly established that these membranes will still contain ionic impurities [16,20]. Figure 5.6 shows the development of the light scattering profile as a function of time obtained by X. Li. It is noteworthy that even when water droplets have formed throughout the membrane there is still a highly hydrated surface layer present. The transport parameters or apparent diffusion coefficients have been estimated using the model of X. Li presented in Chapter 1. The solid lines in Figure 5.6 are the fits to the data at the edges with equations 1.18 and 1.17 which are given as:

$$\Delta A_2^b(x, t) = \Delta A_b^0 \left\{ 1 - \frac{4}{\pi} \sum_{n=1}^{\infty} \frac{1}{(2n-1)} \exp \left[ -\frac{D_2^b (2n-1)^2 \pi^2 t}{l^2} \right] \sin \frac{(2n-1)\pi x}{l} \right\} \quad (1.17)$$

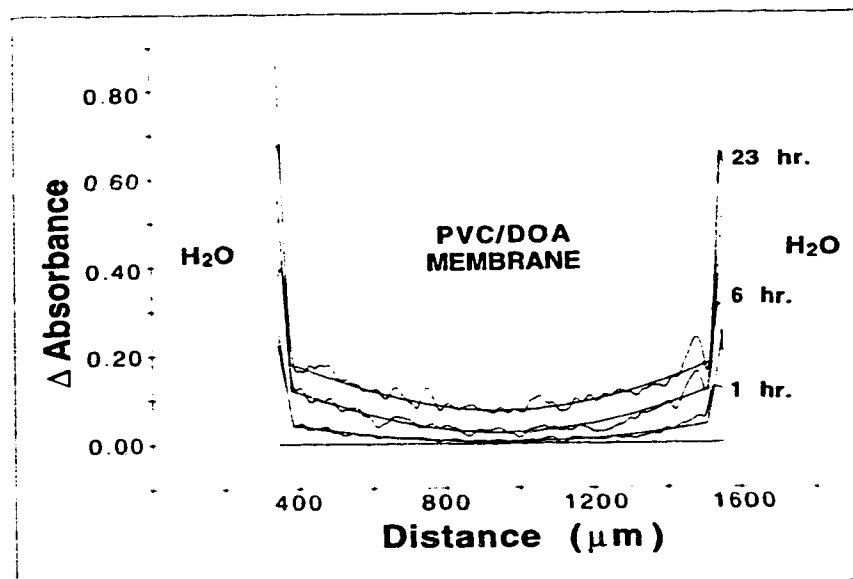


Figure 5.6 Absorbance due to light scattering in a PVC/DOA membrane over 23 hours of water exposure. The solid lines are fits according to equations (1.18) and (1.17) for the surface and bulk regions, respectively. (adapted from X. Li's Thesis, 1992, p101)

$$\Delta A_2^s(x,t) = \Delta A_{2,\max}(x,t) \left[ 1 - \frac{1}{\operatorname{erf} \frac{x_k}{2\sqrt{D_2^s t}}} \operatorname{erf} \frac{x}{2\sqrt{D_2^s t}} \right] \quad (1.18)$$

Using equations 1.17 and 1.18 the apparent diffusion coefficients for the scattering centers in the bulk,  $D_2^b$ , and in the surface region,  $D_2^s$ , were estimated and are given in Table 5.1. The approximations associated with this have been discussed in Chapters 1 and 2. Note in particular that absorbance appears to the power 1 rather than 1/2 in equations 1.17 and 1.18, so that the diffusion coefficient of droplets is obtained. This analysis does not provide the actual diffusion coefficient of water molecules in the membrane in the presence of droplets, but it does allow for an estimation of the overall rate of the water uptake process.

The slow decrease in the rate of penetration of the water-rich boundary into the membrane is evidenced by the diffusion coefficients for the scattering centers in the near-surface region (see Table 5.1). There is a decrease in  $D_2^s$  as a function of time. This shows that the appearance of a surface region is not due just to a steady but slow diffusion process; instead, the ingress of water slows after the surface becomes hydrated. (As discussed below, this effect is even more drastically indicated by the data in Table 5.2 for a PVC/DOA membrane that contains 1 wt.% Valinomycin and 0.01 wt.% KBPh<sub>4</sub>, for which data was obtained after 290 hours.) Similarly, the apparent diffusion coefficient for scattering centers in the membrane bulk,  $D_2^b$  also decreased with time. The mean absorbance of the membrane due to light scattering ( $A_{\text{mean}}$ ) is also given in Table 5.1. The data indicates that there is a correlation between the increase in water content and the



**Table 5.1**      Diffusion coefficients and absorbance of light scattering centers in a PVC/DOA membrane.

<b>Time (h)</b>	<b><math>D_2^s</math> (<math>\times 10^9 \text{cm}^2/\text{s}</math>)</b>	<b><math>D_2^b</math> (<math>\times 10^7 \text{cm}^2/\text{s}</math>)</b>	<b><math>A_{\text{mean}}</math></b>
0.17	12.0	6.0	0.0035
0.5	6.0	3.0	0.010
1	3.5	1.2	0.016
2	1.5	0.8	0.022
4	1.0	0.35	0.042
6	0.20	0.3	0.058
23	0.15	0.13	0.11

decrease in apparent diffusion in the surface region. The results do clearly indicate that ingress of the water centers is a process that decreases in rate with increasing water concentration. At least in the case of  $D_2^b$ , this decrease can be understood in terms of the dual-sorption model presented in Chapter 2.

The results in Figure 5.6 show that the PVC/DOA matrix develops a surface region that is also about 50  $\mu\text{m}$  thick. This indicates that it is the matrix itself that is responsible for the effect. The hydrophobic valinomycin additive apparently has no influence. It might be expected that the  $\text{KBPh}_4$  salt would influence water uptake, however, at 0.01% it appears that the concentration is too low for it to be significant.

### 5.3-3 Effect of Additives

The ingress of water droplets was evaluated for PVC/DOA membranes containing  $\text{CoTPP(py)Br}$  and the betaine dye referred to as ET-30. The Coporphyrin is able to bind a water molecule in an axial coordination site through exchange with  $\text{Br}^-$ , which gives it a fairly well defined interaction with water. It should be more hydrophilic than Valinomycin, but much less so than the pyridinium phenolate dye ET-30, which absorbs water of hydration to a significant extent. Figure 5.7 compares the surface region that develops after 24 hours and Table 5.2 indicates the approximate width of the surface layer as a function of time for the various additives. It is clear that ET-30 increases the penetration depth of the water-rich region considerably, relative to valinomycin or  $\text{CoTPP(py)Br}$ . However, even after 100 hours this depth has not increased from a plateau of about

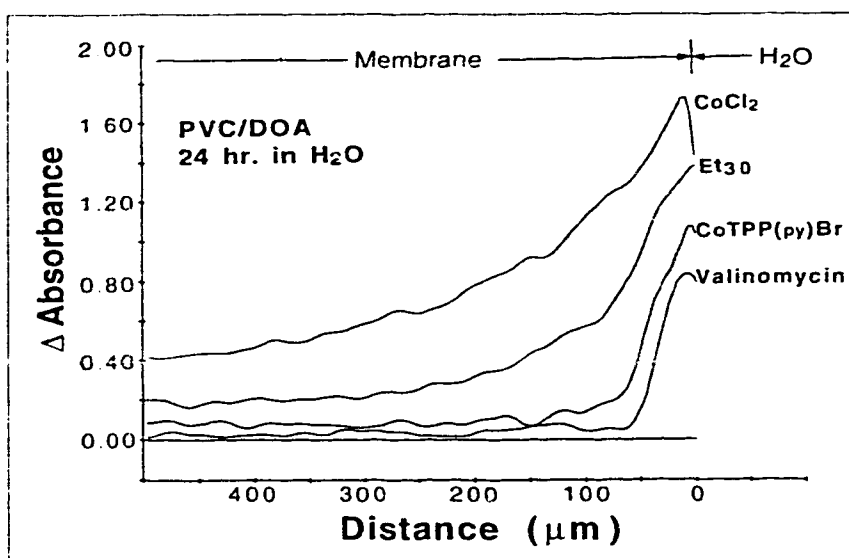


**Figure 5.7** Comparison of changes in absorbance in the surface regions induced by water uptake over 24 hours, for 0.15%  $\text{CoCl}_2$ , 0.1% ET-30, 0.3%  $\text{CoTPP}(\text{py})\text{Br}$ , and 1% valinomycin with 0.01%  $\text{KBPh}_4$ . Water contacted both sides, but only one interface is shown.

200  $\mu\text{m}$ . This would obviously be across the entire width of a conventional ion-selective electrode membrane.

A value of  $D_2^s$  could be evaluated by fitting the absorbance in the surface regions to equation 1.18. This parameter gives a more accurate estimate of the absorbance profile at a given time than does the Nernst layer approximation of the surface layer thickness. These are reported in Table 5.2, where it can be seen that they decrease as a function of time, as would be expected if the thickness of the surface region was stationary in time. However, as  $D_2^s$  is a time or concentration dependent parameter, fitting the data to equation 1.18 provides only a representative, average value of  $D_2^s$  at any given time. The values of  $D_2^s$  in Table 5.2 can not be considered true diffusion coefficients, but they do allow for calculation of the observed absorbance profile at a given point in time, and so provide an empirical measure of the progress of water permeation.

We have used  $\text{CoCl}_2$  as a water-sensitive dye to image the initial stage of water uptake. This dye incorporates water in its inner coordination sphere, and when  $\text{Co}(\text{H}_2\text{O})_6\text{Cl}_2$  forms the dye will also have a significant perturbation on the water uptake properties of the membrane. Figure 5.8 shows the development of light scattering as a function of time after exposure to water on both sides, for a membrane containing 0.15 wt. %  $\text{CoCl}_2$ . By comparing the absorbance due to light scattering in Figure 1.4 at short times, Figure 5.8 up to 28 hours, and Figure 4.9 up to 120 hours the time progression of water uptake can be evaluated. In the first hour a surface region that is not described by the model presented in Chapters 2 and 4 may be present. However, after that the uptake can be represented by the model, as already discussed in Chapter 4, and a uniform distribution will be established after 120 hours or so. Nevertheless, over the first 24 hours the dual-

Table 5.2 Thickness of water-rich region and apparent diffusion coefficients

Composition*	Time** (h)	Thickness <sup>†</sup> ( $\mu\text{m}$ )	$D_2^s$ ★ ( $\times 10^9 \text{cm}^2/\text{s}$ )
PVC/DOA	24	55	0.15
	48	55	0.03
1% val., $\text{KBPh}_4$	24	50	0.08
	290	50	0.007
3% $\text{CoTPP}(\text{py})\text{Br}$	24	50	0.1
	48	52	0.05
1% ET-30	23	188	1.3
	100	200	0.3
0.15% $\text{CoCl}_2$	0.75	75	5.5
	23	280	3.0
PVC/NPOE	24	57	0.14
PVC-OH/DOA	24	70	0.23

\* PVC or PVC-OH, ~ 66% plasticizer; other additives as indicated.

\*\* Time of exposure to water on both faces of the membrane.

† Estimated by linear extrapolation of steep portion of absorbance profile (Nernst layer approximation). Error of about  $\pm 20\%$ .

★ Apparent diffusion coefficient of scattering centers in the surface region. Obtained by fitting absorbance profile to equation (1.39) in surface region. Standard deviation of  $\pm 15\%$ .

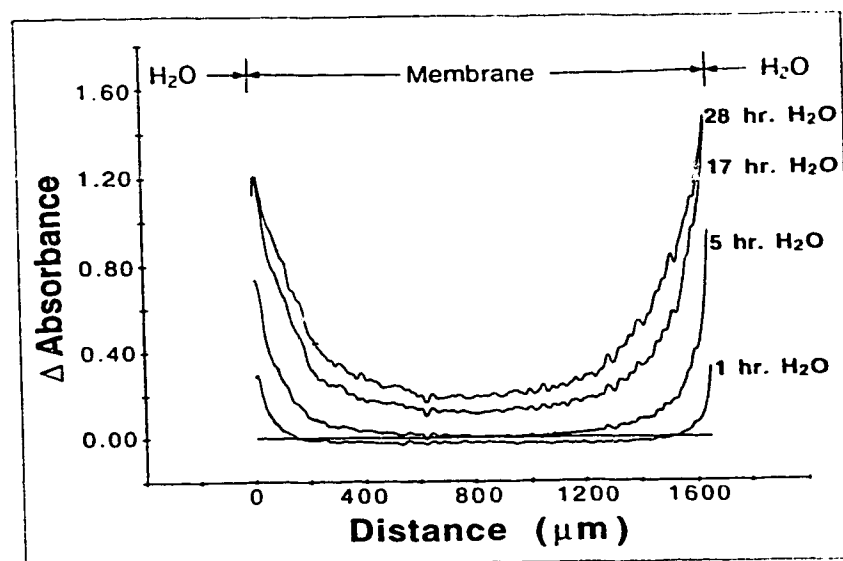


Figure 5.8 Changes in absorbance over 28 hour exposure to water for membrane with 0.15 wt. %  $\text{CoCl}_2$  added.

sorption transport process leads to a region near the surface that is much richer in water than the bulk is.

The formation of a surface region during the approach to equilibrium was influenced by the  $\text{CoCl}_2$  concentration. Harrison *et al.* have previously reported that the absorbance profile due to scattering from water droplets clearly obeys Fick's laws of diffusion across the entire membrane when  $\text{CoCl}_2$  is present at 0.78 to 1% [5]. In that study a distinct water-rich surface region did not form. The transport of water when droplets formed within the bulk membrane could instead be described by a single diffusion coefficient, indicating a greater uniformity of the membrane with a higher salt content. This shows that the hydrophilic salt overcomes the tendency of the membrane matrix to form a surface region.

#### 5.3-4 Effect of Other Matrices

In the above studies the membrane matrix was constant; however, it is also of interest to explore the effect of the matrix itself. Harrison *et al.* have previously shown that PVC-OH in combination with  $\text{SiCl}_4$  can be used to enhance adhesion on solid substrates [12]. The hydroxyl functionality makes this polymer more hydrophilic than PVC, so we have examined this material using DOA as a plasticizer. An alternative means of increasing the membrane hydrophilicity is to use the more polar plasticizer, NPOE, which is commonly used in  $\text{Ca}^{2+}$ -selective membrane. The distribution of light scattering centers was also examined in this matrix after exposure to water. The results for both systems are given in Table 5.2. They show a modest increase in the size of the water-rich surface region compared with the PVC/DOA matrix, however, the increase is only slightly larger than experimental error.

## 5.4 CONCLUSIONS

The presence of a water-rich region within these PVC based membranes is surprising, and the experiments described here were not designed to elucidate the source of the phenomena. Chan *et al.* have speculated about the reasons why a surface region develops [3]. It may arise from stress within the membrane upon water uptake, as stress can influence the diffusion coefficients [21]. Alternatively, it may be due to a competition between water and plasticizer to fill voids created in the surface region by leaching of the plasticizer into the solution [22], as described elsewhere [3]. This chapter shows that the presence of a water-rich region is not strongly dependent on the polarity of the plasticizer used, as DOA and NPOE have very different polarities. Similarly, small changes in the polymer polarity do not have a significant influence. However, the additives in the membrane play a significant role in establishing the water distribution, and the apparent diffusion coefficient of water droplets within the membranes. Within the range of additives we have examined it appears that the greater the hydrophilicity of the additives, and the greater its concentration, the greater will be the depth of the water-rich region. This also means that the overall water content will increase with increasing hydrophilicity of the additives. For 100 - 200  $\mu\text{m}$  thick membranes with hydrophobic additives the interior will be lower in water droplet content than the surface. If a significant salt concentration is added to the polymer, the water distribution will be much more uniform. Thinner membranes coated on solids will have a more uniform, and on average higher, water content, regardless of the additives present.



## 5.5 REFERENCES

- [1] Tóth, K.; Gráf, E.; Horvai, G.; Pungor, E.; Buck, R. P. *Anal. Chem.* **1986**, *58*, 2741.
- [2] Tóth, K.; Lindner, E.; Pungor, E.; Zippel, E.; Kellner, R. *Fresenius' Z. Anal. Chem.* **1988**, *448*, 331.
- [3] Chan, A. D. C.; Li, X.; Harrison, D. J.; *Anal. Chem.* **1992**, *64*, 2512.
- [4] Harrison, D. J.; Li, X.; Petrovic, S. *In Biosensors and Chemical Sensors. Optimizing Performance Through Polymeric Materials* (P. G. Edelman, J. Wang, Eds), *ACS Symposium Series 487*, American Chemical Society, Washington DC **1992**, Chapter 23, 292-300.
- [5] Li, X.; Petrovic, S.; Harrison, D. J. *Sensors Actuators* **1990**, *B1*, 275
- [6] Craggs, A.; Moody, G. J.; Thomas, J. D. R. *J. Chem. Educ.* **1974**, *51*, 541.
- [7] Schwarzenbach, G.; Flaschka, H. *Complexometric Titrations*, Methuen, Londong, **1969**, [translated by H. M. N. H. Irving].
- [8] Li, X.; Harrison, D. J. *Anal. Chem.* **1991**, *63*, 2168.
- [9] Kumoi, S.; Oyama, K.; Yano, T.; Kobayashi, H.; Ueno, K. *Talanta* **1970**, *17*, 319.
- [10] Johnson, B. P.; Gabrielson, B.; Matulenko, M.; Dorsey, J. G.; *Anal. Lett.* **1986**, *19*, 939.
- [11] Bassett, J.; Denney, R. C.; Jeffery, G. H.; Mendham, J. *Vogel's Textbook of Quantitative Inorganic Analysis* 4th edn, Longman, London, **1978**.
- [12] Satchwill, T.; Harrison, D. J. *J. Electroanal. Chem.* **1986**, *202*, 75.
- [13] Schulthess, P.; Ammann, D.; Kreulter, B.; Caderas, C.; Stepanek, R.; Simon, W. *Anal. Chem.* **1985**, *57*, 1397.
- [14] Oehme, M.; Simon, W. *Anal. Chem. Acta* **1976**, *86*, 21.
- [15] Jan, C. C.; McCreery, R. L. *Anal. Chem.* **1986**, *58*, 2771.

- [16] Morf, W. E.; Simon, W. *Helve. Chim. Acta* **1986**, *69*, 1120.
- [17] Seiler, K.; Morf, W. E.; Rusterholz, B.; Simon, W. *Anal. Sci.* **1989**, *5*, 557.
- [18] Morf, W. E.; Seiler, K.; Rusterholz, Simon, W. *Anal. Chem.* **1990**, *62*, 738.
- [19] Li, X. *Ph. D. Thesis*, **1992**,
- [20] van den Berg, A.; van der Wal, P. D.; Skowrowska-Ptasinska, M.; Sudholter, E. J. R.; Reindhaut, D. N.; Bergveld, P. *Anal. Chem.* **1987**, *59*, 2827.
- [21] Crank, J. *J. Polym. Sci.* **1953**, *11*, 151.
- [22] Messadi, D.; Vergnaud, J. M. *J. Appl. Polym. Sci.* **1982**, *27*, 3945.

## **Chapter 6**

# **A Study of the Water-Rich Surface Region In PVC-Based Ion-Selective Membranes**

## **6.1 INTRODUCTION**

Optical and gravimetric studies have revealed a unique behavior of water in PVC/DOA based ion-selective electrode (ISE) membranes [1-4]: a many-micron-thick, water-rich surface region develops during the process of water uptake, and the water distribution remains non-uniform, even after many days of exposure. Our studies on PVC/NPOE based ISE membranes (see Chapter 3) have also shown the existence of this surface phenomenon. A comparative study of effects of additives on the surface layers has been presented in Chapter 5. However, those studies did not examine the origin of highly hydrated surface layers.

Given the presence of such a non-uniform distribution of water in PVC based ISE membranes, it is important to understand why it may arise. It has been suggested by Harrison *et al.* that the internal stress developed within plasticized PVC membranes upon uptake of water may account for the heterogeneity [1-2, 5], since diffusion rates within a polymer can be changed substantially by stress [6].

A. D. C. Chan *et al.* have also postulated that leaching of plasticizer from the surface of membranes to the external aqueous solution could provide a kinetic interpretation of the effect [4]. Loss of plasticizer would result in a decrease in volume or the formation of voids in the membrane matrix. It is possible that water from the aqueous solution competes with plasticizer from the membrane bulk to fill these voids. A water-rich region would then be established near the surface where the water flux was greater, which would essentially disappear at the point in the membrane where the flux of plasticizer became greater. A similar model has been suggested to interpret data for plasticized PVC exposed to more lipophilic solvents [7].

In an attempt to differentiate the above two explanations, we have used the SIP method to study the effect of the plasticizer on the water-rich surface layer in PVC based ISE membranes. Experiments on ion-selective electrode membranes plasticized with some polymeric plasticizers will be reported here. Results with polymeric plasticizers will be compared with those of membranes plasticized with the conventional plasticizers (*e.g.*, DOA and NPOE). Polymeric plasticizers were chosen because they have very high lipophilicities and presumably lower mobility than low molecular weight plasticizers. A uniform distribution of water across the membrane might then be expected if the kinetic interpretation is valid, since leaching of the plasticizer would occur to a much lesser extent. Based on the experimental results obtained, we propose an approximate water uptake model which incorporates the development of a water-rich surface layer in PVC based ISE membranes. A comparison of calculated results with experimental data will also be presented in this chapter.

## 6.2 MODELING AND NUMERICAL METHODS OF ANALYSIS OF THE SURFACE REGION

In Chapters 2 and 4, we proposed a dual-sorption model to describe the transport of water inside PVC based ion-selective electrode membranes. An explicit finite difference method was developed to simulate the diffusion process. Calculated results are in good agreement with the experimental data obtained with PVC/DOA membranes doped with the hydrophilic salt,  $\text{CoCl}_2$ . However, the proposed model and numerical method do not consider the development of a water-rich surface layer observed in commonly used PVC/DOA ISE membranes that do not contain hydrophilic salts.

The development of the water-rich surface layer as understood according to the kinetic interpretation may be represented by the schematic diagram shown in Figure 6.1. If there were no loss of plasticizer from the membrane to the external aqueous solution, then uniform concentration distributions of both plasticizer and water would be expected once the equilibrium water concentration was reached, as shown in Figure 6.1(a). However, when plasticizer leaches from the membrane surface, voids will be formed in the membrane matrix. These may be filled by water from the aqueous phase or by plasticizer from the membrane bulk. As a result, a gradient of plasticizer near the membrane surface will generate a gradient of water concentration, as shown in Figure 6.1(b). The thickness of this region will be controlled by the relative water and plasticizer fluxes.

The formation of these surface layers may also be understood in terms of the equilibrium water uptake model (Chapter 2). As described by equation 2.7:

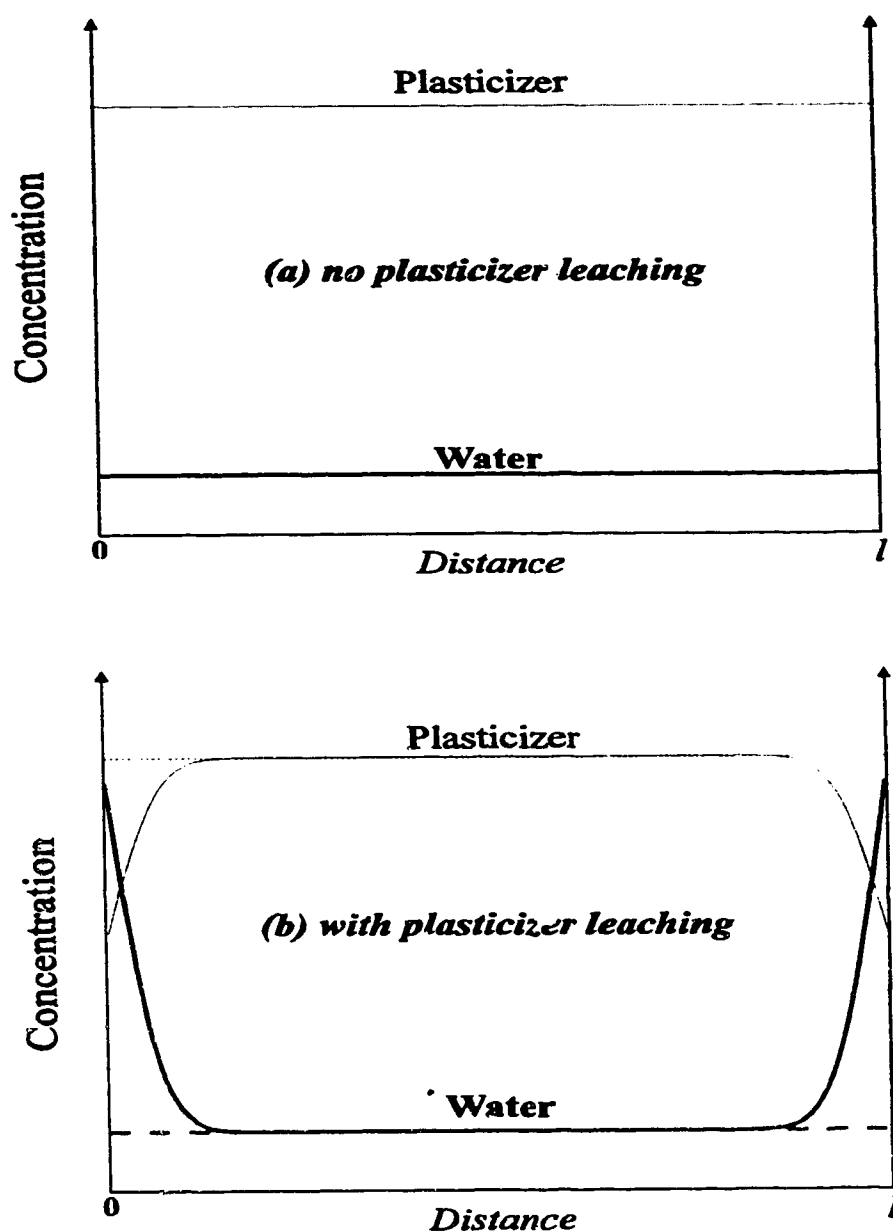


Figure 6.1 Hypothetical concentration profiles of plasticizer and water across the thickness of membrane at the equilibrium water uptake. (a) Assuming no loss of plasticizer; (b) With the loss of plasticizer.

$$C_w = \frac{C_i^s \rho_w / M_w}{C_{aq} + p} \quad (2.7)$$

the equilibrium concentration of water in membrane,  $C_w$ , is determined by the elastic pressure of the polymer matrix,  $p$ . Presumably, loss of plasticizer can result in a change of both  $p$  and  $C_w$ . Therefore, with the development of a plasticizer gradient near the surface as shown in Figure 6.1(a), a gradient of  $p$  forms and results in a gradient of equilibrium water concentration in a membrane according to equation 2.7.

Leaching of the plasticizer and subsequent back-filling by solvent is known as a double transfer process. A knowledge of the kinetics of a double transfer in the near surface region would be needed to truly model this process. In the modeling of matter transport between plasticized PVC and more lipophilic liquids such as alcohols, some empirical formulas for  $D_2^s$  have been used [7, 8-11]. An effort to develop an empirical formula to describe the double transport kinetics in PVC based ISE membranes is outside of the scope of this thesis.

It is also possible to model transport using an apparent  $D_2^s$  in the surface region that is a function of time, providing an empirical description of the changes occurring. However, at this stage of the study this approach was not taken, since a satisfactory function for  $D_2^s$  versus time was not readily apparent. Because of the empirical aspects of any function we could determine it did not seem justified to pursue this, given the increased degree of programming complexity that would be introduced. Instead a more approximate model utilizing a single  $D_2^s$  over time was evaluated to describe the surface region.

The model adapted for numerical calculations of the presence of a surface region is based on the dual sorption model introduced in Chapter 2. Added to this

is a third, separate diffusion process, with a much lower diffusion coefficient which obeys Fick's laws of diffusion. This process is driven by the double transfer process, but represented by a simple Fick's law diffusion of water alone within the model. The various aspects of the model are formulated as follows:

- (1) Besides the two modes of water sorption described by the dual-sorption model (*i.e.*, sorptions which involve the diffusion of mobile water molecules in the membrane phase and immobilization of water molecules at impurity sites within the membrane), there is a third one which occurs due to the loss of plasticizer from the membrane surface region.
- (2) These three sorption modes occur simultaneously at the near surface region while dual-sorption dominates in the bulk.
- (3) Sorption by the first two modes will cease at positions where water reaches the equilibrium concentration in the membrane bulk,  $C_{eq}^b$ , however, sorption by the third mode may continue. Sorption of the third mode is independent of other two and occurs in the near surface region until it reaches its own equilibrium value,  $C_{eq}^s$ .
- (4) The sorption of the third mode can be described by an apparent diffusion coefficient of water at the surface,  $D_2^s$ .

Assumption 4 is made since we have no means to incorporate the true diffusion coefficient of water molecules,  $D$ , into the third mode. In a more sophisticated model  $D_2^s$  could be made time dependent, or the double transfer kinetics could be explicitly incorporated. However, this is outside the scope of this thesis.



An explicit-finite-difference method (Scheme III) has been developed to simulate the water uptake process described by this new model, as shown in Figure 6.2, where  $(C_i^n)_b$  and  $(C_i^n)_s$  indicate the water concentration determined by the dual-sorption modes and the third mode, respectively. In this simulation,  $(C_i^n)_s$  is always calculated independently using Scheme II, which is based on the following difference equation (Fick's second law):

$$(C_i^{n+1} - C_i^n)_s = \frac{D_z^s t}{h^2} (C_{i+1}^n - 2C_i^n + C_{i-1}^n)_s \quad (6.1)$$

$(C_i^n)_b$  is calculated using Scheme I (Chapter 4). For each iteration, the sum of  $(C_i^n)_b$  and  $(C_i^n)_s$  calculated in the previous step will be assigned as the initial value for  $(C_i^n)_b$ . The routine will bypass the transport step of Scheme I if  $(C_i^n)_b$  is greater than the equilibrium concentration of water in the bulk,  $C_{eq}^b$ , following the assumption 3 above.

### 6.3 EXPERIMENTAL

Membranes were prepared from about 33 wt.% PVC (Polysciences Chromatographic grade), 66 wt.% plasticizer and small amounts of ionophore and lipophilic salts, except where indicated. DOA and NPOE were obtained from Fluka (Selectophore grade). The polymeric plasticizers, Paraplex G-25 and G-62, were obtained from C. P. Hall Inc. (Chicago, IL) and ethylene/vinyl acetate (EVA-

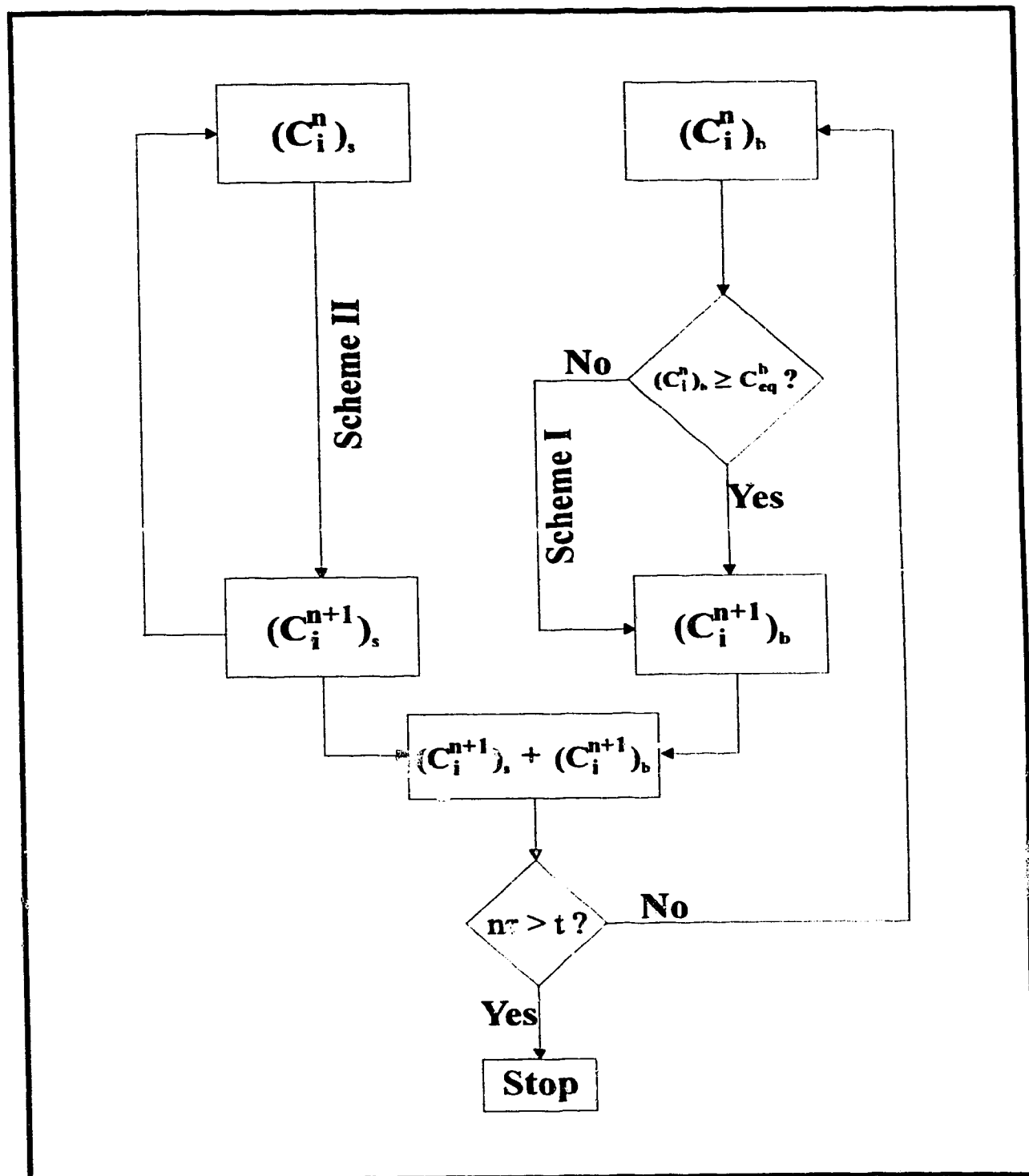


Figure 6.2 Scheme III of numerical calculation. Schemes I and II are contained within this scheme.

45 (or 70), vinyl acetate content 45 (or 70) wt.%) were obtained from Scientific Polymer Products Inc. (Ontario, NY). Valinomycin (Aldrich) was used as received. Potassium tetrakis(4-chlorophenyl) borate (KTpClPB) was obtained from Fluka (Selectophore grade).

A spatial imaging photometer was used to measure the absorbance profiles across the membranes as a function of time after exposure to water. The instrument design and the experimental procedures have been described in detail in Chapters 1 to 3.

## 6.4 RESULTS AND DISCUSSION

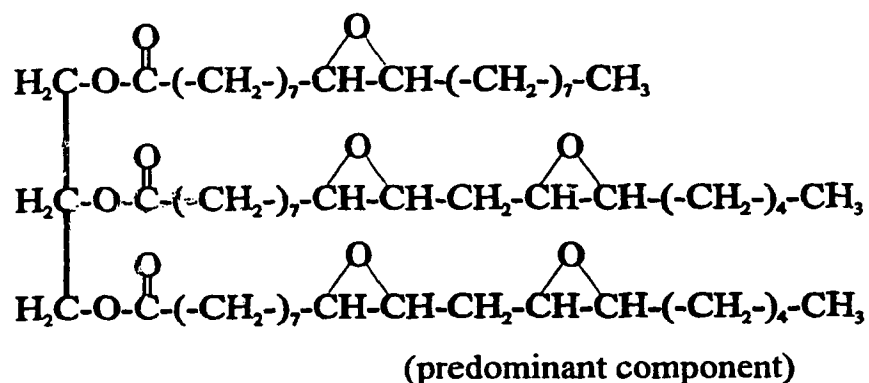
### 6.4-1 Water Distribution in PVC/polymeric-Plasticizer ISE Membranes

Using the SIP a number of polymeric plasticizers, which are available commercially for plasticizing PVC, were tested as components of ion-selective electrode membranes. Table 6.1 lists the polymeric plasticizers studied as well as DOA and identifies some of their relevant parameters, as given by the manufacturer and reference 12. G-25 is a polyester of sebacic acid, and so should be similar in chemical characteristics to DOA, while G-62 is an epoxidized soybean oil and EVA is an ethylene vinyl acetate copolymer. They may be idealized as the structures shown in Figure 6.3 [12-13]. It can be seen from Table 6.1 that G-25 and EVA have very high molecular weight while G-62 has a moderate one. Those polymeric plasticizers are expected to have much higher lipophilicity and lower water extractability in PVC matrix than DOA has.

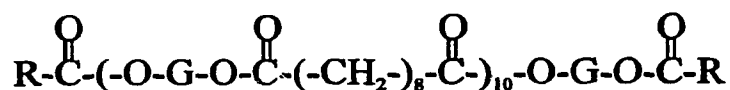
The use of G-25 and G-62 as plasticizer for PVC based ion-selective electrode membranes has been examined by Harrison *et al.* [14]. Both plasticizers

Table 6.1 Types of plasticizers used and their properties.

Plasticizer	Type	Molecular Weight	Weight loss in PVC			Dielectric Constant
			water, 24 hr. at 50°C	hot soapy water, 4 days	5%NaOH, 23°C, 4 days	
<b>DOA</b>	Adipate	370.6	0.10%	/	/	4.13
<b>G-62</b>	Epoxidized soybean oil	1000	/	1.7%	1.0	5.47
<b>G-25</b>	Polyester sebacate	8000	/	1.0%	0.4	/
<b>EVA</b>	Ethylene/ vinyl acetate	>250,000	/	/	/	2.60-2.98



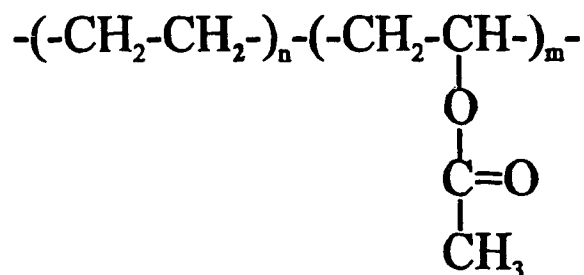
G-62



G-25

where R = alkyl moiety ( $\text{C}_n\text{H}_{2n+1}$ ) in a fatty acid; or rarely an aryl hydrocarbon radical.

G = alkylene bridge ( $\text{C}_n\text{H}_{2n}$ ) of a glycol. The bridge may be linear or branched.



EVA

$$\frac{n}{m} = \frac{55}{45}$$

EVA-45

$$\frac{n}{m} = \frac{30}{70}$$

EVA-70

Figure 6.3 The symbolized structures of polymeric plasticizers [12].

gave functional potassium and ammonium selective electrodes and increased sensor lifetime to varying degrees under accelerated aging conditions (high temperature). They did not yield functional calcium selective electrodes. Christian *et al.* have used EVA-45 alone as an alternative to PVC for the calcium ion-selective electrode preparation [13]. A long lifetime, and improved stability and selectivity of the sensors has been reported.

**Membranes with  $\text{CoCl}_2$**  Membranes with 0.15 wt.% hydrophilic salt,  $\text{CoCl}_2$ , were first examined by SIP. Figures 6.4 to 6.6 show the observed absorbance profiles of light scattering centers after an extended period of water uptake for G62, G25, and EVA-45 plasticized PVC membrane, respectively. It can be seen that the behavior of water in these membranes exhibits the same characteristics that have been observed in conventional PVC/DOA ISE membranes containing  $\text{CoCl}_2$  (see Figure 4.9 in Chapter 4), *i.e.*, an eventual uniform distribution of water across the membranes. The SIP data have also been analyzed using the water uptake models presented in Chapters 1 and 2. Anhydrous  $\text{CoCl}_2$  was added as the water sensitive dye to image the initial stage of water uptake in the membranes. Equation 1.15 was used to fit the bleaching data to obtain the values of apparent diffusion coefficients of dissolved water,  $D_1$ . The calculated results have been summarized in Table 6.2 and compared with the values obtained for PVC/DOA and PVC/NPOE membranes. It was found that the diffusion rates of dissolved water in PVC/polymeric-plasticizer membranes are close to those in PVC/NPOE membranes.

**Membranes with no salt.** Blank membranes consisting of PVC and polymeric plasticizer alone have been examined to evaluate the effect of plasticizer on the distribution of water in the near surface region of membranes. Figure 6.7 shows the light scattering profiles which develop 24 hours after water uptake inside those membranes. It can be seen from Figure 6.7 that there is no surface

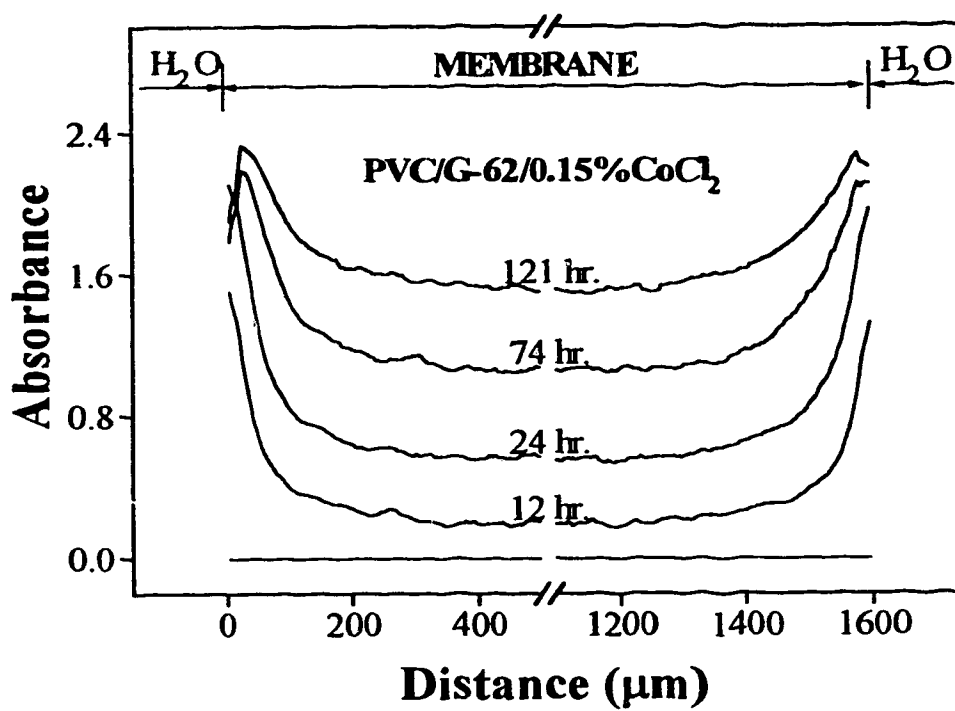


Figure 6.4 Changes in absorbance over 121 hour exposure to water for a PVC/G-62 membrane with 0.15 wt.%  $\text{CoCl}_2$  added.

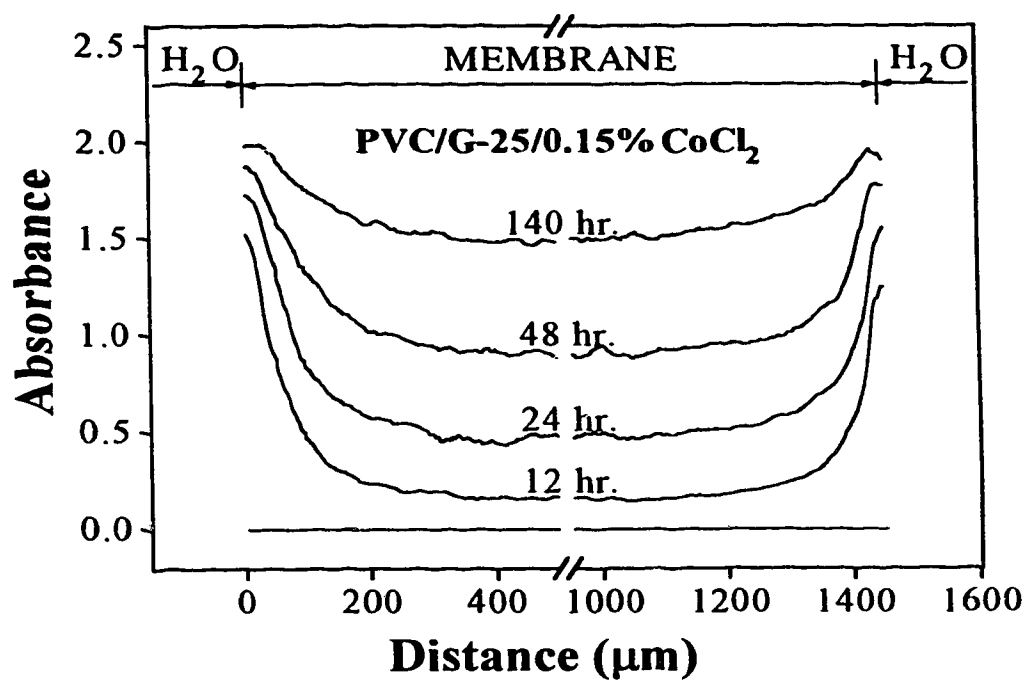


Figure 6.5 Changes in absorbance over 140 hour exposure to water for a PVC/G-25 membrane with 0.15 wt.%  $\text{CoCl}_2$  added.



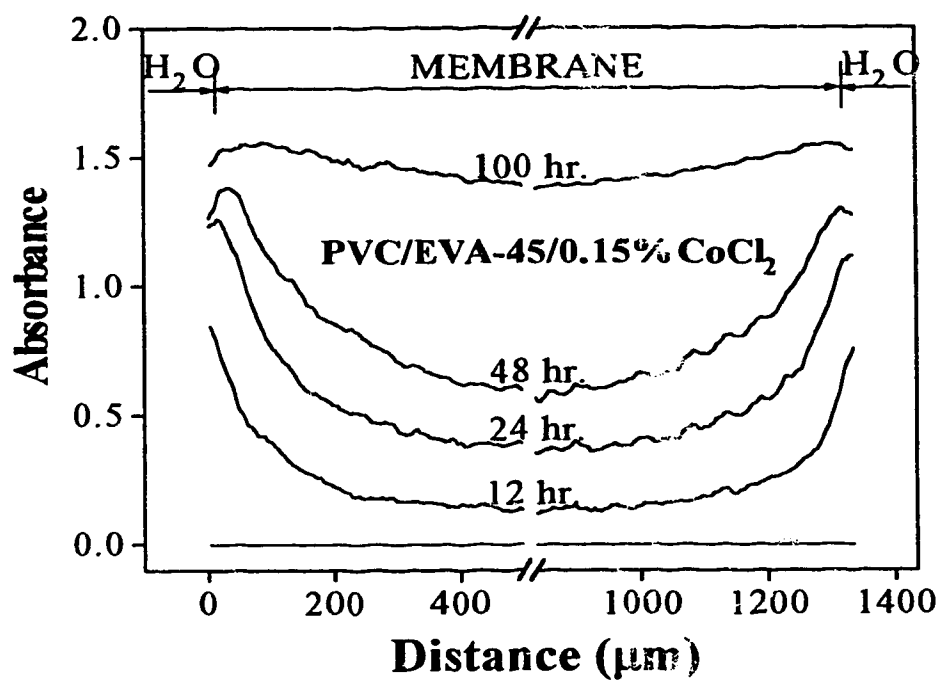


Figure 6.6 Changes in absorbance over 100 hour exposure to water for a PVC/EVA-45 membrane with 0.15 wt.%  $CoCl_2$  added.

Table 6.2 Apparent diffusion coefficients of dissolved water at initial stage of water uptake in PVC based ISE membranes.

MEMBRANES*	$D_1^\dagger$ ( $\times 10^7 \text{ cm}^2/\text{s}$ )	
	(0.33%CoCl <sub>2</sub> )	(0.67%CoCl <sub>2</sub> )
PVC/DOA	7.8	3.2
PVC/NPOE	3.1	1.2
PVC/G-25	2.5	/
PVC/EVA-45	2.3	0.52

\* consisting of 33 wt.% PVC and 67 wt.% plasticizer.

† calculated by fitting SIP data to equation 1.15.

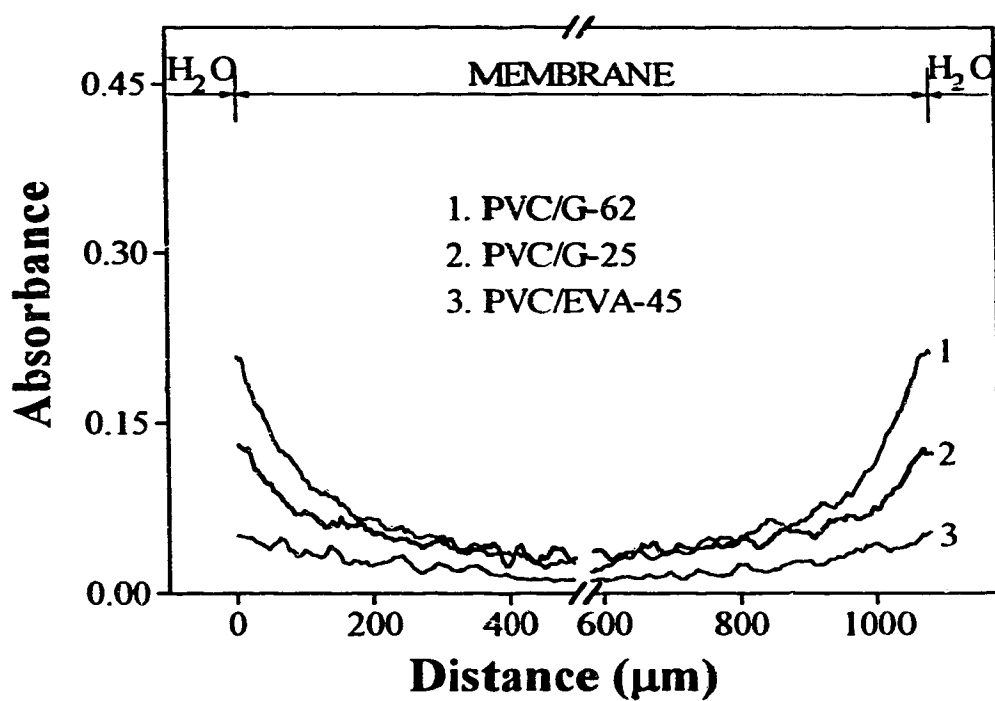
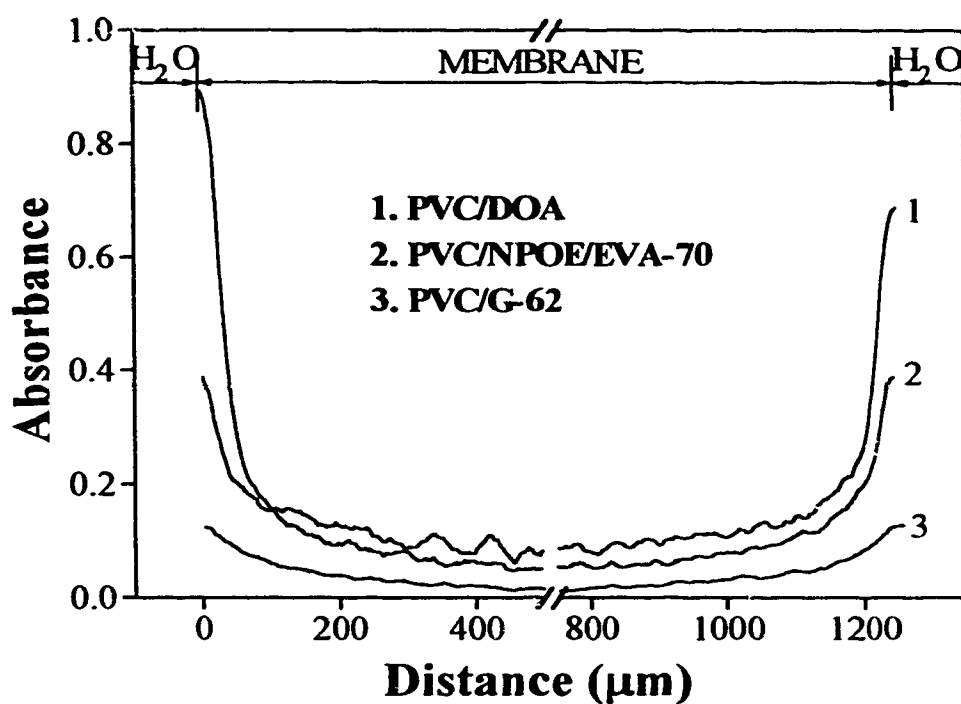


Figure 6.7 Absorbance due to light scattering in PVC/polymeric-plasticizer membranes after 24 hours of water exposure. (1) PVC/G-62; (2) PVC/G-25; (3) PVC/EVA-45.

region which can be distinguished from the membrane bulk in those membranes tested. At any given time, the gradients of water concentration seen in Figure 6.7 can be modeled by Fick's law using a single diffusion coefficient. This indicates a more conventional diffusion process with no surface region present, although the diffusion coefficient does still change over time, consistent with the dual sorption model.

We have also examined membranes consisting of 30 wt.% PVC, 25 wt.% EVA-70, and 45 wt.% NPOE. The observed water distribution after 24 hour of water exposure is shown in Figure 6.8. The profiles for a PVC/DOA and a PVC/G-62 membrane are also included in the figure for a comparison of the distributions of water. It is clear that a water-rich region is present in both the DOA and NPOE/EVA-70 plasticized membranes. The thickness of the region is not identical, but not substantially different, while the magnitude of light scattering is reduced by the added EVA-70. (Chapter 3 shows that PVC/NPOE membranes behave essentially the same as PVC/DOA matrices.) In contrast the G-62 plasticized membrane shows much lower scattering and no real evidence of a surface region that exhibits a different apparent diffusion coefficient.

Results shown in Figures 6.7 and 6.8 clearly demonstrate a correlation between the presence of a water-rich surface region and the nature of the plasticizer, specifically their mobility in the polymer matrix and solubility or extractability into the aqueous phase. We expected that the higher molecular weight plasticizers would be less extractable, creating less void volume in the region near the surface that could be occupied by water droplets. The data in Figures 6.7 and 6.8 show this expectation was borne out. This strongly suggests that the water-rich surface region does result from the loss of plasticizer.



**Figure 6.8** Absorbance due to light scattering in PVC based membranes after 24 hours of water exposure. (1) 32% PVC, 67% DOA, 1% Valinomycin, and 0.1% KTpClPB; (2) 30% PVC, 25% EVA-70, and 45% NPOE; (3) 33% PVC and 67% G-62.

The data for the various polymeric plasticized membranes was analyzed using the approximate model of water uptake introduced in Chapter 1 to obtain apparent diffusion coefficients. Table 6.3 lists the surface and bulk values for the light scattering centers,  $D_2^s$  and  $D_2^b$ , calculated using equations 1.17 and 1.18. It can be seen that  $D_2^b$  at 24 hour is approximately the same for all the membrane compositions. The polymeric plasticizer did not require a separate surface layer and showed much lower absorbance (concentration) at the surface of the membranes. It can also be seen from Table 6.3 that  $D_2^b$  in the polymeric membranes decreased with time, as observed for PVC/DOA membranes. This effect was accounted for by the dual sorption model in PVC/DOA membranes, This model likely also describes the polymerically plasticized membranes, since they will also contain ionic sites, and the same trend is seen for  $D_2^b$ .

#### 6.4-2 Numerical Analysis of Surface Region

Scheme III proposed in Section 6.2 has been used to simulate the water uptake in a PVC/DOA membrane containing 1 wt.% valinomycin and 0.1 wt.% KTpClPB. Several parameters are of importance in the simulation. The values of  $D$  and  $s_0$  for PVC/DOA membranes have been given as  $1.5 \times 10^{-6}$  cm<sup>2</sup>/s and 50.8 mM, respectively, in Chapter 2. The equilibrium concentration of water in droplets in the membrane bulk,  $C_{eq}^b$ , is obtained as 0.24 M from the desorption experiment carried out by A. D. C. Chan *et al.*[4]. The equilibrium concentration of water in droplets at the membrane surfaces,  $C_{eq}^s$ , is estimated from the SIP data for the 24 hour water exposure in Figure 6.8. The maximum absorbance at the membrane surface,  $A_{max}^{surf}$ , is about 0.8 while the average value of the absorbance in the bulk

**Table 6.3** Apparent diffusion coefficients of water at late stages of water uptake in PVC based ISE membranes.

<b>Membranes (wt/wt)</b>	<b>Time (hr.)</b>	<b><math>D_2^{b*}</math> (<math>\times 10^9 \text{ cm}^2/\text{s}</math>)</b>	<b><math>D_2^{s\dagger}</math> (<math>\times 10^{10} \text{ cm}^2/\text{s}</math>)</b>	<b><math>A_{2,\text{max}}</math></b>
PVC/DOA*	24	10.4	1.35	0.95
PVC(30)/EVA-70(45)/NPOE(25)	24	7.52	2.78	0.46
PVC(33)/G-62(67)	24	8.40	/	0.23
	11	13.7	/	0.18
	6	25.4	/	0.13
PVC(33)/G-25(67)	48	3.42	/	0.17
	24	10.1	/	0.15
	13	17.6	/	0.11
PVC(33)/EVA-45(67)	48	2.39	/	0.06
	24	8.16	/	0.05

\* calculated by fitting SIP data to equation 1.17.

† calculated by fitting SIP data to equation 1.18.

\* consisting of 32% PVC, 67% DOA, 1% Valinomycin, and 0.1% KTpCIPB.

region of the membrane,  $A_{\text{mean}}^{\text{bulk}}$ , is about 0.15. Given  $C_{eq}^b$  (0.24 M),  $C_{eq}^s$  can be estimated using equation 2.31 as:

$$C_2 \propto \sqrt{A_2} \quad (2.31)$$

$$C_{eq}^s = C_{eq}^b \frac{\sqrt{A_{\text{max}}^{\text{surf}}}}{\sqrt{A_{\text{mean}}^{\text{bulk}}}} \approx 0.55 \text{ (M)} \quad (6.2)$$

$D_2^s$  can be estimated by fitting SIP data in Figure 6.8 in the surface region using equation 1.17 with  $C$  proportional to  $\sqrt{A}$ . A value of  $1.4 \times 10^{-10} \text{ cm}^2/\text{s}$  ( $D_2^s$  at 24 hour) has been obtained and used in the simulation. The boundary condition used in the calculation is determined by using equation 4.20 to fit X. Li's data on PVC/DOA membranes [15].

$$C^s = C_{eq}^s [1 - \exp(-\beta t)] \quad (4.20)$$

The result is shown in Figure 6.9. The value of  $\beta$  obtained was 0.5. This is for a blank membrane, while the value for  $\beta$  in PVC/DOA membranes containing 0.15%  $\text{CoCl}_2$  was about 0.3 (Chapter 4). Another important parameter in the simulation is the concentration of impurity ions,  $C_i^s$ . It has been generally accepted that PVC based ion-selective membranes contain ionic impurities [16, 17]. Those ionic components may arise from PVC (*i.e.*, polymer-bound initiating groups and reminders of surfactants used during emulsion or suspension polymerization), ionophore, and plasticizer. The concentration of those ions may be taken as about 0.1 mM [18]. Also 0.1 wt.% KTpClPB has been added to the membrane.



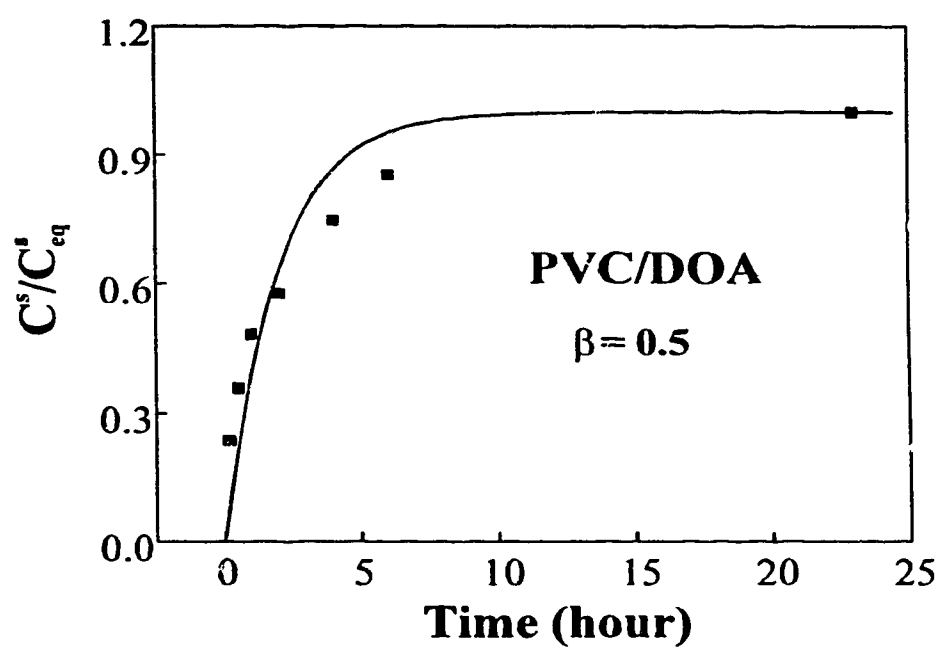


Figure 6.9 The plot of  $C^s / C_{eq}^s$  as a function of time.

Therefore, we estimated  $C_1^s$  as about 4.1 mM. All parameters discussed above are summarized in Table 6.4.

Figures 6.10a and 6.10b show the concentration and absorbance profiles of water developed across the membrane sheet, calculated using Scheme III at various times and the parameters in Table 6.4. The experimental data obtained using the SIP is also given in the figures. In Figure 6.10a, absorbance has been converted to concentration according to equation 2.31. All curves were normalized to the value of maximum concentration (or absorbance) at the water/membrane surface. Compared with the calculation using scheme I in Figure 4.7, it can be seen that the presence and behavior of the highly hydrated surface layer over time are represented by the calculation of Scheme III.

Figures 6.10a and 6.10b demonstrate that the proposed model provides a good simulation of the transport of water inside PVC-based ISE membranes. It should be pointed out that this method can only be taken as a semi-quantitative approach to the problem since an apparent diffusion coefficient,  $D_2^s$ , has been used in the calculations. Moreover, a single  $D_2^s$  has been used because the program written did not allow  $D_2^s$  to vary. As shown in Table 5.1,  $D_2^s$  actually decreases with time. Therefore, using the single value at 24 hour may underestimate the development of the surface layer at the earlier stages of water uptake. The value of  $D_2^s$  at 1 hour ( $1.3 \times 10^{-9}$  cm<sup>2</sup>/s) was obtained from X. Li's thesis [15] and also used in the simulation and the result is shown in Figure 6.11, in which the simulation using  $D_2^s$  at 24 hour and the SIP data are also included for the comparison. It can be seen that there is essentially no difference for the short time between two simulations. The calculation using  $D_2^s$  at 1 hour gives better result for the 6 hour water uptake, but it gives very poor simulation for the 24 hour uptake near the surface region. Figure 6.11 indicates that using  $D_2^s$  for the long time may give

Table 6.4 Parameters of Numerical Calculation (Scheme II)

$D = 1.5 \times 10^{-6} \text{ cm}^2/\text{s}$	$D_2^c = 1.4 \times 10^{-10} \text{ cm}^2/\text{s}$
$s_0 = 50.8 \text{ mM}$	$C_i^c = 4.1 \text{ mM}$
$C_{2,eq}^{bulk*} = 0.19 \text{ M}$	$C_{2,eq}^{surf\dagger} = 0.50 \text{ M}$
$h = 8.27 \text{ }\mu\text{m}$	$\tau = 0.34 \text{ second}$

\*  $C_{2,eq}^{bulk}$  is the equilibrium concentration of water in droplets in the membrane bulk and equals to  $(C_{eq}^{bulk} - s_0)$ .

†  $C_{2,eq}^{surf}$  is the equilibrium concentration of water in droplets at the membrane surfaces and equals to  $(C_{eq}^{surf} - s_0)$ .

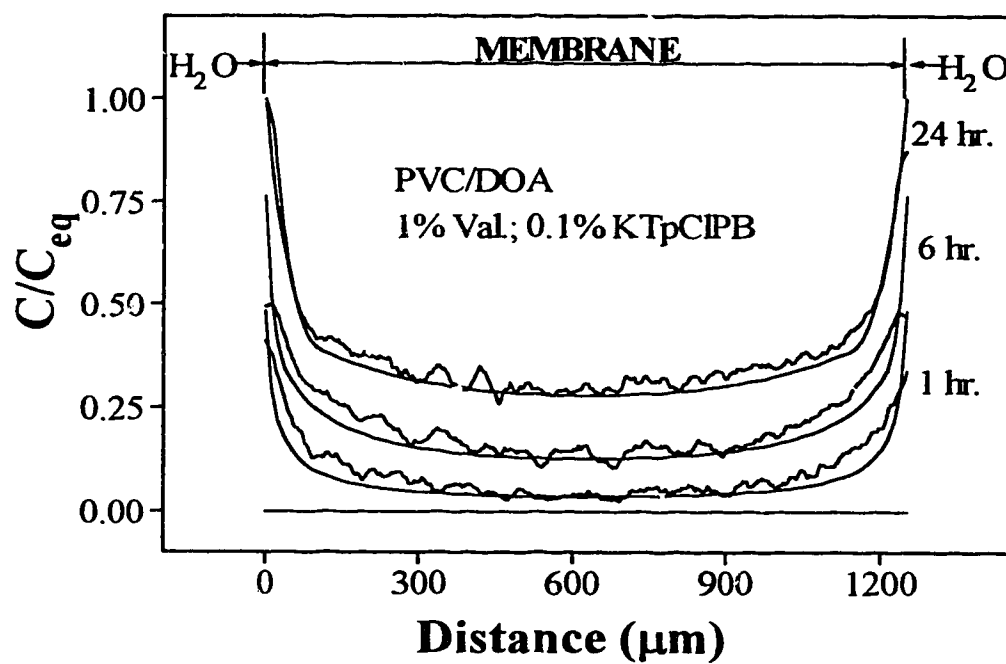


Figure 6.10a Profiles of concentration of water developed through the membrane calculated using Scheme III and observed SIP data.

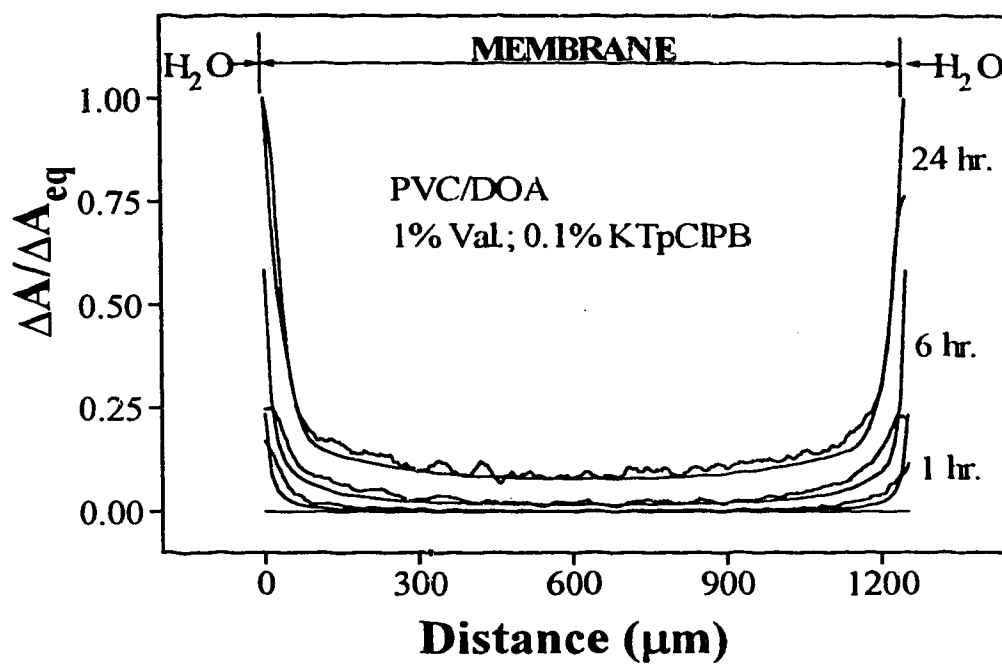


Figure 6.10b Profiles of absorbance of water developed through the membrane calculated using Scheme III and observed SIP data.

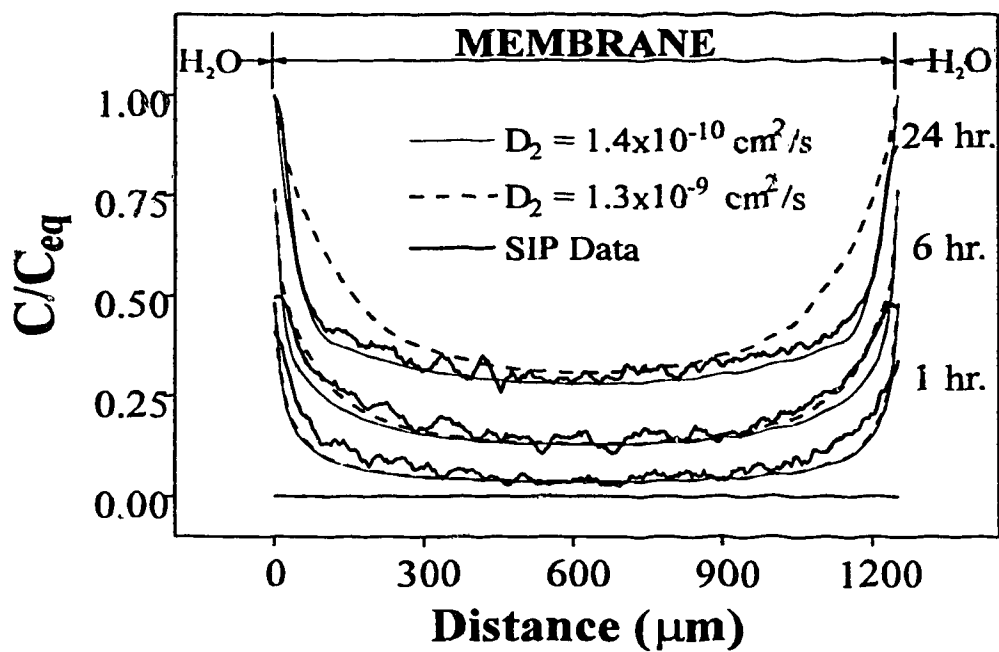


Figure 6.11 Comparison of profiles of concentration of water developed through the membrane calculated using different  $D_2^s$  (see text for the discussion).

better simulations in general. A more accurate simulation could be achieved with a better understanding of the transfer mechanism at the surface region.

The approximate surface sorption model developed in this chapter does not limit the "surface region" to the surface. In fact, after the bulk has all come to equilibrium the further transport of water in the "surface region" becomes a single Fickian type diffusion process. For the value of  $D_2^*$  that described the data in Figure 6.10 reasonably well it is instructive to consider how the surface layer would be predicted to change using this model. Figure 6.12 shows a plot of Fickian diffusion across a membrane with  $D_2^* = 1.4 \times 10^{-10} \text{ cm}^2/\text{s}$ . It is clear that the steady state result is a uniform distribution, but after 12 days an apparent surface region exists that is 200  $\mu\text{m}$  thick, and it takes over 100 days to approach equilibrium.

In Chapter 5 it was shown that the surface region reaches a stable thickness after about 2 days and is unchanged 10 days later. Consequently, the model used here does not truly describe the surface region behavior. Nevertheless, the very slow development of a uniform distribution evidenced by Figure 6.12 shows that the model models a good approximation of the experimental results.

## 6.5 CONCLUSIONS

The behavior of water in the PVC membrane plasticized with polymeric plasticizers was investigated. No surface layer has been observed in these membranes during the water uptake process. This is strong evidence for the hypothesis that loss of plasticizer from ISE membranes to external aqueous solutions is the main source of development of surface layer. As expected,

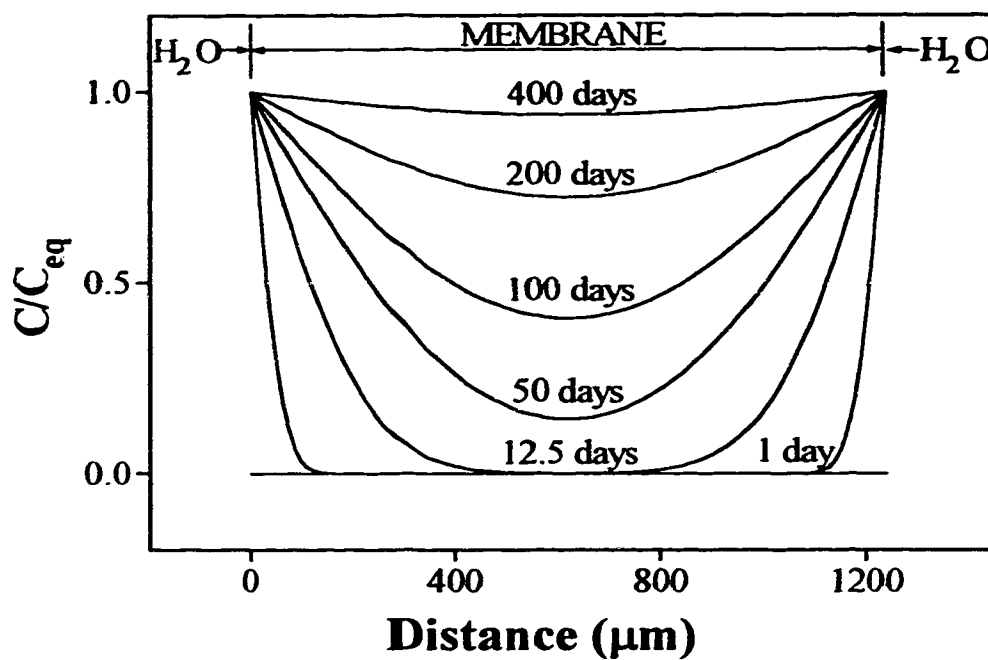


Figure 6.12 Profiles of concentration of water developed through the membrane calculated using Scheme II ( $D_2^* = 1.4 \times 10^{-10} \text{ cm}^2/\text{s}$  and  $l = 1252 \mu\text{m}$ ).



osmotic-pressure effects also govern water uptake ~~inside~~ these membranes, as evidenced by the uniform distribution of water with the hydrophilic salt  $\text{CoCl}_2$  added to the membranes. Based on the observed experimental results, a triple-sorption model has been proposed to describe this unique behavior of water inside ISE membranes. A preliminary result of a numerical analysis of the water transport has also been given and provided a useful means to analyze the process. However, a more detailed model will be needed, with more accurate input parameters, if more accurate descriptions of the curves are to be obtained.

The presence of a water-rich surface layer has important consequences for understanding the behavior of polymer-based ion-selective membrane electrodes, since heterogeneous distributions have not normally been assumed in the theoretical treatments of poly(vinyl chloride)-based systems [4]. The studies presented in this chapter clarify the origin of water-rich surface region inside liquid PVC based ISE membranes. The results also suggest that using polymeric plasticizer may improve the performance of ion sensors made with these membranes, as reported in a few papers [13-14].

## 6.6 REFERENCES

- [1] Harrison, D. J.; Li, X.; Petrovic, S. *In Biosensors and Chemical Sensors. Optimizing Performance Through Polymeric Materials* (P. G. Edelman, J. Wang, Eds), ACS Symposium Series 487, American Chemical Society, Washington DC 1992, Chapter 23, 292-300.
- [2] Li, X.; Petrovic, S.; Harrison, D. J. *Sensors Actuators* 1990, B1, 275.
- [3] Li, X. *Transport Behavior of Water and Ions in Polyvinylchloride Based Ion-Selective Membranes* Ph. D. Thesis, University of Alberta, Edmonton, Canada, 1992.
- [4] Chan, A. D. C.; Li, X.; Harrison, D. J. *Anal. Chem.* 1992, 64, 2512-2517.
- [5] Harrison, D. J.; Teclemariam, A.; Cunningham, L. L. *Anal. Chem.* 1989, 61, 246-251.
- [6] Crank, J. *J. Polymer Sci.* 1953, 11, 151-168.
- [7] Vergnaud, J. M. *Liquid Transport Process in Polymeric Materials*; Prentice-Hall: Englewood Cliffs, NJ, 1991.
- [8] Ziemiński, K. F.; Peppas, N. A. *Journal of Applied Polymer Science* 1983, 28, 1751-1765.
- [9] Taverdet, J. L.; Vergnaud, J. M. *Journal of Applied Polymer Science* 1986, 31, 111-122.
- [10] Aboutaybi, J.; Bouzon, J.; Vergnaud, J. M. *Europ. Polym. J.* 1990, 26, 285-91.
- [11] Vergnaud, J. M. *Liquid Transport Process in Polymeric Materials*; Prentice-Hall: Englewood Cliffs, NJ, 1991.
- [12] Sears, J. K.; Darby, J. R. *The Technology of Plasticizers* John Wiley & Sons, New York, 1982.

- [13] El-Jammal, A.; Bouklouze, A. A.; Patriarche, G. J.; Christian, G. *Talanta* **1991**, *38*, 929-935.
- [14] Harrison, D. J.; Teclemariam, A.; Li, Z.; Li, X.; Chan, A. D. C. *Technical Digest, Hilton Head Island Sens. Actuat. Workshop* **1992**, 50.
- [15] Li, X. *Transport Behavior of Water and Ions in Polyvinylchloride Based Ion-Selective Membranes* Ph. D. Thesis, University of Alberta, Edmonton, Canada, **1992**, p102
- [16] Morf, W. E.; Simon, W. *Helv. Chim. Acta* **1986**, *69*, 1120-1132.
- [17] van den Berg, A.; van der Wal, P. D.; Skowrowska-Ptasinska, M.; Sudholter, E. J. R.; Reinhoudt, D. N. *Anal. Chem.* **1987**, *59*, 2827-2829.
- [18] Armstrong, R. D.; Horvai, G. *Electrochimica Acta* **1990**, *35*, 1-7.

## **Chapter 7**

# **Conclusions**

Poly(vinyl chloride) (PVC) based ion-selective electrode membranes are the key component of both conventional ion-selective electrodes (ISE) and ion-sensitive field-effect transistors (ISFET). Fundamental research on working mechanisms of ISE membranes is essential for solving many existing problems in the applications of those ion sensors. It was the primary goal of this thesis work to study the transport and distribution of water in those membranes, which is believed to play critical roles in the performance of sensors. In this concluding chapter, the contributions model will be summarized. As well, possible future studies designed to further the understanding of the behavior of water in PVC based ISE membranes will be discussed.

## **7.1 SUMMARY OF CONTRIBUTIONS**

The research presented in this thesis is based on the pioneering work of X. Li in our group on the behavior of water inside PVC based ion-selective electrode membranes [1]. The progress made in the present work can be summarized in the following two aspects.

First, our efforts have been directed towards a better understanding of the transport mechanism of water in PVC based ISE membranes. In Chapter 2, an equilibrium water uptake model based on an osmotic pressure argument originally proposed for rubber has been adapted to PVC membranes. Experimental work has been carried out to evaluate this model. The results obtained confirm that osmotic pressure effects are the main driving force for water uptake in PVC based ion-selective electrode membranes. A dual-sorption model has also been proposed to describe the kinetics of water uptake in those membranes. The model has been used to explain the observed experimental data with PVC/DOA membranes. Analysis of SIP data gives the true diffusion coefficient and solubility of water inside PVC based ISE membranes. To evaluate the generality of both theories, we have studied the behavior of water in PVC/NPOE membrane, as well as the effects of salts of lipophilic anions, tetraphenylborate, as shown in Chapter 3. Results are consistent with the proposed models. In Chapter 4, a numerical analysis technique has been used to simulate the transport process described by the dual-sorption model in membranes doped with salts. An explicit-finite-difference method has been developed and the calculated results are in good agreement with the experimental ones. Those results provide further support of the proposed theories of water uptake in PVC based ISE membranes.

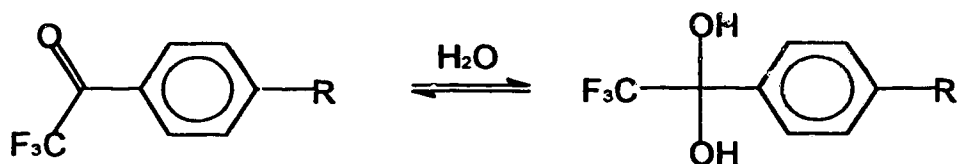
Secondly, efforts have also been directed towards a better understanding of the water-rich surface region observed in PVC based ISE membranes. In Chapter 5, the effects of additives on this highly hydrated surface layer have been studied in detail. Results show that the surface layer thickness is not strongly dependent on the nature of conventional plasticizers such as DOA or NPOE. However, additives to the membrane play a significant role in establishing the steady-state water distribution and determining whether or not it is uniform. The studies of water distribution inside PVC based membranes plasticized with polymeric plasticizers

have provided evidence that loss of plasticizer from the membrane to the external aqueous solution is a main source of the water-rich surface layer. An uptake model incorporating this surface layer has been proposed. Results of numerical analysis show a reasonably good simulation of experimental data.

Results presented here as well as the previous work of SIP [1], NMR, mass desorption [2], and electrical impedance studies [3] in our group have provided a much more detailed picture of water inside PVC based ion selective membranes. This level of understanding of the behavior of water in membrane phase should prove helpful in the designing of solid contact, membrane based ion sensors, and those fabricated using microelectronics techniques.

## 7.2 FUTURE STUDIES

The spatial imaging photometer (SIP) has provided a unique means of quantitatively probing the internal concentration profiles of water inside PVC based ISE membranes with high spatial resolution. In order to observe the initial water uptake process, dehydrated  $\text{CoCl}_2 \cdot 6\text{H}_2\text{O}$  has been used as a water-sensitive dye. This hydrophilic salt will disturb the system of ISE membrane studied. Less disturbing dye for water would be desirable. For example, trifluoroacetophenones, which have been used in optical humidity sensors [4], could be suitable alternative dyes for the studies of water transport in ISE membranes. Upon contacting with water, those compounds undergo reversible hydration [5]:



This interaction leads to a loss in the electron delocalization of the carbonyl group with the aromatic ring and, therefore, to a hypsochromic shift of the absorbance band. It is also possible to immobilize those compounds by attachment to the polymer matrix [6]. This could give much more information on water transport inside membranes.

Using the SIP method and the dual-sorption model, we have determined the true diffusion coefficients of water inside PVC based ISE membranes,  $D$ , which has not previously been reported. The accuracy of  $D$  is very important in numerical simulations. Another possible method to measure  $D$  is the technique of pulsed field gradient spin-echo (PGSE)  $^1\text{H}$  NMR, which has been used to measure the diffusion coefficient of water in perfluorosulfonate ionomeric membranes [7]. With this technique, we will be able to substantiate the values of  $D$  obtained with the SIP method, and therefore, the dual-sorption model proposed. It is also possible to use this technique to measure the diffusion coefficients of other components of ISE membrane, such as, ionophores, tetraphenylborates, and plasticizers.

In formulating the water uptake model, we have assumed that water droplets develop during the uptake process. NMR studies by A. D. C. Chan have provided evidence of the droplets. However, while light scattering centers are readily observed by microscopy their composition is not readily determined. It is also interesting to know the distribution of size of these droplets. This task may be carried out by the state-of-art microscopic techniques [8-9]. Among them, confocal laser scanning microscopy (CLSM) could be the best choice for the observation of water droplets since CLSM has the advantage of non-destructive imaging and the ability to image object inside the membrane matrix [8, 10]. In such a microscope, an object is illuminated with a small (diffraction limited) spot derived from a focused laser beam. The illuminated spot is viewed with a spatially

restricted optical system so that only signals emanating from this spot are detected. An image of the complete specimen is built up by a raster scan. Therefore, CLSM offers improved rejection of out-of-focus noise and greater resolution than conventional imaging. Recently, CLSM has been used to determine the distribution of pH, free  $\text{Ca}^{2+}$ , electrical potential, and volume inside cultured adult rabbit cardiac myocytes [11]. With an appropriate fluorescent dye for water, it is possible to use CLSM to directly imaging the water droplets inside PVC based membranes.

On the basis of our observations of water inside PVC based ISE membranes, the drifting problem of ion sensors may be related to the transport process of water. By inserting reference electrodes into an optical cell, we could monitor the drifting and water transport simultaneously, and then correlate those two processes to each other. P. Glavina has shown that such measurements are possible [12]. If the correlation exists, then an investigation of method to control the water uptake process would be very useful in improving the performance of ion sensors made with PVC based ISE membranes.

Finally, further investigations of the surface layer should be carried out to gain a better understanding of mechanism of double-transfer (plasticizer out and water in), which is essential for the development of a quantitative water uptake model in PVC based ion-selective electrode membranes.



### 7.3 REFERENCES

- [1] Li, X. *Transport Behavior of Water and Ions in Polyvinylchloride Based Ion-Selective Membranes* Ph.D. Thesis, University of Alberta, Edmonton, Canada, 1992.
- [2] Chan, A. D. C. *Analysis of Electrical and Physical Properties of Ion-Selective Liquid Membranes* Ph.D. Thesis, University of Alberta, Edmonton, Canada, 1992.
- [3] Verpoorte, E. *Analysis of The Permeability and Behavior of Dissociable Species in Ion-Selective Membranes* Ph.D. Thesis, University of Alberta, Edmonton, Canada, 1991.
- [4] Wang, K.; Seiler, K.; Haug, J. P.; Lehmann, B.; West, S.; Hartman, K.; Simon, W. *Anal. Chem.* 1991, 63, 970-974.
- [5] Behringer, Ch.; Lehmann, B.; Haug, J. P.; Seiler, K.; Morf, W. E.; Simon, W. *Anal. Chim. Acta* 1990, 233, 41-47.
- [6] Rosatzin, T.; Holy, P.; Seiler, K.; Rusterholz, B.; Simon, W. *Anal. Chem.* 1992, 64, 2029-2035.
- [7] Zawodzinski, T.; Neeman, M.; Sillerud, L. O.; Gottesfeld, S. *J. Phys. Chem.* 1991, 95, 6040-6044.
- [8] Herman, B.; Jacobson, K. *Optical Microscopy for Biology* Wiley & Sons, Inc., New York, 1989.
- [9] Hayat, M. A. *Principles and Techniques of Electron Microscopy* MacMillan Press, Hong Kong, 1989.
- [10] White, J. G.; Amos, W. B.; Fordham, M. *J. Cell Biol.* 1987, 105, 41-48.
- [11] Chacon, E.; Reece, J. M.; Nieminen, A. L.; Zahrebelski, G.; Herman, B.; Lemasters, J. J. *Biophysical Journal* 1994, 66, 942-952.
- [12] Glavina, P. Ph.D. Thesis, to be completed.

## **APPENDIX A. COMPUTER PROGRAMS FOR SIP EXPERIMENTS**

The program used to acquire and display the experimental data using a Compaq 286, i.e., *START2.POT*, was created by X. Li and D. J. Harrison\*. Two new ASYST programs have been written in order to analyze the data on a PC486 using the **Origin** software package.

SIP data were originally saved as an ASYST file in the floppy disk. Each file consists of two sets of data: SCAT.DATA and REF for two light sources of different wavelength. These data must be saved separately using SV.POT (Program A.1) before they can be transferred to text files using FILETRAN.PRG (Program A.2). The following example describes how to transfer a SIP data file "WATER" to text files:

► **To save the SIP data file as two separate ASYST files to the floppy disk:**

1. Load *START2.POT* and *SV.POT* by typing the following at the ASYST command prompt:

```
OK LOAD START2.POT           ↵
OK LOAD SV.POT               ↵
```

2. Read the SIP data file from drive A by typing the following at the ASYST command prompt:

```
OK FILE.READA               ↵
"NAME OF FILE TO READ"     WATER ↵
```

---

\* Li, X. Ph.D. Thesis, University of Alberta, Edmonton, 1992, Appendix A.

3. Save SCAT.DATA to drive A by typing the following at the command prompt:

```

OK SAVESB                                ↵
"INPUT FILENAME" :=      WATER1          ↵

```

4. Save REF to drive A by typing the following at the command prompt:

```

OK SAVEFB                                ↵
"INPUT FILENAME" :=      WATER2          ↵

```

► **To transfer the ASYST files to text files:**

A version of ASYST is saved under the name FILETRAN, which contains all the words defined in the program FILETRAN.PRG. It may be loaded from DOS as described below:

1. Run the transferring program by typing the following at the DOS and ASYST command prompt:

```

> FILETRAN                                ↵
OK GO                                     ↵

```

2. Press F1 key to read the ASYST files.
3. Press F4 key to display the data.
4. Press F3 key to transfer the files:

```

OK  "FILENAME"      WATER1      ↵
    "FILENAME"      WATER2      ↵
                                ..... ↵
                                END    ↵

```

5. Press F10 key to quit. All ASYST files will be transferred to text files and saved in drive C with the names as TWATER1 and TWATER2, etc. These text files can be imported to an Origin file for the data analysis.

➤ **To import a text file to an Origin file:**

1. Open an Origin worksheet in Windows.
2. Open the dialog box "ASCII Import Options" by clicking **File** → **Import** → **Options....**
3. Choose **New Columns** in the box of "Import into worksheet as" and then click **Import Now...**
4. Highlight the data file you want from the **File Open** box and click **OK**. The file will be imported to the first column of the worksheet. For more instructions, see pages 129-133 of Reference Manual of Origin.

➤ **To plot and analyze data in an Origin file:**

Detailed instructions have been given in pages 72-99 of the Reference Manual of Origin for plotting data, and in pages 104-121 of the Reference Manual for data analysis. A few hints are given as follows:

1. The original transmittance raw data are imported directly to an Origin file. Absorbance calculation and reference subtraction can be done easily in Origin (see p166).
2. A template file, **RAWDATA.OTW**, has been created and saved for the data import and absorbance calculation. This file can be modified (see p128).

3. To flip over the x-axis, reverse the data sequence of the column **X** in the worksheet.
4. To set x-axis (or y-axis) scale type and increment, tick labels and marks, double click the axis and open the box of "**The X Axes**" and choose your options (see p84).
5. To put a break in an Origin plot, open the sub-box of "**Axis Break**" in the "**The X Axis**" box and choosing your options (see p96).
6. To get rid of data outside of the membrane, highlight the data in the work sheet and choose the **DELETE** command in the **Edit** menu (see p137).
7. The data plot can be fitted with water uptake models (see p109). Several curve fitting functions for the approximate water uptake models have been created and built in the **Fit** Menu. Table A1 shows these functions and corresponding parameters with units.

**PROGRAM A.1:**

\ ASYST FILE:       **SV.POT**

\ This program saves original SIP data as well as calculated data files individually  
 \ to the floppy disk in driver A.

\                   Created by: Zhong Li  
 \                               June, 1993

\ -----

**: FILE.FORMC**

FILE.TEMPLATE

REAL DIM[ 511 ] SUBFILE

END

;

**: CREATE.DATA.FILEC**

FILE.FORMC

CR ." NAME OF FILE TO WRITE ? "

"INPUT FILENAME " :=

\ " A:" FILENAME "CAT " .DAT" "CAT FILENAME "=

\ FILENAME DEFER> FILE.OPEN

\ CR CR ." FILE ALREADY EXISTS USE IT ? (Y/N) "

\ Y/N? YES.NO 0 =

\ IF FILE.CLOSE ESCAPE

\ THEN FILE.CLOSE

\ FILE.FORMC

FILENAME DEFER> FILE.CREATE

;

**: SAVEAB**

CREATE.DATA.FILEC

FILENAME DEFER> FILE.OPEN

1 SUBFILE ANAL.DATA ARRAY>FILE

FILE.CLOSE

.

**: SAVEABSM**

```
CREATE.DATA.FILEC  
FILENAME DEFER> FILE.OPEN  
1 SUBFILE ABSO ARRAY>FILE  
FILE.CLOSE
```

;

**: SAVEXD**

```
CREATE.DATA.FILEC  
FILENAME DEFER> FILE.OPEN  
1 SUBFILE XD ARRAY>FILE  
FILE.CLOSE
```

;

**: SAVESB**

```
CREATE.DATA.FILEC  
FILENAME DEFER> FILE.OPEN  
1 SUBFILE SCAT.DATA ARRAY>FILE  
FILE.CLOSE
```

;

**: SAVEFB**

```
CREATE.DATA.FILEC  
FILENAME DEFER> FILE.OPEN  
1 SUBFILE REF ARRAY>FILE  
FILE.CLOSE
```

**PROGRAM A.2:**

**\ ASYST FILE:        FILETRAN.PRG**

**\ This program is written for transferring ASYST data files to text files.**

**\ The maximum number of files which could be handled at one time is 40.**

**\ After the last file name input, type END to respond the ENTER FILENAME.**

**\                      Created by:    Zhong Li**

**\                                      June, 1993**

**\ -----**

**REAL DIM[ 511 ] ARRAY SPEC                      \ For the working copy of the file.**

**DIM[ 511 ] ARRAY SPEC2**

**12 STRING FILENAME**

**DIM[ 41 , 12 ] STRING.ARRAY FILE.NAME    \ Auto data transferring**

**INTEGER SCALAR M**

**\ TEXT WINDOWS**

**13 0 24 38 WINDOW {FKEYS}**

**13 42 24 78 WINDOW {NOTES}**

**: PORT1                                      \ Top 1/2 of the screen**

**NORMAL.COORDS 1 0.22 VUPOINT.SIZE 0 0.78 VUPOINT.ORIG**

**VUPOINT.CLEAR**

**;**

**: PORT2                                      \ Bottom 1/2 of the screen**

**NORMAL.COORDS 1 0.22 VUPOINT.SIZE 0 0.50 VUPOINT.ORIG**

**VUPOINT.CLEAR**

**;**

**: CURSORS                                      \ Activates the cursors for on screen readout**

**NORMAL.COORDS ARRAY.READOUT .5 .9 READOUT>POSITION**

**;**

**: PLOTA**

**VERTICAL GRID.OFF HORIZONTAL GRID.OFF AXIS.FIT.OFF**



```

WORLD.COORDS 0 1024 WORLD.SET Y.AUTO.PLOT CURSORS
;

: PLOT.SPECTRUM
  PORT1 SPEC PLOTA
  PORT2 SPEC2 PLOTA
;

: GET.FILENAME
  0 M := {NOTES}
  BEGIN
    1 M + M :=
    ." ENTER FILENAME " "INPUT
    FILE.NAME "[ M ] " := CR
    FILE.NAME "[ M ] " END " :=
  UNTIL
  M 1 - M :=
  SCREEN.CLEAR STACK.CLEAR
;

: GET.NAME                                     \ For single file reading
  {NOTES} SCREEN.CLEAR ." ENTER FILENAME " CR "INPUT FILENAME " :=
  CR
;

: RAW.DATA.TEMPLATE
  FILE.TEMPLATE
  REAL DIM[ 511 ] SUBFILE
  REAL DIM[ 511 ] SUBFILE
  END
;

: SAVE.RAW.DATA
  RAW.DATA.TEMPLATE {NOTES} SCREEN.CLEAR GET.NAME
  FILENAME DEFER> FILE.CREATE FILENAME DEFER> FILE.OPEN
  SPEC 1 SUBFILE ARRAY>FILE

```

```

SPEC2 2 SUBFILE ARRAY>FILE
FILE.CLOSE
CR CR ." FILE - " FILENAME "TYPE ." IS SAVED! "

```

```
;
```

#### : READ.DATA

```

FILENAME DEFER> FILE.OPEN
SPEC 1 SUBFILE FILE>ARRAY
SPEC2 2 SUBFILE FILE>ARRAY
FILE.CLOSE
CR CR ." FILE - " FILENAME "TYPE ." IS READ! "

```

```
;
```

#### : READ.RAW.DATA

```
1 M := {NOTES} SCREEN.CLEAR GET.NAME READ.DATA
```

```
;
```

#### : SPEC.PLOT

\ Plot spec on the top 1/2 of the screen

```

{NOTES} SCREEN.CLEAR
1 M <> IF
  READ.RAW.DATA
THEN
PLOT.SPECTRUM {NOTES} SCREEN.CLEAR

```

```
;
```

#### : DATA.TRANS

\ Transfer data files to text

```

GET.FILENAME
M 1 + 1 DO
FILE.NAME "[ I ] FILENAME ":= READ.DATA
" T" FILENAME "CAT FILENAME ":=
FILENAME DEFER> OUT>FILE
{NOTES} 512 1 DO
  SPEC [ I ] . CR
  LOOP
  OUT>FILE.CLOSE
  LOOP

```

```

512 1 DO
SPEC2 [ 1 ] . CR
LOOP
OUT>FILE.CLOSE
{NOTES} SCREEN.CLEAR
M . ." DATA.TRANSFERS HAVE BEEN DONE! "
;

: MAIN.MANU
{NOTES} SCREEN.CLEAR
{FKEYS} SCREEN.CLEAR
." F1> READ DATA FROM DISK " CR
." F2> SAVE DATA ONTO DISK " CR
." F3> TRANSFER DATA TO TEXT FILE " CR
." F4> PLOT SPECTRUM ON SCREEN " CR
." F5> NOP " CR
." F6> NOP " CR
." F7> NOP " CR
." F8> NOP " CR
." F9> NOP " CR
." F10> LEAVE MANU "
;

: GET.OUT
{NOTES} NORMAL.DISPLAY CLEAR.FUNCTION.KEYS
;

: MAIN.KEYS
F1 FUNCTION.KEY.DOES READ.RAW.DATA
F2 FUNCTION.KEY.DOES SAVE.RAW.DATA
F3 FUNCTION.KEY.DOES DATA.TRANS
F4 FUNCTION.KEY.DOES SPEC.PLOT
F5 FUNCTION.KEY.DOES NOP
F6 FUNCTION.KEY.DOES NOP
F7 FUNCTION.KEY.DOES NOP
F8 FUNCTION.KEY.DOES NOP

```

F9 FUNCTION.KEY.DOES NOP  
F10 FUNCTION.KEY.DOES ESCAPE

;

**: GO**

0 M :=

GRAPHICS.DISPLAY STACK.CLEAR MAIN.KEYS MAIN.MANU

INTERPRET.KEYS

ONESCAPE: GET.OUT {NOTES}

ONERR: BELL INTERPRET.KEYS

;

BELL BELL

**Table A1. Curve Fitting for Water Uptake**

Function	Model	Parameter
Stage1	$\Delta A_1 = \Delta A_{1,\max} \left( 1 - \operatorname{erf} \frac{x}{2\sqrt{D_1 t}} \right)$	P1: $\Delta A_{1,\max}$ P2: $D_1$ P3: t in sec. x: $\mu\text{m}$
Stage2	$\Delta A_2 = \Delta A_{2,\max} \left( 1 - \frac{1}{\operatorname{erf} \frac{x_k}{2\sqrt{D_2 t}}} \operatorname{erf} \frac{x}{2\sqrt{D_2 t}} \right)$	P1: $\Delta A_{2,\max}$ P2: $D_2$ P3: t in hr. P4: $x_k(\mu\text{m})$ x: $\mu\text{m}$
Bulk (n=5)	$\Delta A = \Delta A_{\max} \left\{ 1 - \frac{4}{\pi} \sum_{n=1}^{\infty} \frac{1}{(2n-1)} \exp \left[ -\frac{(2n-1)^2}{d^2} \pi^2 D t \right] \sin \left[ \frac{(2n-1)}{d} \pi x \right] \right\}$	P1: $\Delta A_{\max}$ P2: D P3: t in sec. P4: d(cm) x: cm
Bulk1 (n=6)	$\Delta A = \Delta A_{\max} \left\{ 1 - \frac{4}{\pi} \sum_{n=1}^{\infty} \frac{1}{(2n-1)} \exp \left[ -\frac{(2n-1)^2}{d^2} \pi^2 D t \right] \sin \left[ \frac{(2n-1)}{d} \pi x \right] \right\}$	P1: $\Delta A_{\max}$ P2: D P3: t in sec. P4: d(cm) x: cm
Bulk2 (n=6)	$\Delta A = \Delta A_{\max} \left\{ 1 - \frac{4}{\pi} \sum_{n=1}^{\infty} \frac{1}{(2n-1)} \exp \left[ -\frac{(2n-1)^2}{d^2} \pi^2 D t \right] \sin \left[ \frac{(2n-1)}{d} \pi x \right] \right\}$	P1: $\Delta A_{\max}$ P2: D P3: t in sec. P4: d(cm) x: $\mu\text{m}$
Bulk3 (n=11)	$\Delta A = \Delta A_{\max} \left\{ 1 - \frac{4}{\pi} \sum_{n=1}^{\infty} \frac{1}{(2n-1)} \exp \left[ -\frac{(2n-1)^2}{d^2} \pi^2 D t \right] \sin \left[ \frac{(2n-1)}{d} \pi x \right] \right\}$	P1: $\Delta A_{\max}$ P2: D P3: t in sec. P4: d(cm) x: $\mu\text{m}$

## **APPENDIX B. COMPUTER PROGRAMS FOR NUMERICAL SIMULATIONS**

Several FORTRAN programs have been written to simulate solutions of the diffusion equation in Chapter 2. *PROGRAM B.1* can be used to calculate the analytical solution, equation 1.13, while *PROGRAMS B.2-B.6* can be used to simulate the numerical solutions. Examples of the calculations are given as follows:

### **Program B.1**

► To calculate the analytical solution of

$$C_1(x, t) = C_1^0 \left\{ 1 - \frac{4}{\pi} \sum_{n=1}^{\infty} \frac{1}{(2n-1)} \exp \left[ -\frac{D_1 (2n-1)^2 \pi^2 t}{l^2} \right] \sin \frac{(2n-1)\pi x}{l} \right\} \quad (1.13)$$

1. Run the program ABXT.FOR by typing the following at the DOS command prompt:

ABXT > (FILENAME TO BE SAVED)

J

2. Input the parameters successively :

$n$ ,  $C_1^0$  (in any units desired),  $D_1$  (cm<sup>2</sup>/s),  $t$  (second),  $l$  (cm)

3. Press ENTER to start the calculation. The calculated result will be saved as a text file which can be imported to an Origin file for the display of the result.

### Programs B.2, B3, B5 & B.6

#### ► To simulate the numerical solution (Scheme I):

1. First you save the parameters in file DATA. Input the parameters by typing the following at the DOS command prompt:

**EDIT DATA**

┘

2. Type the values of the parameters in the following sequence:

$s_0$  (mM),  $C_i^s$  (mM),  $D$  (cm<sup>2</sup>/s),  $C_{cq}^s(x=0)$  (mM),  $C_{cq}^s(x=l)$  (mM)  
 $l$  (cm), # of data point,  $C(t=0)$  (mM),  $\tau$  (s)  
 final time (s), how many curves to save  
 times for each curve

(note that:  $\tau \leq \frac{l^2}{2Dn^2}$  is required)

For example:

50.8, 45.8, 1.5E-6, 2900., 2900.  
 0.0827, 101, 0.0, 0.34  
 432000., 8  
 600., 1800., 3600., 10800., 21600., 43200., 86400., 172800.  
 (The positions of . and , are critical.)

3. Save the DATA file and quit.
4. Start the simulation by typing the following at the DOS command prompt:

**ZHONG1**

J

The calculated curves will be saved in a single text file named RESULT, which can be imported to an Origin file for the display of the result.

**Programs B.4****► To simulate the numerical solution (Scheme II):**

1. First you save the parameters in file DATA. Input the parameters by typing the following at the DOS command prompt:

**EDIT DATA**

J

2. Type the values of parameters as the following sequence:

$s_0$  (mM),  $C_i^s$  (mM),  $D$  (cm<sup>2</sup>/s),  $C_{eq}^b(x=0)$  (mM),  $C_{eq}^b(x=l)$  (mM),

$C_{eq}^s(x=0)$  (mM),  $C_{eq}^s(x=l)$  (mM),  $D_2^s$  (cm<sup>2</sup>/s)

$l$  (cm), # of data point,  $C(t=0)$  (mM),  $\tau$  (s)

final time (s), how many curves to save  
times for each curve

(note that:  $\tau \leq \frac{l^2}{2Dn^2}$  is required)

For example:

50.8, 4.1, 1.5E-6, 190., 190., 500., 500., 1.0E-10

0.0200, 26., 0.0, 0.050

86400., 7

600., 1800., 3600., 7200., 14400., 21600., 43200.

(The positions of . and , are critical.)



3. Save the DATA file and quit.
4. Start the simulation by typing the following at the DOS command prompt:

**ZHONG3**

」

The calculated curves will be saved in a single text file named RESULT, which can be imported to an Origin file for the display of the result.

**PROGRAM B.1:**

C -----  
 C FORTRAN FILE:           **ABXT.FOR**  
 C THIS IS A FORTRAN PROGRAM TO SIMULATE THE ANALYTICAL  
 C SOLUTION OF INFINIT SERIES (equation 1.13) WHEN THE PARAMETERS  
 C ARE GIVEN.

C                           Created by:   Zhong Li  
 C   October, 1993

C -----

```

PROGRAM REFINDEX
parameter(pi=3.14159)
real*8 Ab0,d,D1,t,x1,x2,dltx,Abxt
C   d in cm; t in sec; x in cm; x1=0; x2=/
write(*,*)' Please enter n:'
read(*,*)n
write(*,*)' Please enter the A_b^0, d, D, t:'
read(*,*)Ab0,d,D1,t
write(*,*)' Please enter the range of x:'
read(*,*) x1,x2
dltx=(x2-x1)/1000
do i=0,1000
    x=x1+i*dltx
    Abxt=0
    do j=1,n
        n2=2*j-1
        Abxt=Abxt+1./n2*dexp(-(n2*pi/d)**2*D1*t)*dsin(n2*pi*x/d)
    enddo
    Abxt=Ab0*(1-4*Abxt/pi)
c   write(*, '(a,f8.3,10x,a,f8.3)') x='x',x,'A_b(x,t)='Abxt
    write(*, '(f9.3,10x,f8.3)')x,Abxt
enddo
stop
end
  
```

**PROGRAM B.2:**

PROGRAM MAIN

```

C -----
C  FORTRAN File:      ZHONG1.FOR
C  THIS A FORTRAN PROGRAM TO SIMULATE THE NUMERICAL RESULTS
C  OF DUAL-SORPTION MODEL FOR BULK REGION WITH A VARYING
C  SURFACE CONCENTRATION (SCHEME I)

```

```

C              Created by:  Zhong Li
C                      Feburary, 1994
C -----

```

```

      DIMENSION C(10000),C1(10000),SK(20)
      OPEN(6,FILE='DATA')
      OPEN(7,FILE='RESULT')
C
      READ(6,*) A,B,D,G1,G2
      WRITE(7,100) A,B,D,G1,G2
      READ(6,*) X,NX,CI,TH
      WRITE(7,200) X,NX,CI,TH
      READ(6,*) T0,NT
      WRITE(7,300) T0,NT
      READ(6,*) (SK(I),I=1,NT)
      WRITE(7,500) (SK(I),I=1,NT)
C
      T=0.0
      H=X/(NX-1)
      DO 10 I=1,NX
10    C1(I)=CI
1    T=T+TH
      DO 20 I=1,NX
      IF(I.EQ.1) THEN
      IF (MOD(INT(T/TH),1000).EQ.0) WRITE(0,50) T

```

```

      TT=T/10000.
      C(1)=G1*(1.0-EXP(-TT))
ELSE IF(I.EQ.NX) THEN
      TT=T/10000.
      C(NX)=G2*(1.0-EXP(-TT))
ELSE
      DD=D*TH/(H*H)
      F1=A*C1(I-1)/(C1(I-1)+B)
      F2=A*C1(I)/(C1(I)+B)
      F3=A*C1(I+1)/(C1(I+1)+B)
      CC=DD*(F1-2.0*F2+F3)+F2+C1(I)
      S=A+B-CC
      SS=S*S+4.0*B*CC
      C(I)=0.5*(-S+SQRT(SS))
END IF
20  CONTINUE
    IF(T.GE.T0) THEN
      WRITE(7,400) T,(C(I),I=1,NX)
    ELSE
      DO 30 I=1,NX
30      C1(I)=C(I)
50      FORMAT(1X,'T=',E20.5)
      J1=0
      DO 40 J=1,NT
      IF (ABS(T-SK(J)).LE.0.17) J1=J1+1
40  CONTINUE
      IF(J1.EQ.1) WRITE(7,400) T,(C(I),I=1,NX)
      GO TO 1
    END IF
C
100  FORMAT(1X,'A=',F15.9,2X,'B=',F15.9,2X,'D=',E15.9,2X,'G1=',
*      F15.9,2X,'G2=',F15.9)
200  FORMAT(1X,'X=',F15.9,2X,'NX=',I5,2X,'CI=',F15.9,2X,'TH=',
*      F15.9)
300  FORMAT(1X,'T0=',F15.9,2X,'NT=',I5)
400  FORMAT(5X,'CONCENTRATION VALUE ', 'T=',E20.9/(2X,F15.9))

```

```
500  FORMAT(1X,'SPECIFIC TIME TO PRINT OUT'/4(1X,E20.9))  
      STOP  
      END
```

**PROGRAM B.3:****PROGRAM MAIN**

```

C -----
C  FORTRAN File:      ZHONG2.FOR
C  THIS A FORTRAN PROGRAM TO SIMULATE THE NUMERICAL RESULTS
C  OF DUAL-SORPTION MODEL FOR BULK REGION WITH A CONSTANT
C  SURFACE CONCENTRATION (SCHEME I)

```

```

C              Created by:  Zhong Li
C                      Feburary, 1994
C -----

```

```

      DIMENSION C(10000),C1(10000),SK(20)
      OPEN(6,FILE='DATA')
      OPEN(7,FILE='RESULT')
C
      READ(6,*) A,B,D,G1,G2
      WRITE(7,100) A,B,D,G1,G2
      READ(6,*) X,NX,CI,TH
      WRITE(7,200) X,NX,CI,TH
      READ(6,*) T0,NT
      WRITE(7,300) T0,NT
      READ(6,*) (SK(I),I=1,NT)
      WRITE(7,500) (SK(I),I=1,NT)
C
      T=0.0
      H=X/(NX-1)
      DO 10 I=1,NX
10    C1(I)=CI
1    T=T+TH
      DO 20 I=1,NX
      IF(I.EQ.1) THEN
      IF (MOD(INT(T/TH),1000).EQ.0) WRITE(0,50) T

```

```

C      TT=T/10000.
      C(1)=G1
      ELSE IF(I.EQ.NX) THEN
C      TT=T/10000.
      C(NX)=G2
      ELSE
      DD=D*TH/(H*H)
      F1=A*C1(I-1)/(C1(I-1)+B)
      F2=A*C1(I)/(C1(I)+B)
      F3=A*C1(I+1)/(C1(I+1)+B)
      CC=DD*(F1-2.0*F2+F3)+F2+C1(I)
      S=A+B-CC
      SS=S*S+4.0*B*CC
      C(I)=0.5*(-S+SQRT(SS))
      END IF
20    CONTINUE
      IF(T.GE.T0) THEN
      WRITE(7,400) T,(C(I),I=1,NX)
      ELSE
      DO 30 I=1,NX
30      C1(I)=C(I)
50      FORMAT(1X,'T=',E20.5)
      J1=0
      DO 40 J=1,NT
      IF (ABS(T-SK(J)).LE.0.17) J1=J1+1
40      CONTINUE
      IF(J1.EQ.1) WRITE(7,400) T,(C(I),I=1,NX)
      GO TO 1
      END IF
C
100   FORMAT(1X,'A=',F15.9,2X,'B=',F15.9,2X,'D=',E15.9,2X,'G1=',
* F15.9,2X,'G2=',F15.9)
200   FORMAT(1X,'X=',F15.9,2X,'NX=',I5,2X,'CI=',F15.9,2X,'TH=',
* F15.9)
300   FORMAT(1X,'T0=',F15.9,2X,'NT=',I5)
400   FORMAT(5X,'CONCENTRATION VALUE ', 'T=',E20.9/(2X,F15.9))

```

```
500  FORMAT(1X,'SPECIFIC TIME TO PRINT OUT'/4(1X,E20.9))  
      STOP  
      END
```



**PROGRAM B.4:****PROGRAM MAIN**

```

C -----
C   FORTRAN File:      ZHONG3.FOR
C   THIS A FORTRAN PROGRAM TO SIMULATE THE NUMERICAL RESULTS
C   OF DUAL-SORPTION MODEL WITH SURFACE ALWAYS ASSOCIATED
C   (SCHEME II).

```

```

C               Created by:  Zhong Li
C                               Feburary, 1994
C -----

```

```

      DIMENSION C(10000),C1(10000),SK(20),W(10000),W1(10000)
      OPEN(6,FILE='DATA')
      OPEN(7,FILE='RESULT')
C
      READ(6,*) A,B,D,G1,G2,P1,P2,D1
      WRITE(7,100) A,B,D,G1,G2,P1,P2,D1
      READ(6,*) X,NX,CI,TH
      WRITE(7,200) X,NX,CI,TH
      READ(6,*) T0,NT
      WRITE(7,300) T0,NT
      READ(6,*) (SK(I),I=1,NT)
      WRITE(7,500) (SK(I),I=1,NT)
C
      T=0.0
      H=X/(NX-1)
      DO 10 I=1,NX
      W1(I)=0.0
10    C1(I)=CI
1    T=T+TH
      DO 20 I=1,NX
      IF(I.EQ.1) THEN

```

```

IF (MOD(INT(T/TH),1000).EQ.0) WRITE(0,50) T
  TT=T/12551.
  W(1)=P1*(1.0-0.6*EXP(-TT/1.4))
  C(1)=G1*(1.0-0.75*EXP(-TT))+W(1)
ELSE IF(I.EQ.NX) THEN
  TT=T/12551.
  W(NX)=P2*(1.0-0.6*EXP(-TT/1.4))
  C(NX)=G2*(1.0-0.75*EXP(-TT))+W(NX)
ELSE
  DD=D*TH/(H*H)
  DW=D1*TH/(H*H)
  W(I)=DW*(W1(I-1)-2.0*W1(I)+W1(I+1))+W1(I)
  F1=A*C1(I-1)/(C1(I-1)+B)
  F2=A*C1(I)/(C1(I)+B)
  F3=A*C1(I+1)/(C1(I+1)+B)
  CC=DD*(F1-2.0*F2+F3)+F2+C1(I)
  S=A+B-CC
  SS=S*S+4.0*B*CC
  C(I)=0.5*(-S+SQRT(SS))+W(I)-W1(I)
END IF
20  CONTINUE
IF(T.GE.T0) THEN
  WRITE(7,400) T,(C(I),I=1,NX)
ELSE
  DO 30 I=1,NX
    C1(I)=C(I)
30    W1(I)=W(I)
50    FORMAT(1X,'T=',E20.5)
    J1=0
    DO 40 J=1,NT
      IF (ABS(T-SK(J)).LE.0.17) J1=J1+1
40    CONTINUE
    IF(J1.EQ.1) WRITE(7,400) T,(C(I),I=1,NX)
    GO TO 1
  END IF
C

```

```
100  FORMAT(1X,'A=',F15.9,2X,'B=',F15.9,2X,'D=',E15.9,2X,'G1=',  
    * F15.9,2X,'G2=',F15.9,2X,'P1=',F15.9,2X,'P2=',F15.9,2X,  
    * 'D1=',E15.9)  
200  FORMAT(1X,'X=',F15.9,2X,'NX=',I5,2X,'CI=',F15.9,2X,'TH=',  
    * F15.9)  
300  FORMAT(1X,'T0=',F15.9,2X,'NT=',I5)  
400  FORMAT(5X,'CONCENTRATION VALUE ',T=',E20.9/(2X,F15.9))  
500  FORMAT(1X,'SPECIFIC TIME TO PRINT OUT'/4(1X,E20.9))  
    STOP  
    END
```

**PROGRAM B.5:****PROGRAM MAIN**

```

C -----
C  FORTRAN File:      BLOCK1.FOR
C  THIS A FORTRAN PROGRAM TO SIMULATE THE NUMERICAL RESULTS
C  OF DUAL-SORPTION MODEL WITH ONE SIDE OF SURFACE BLOCKED
C  (SCHEME I).
C
C                      Created by:  Zhong Li
C                      February, 1994
C -----

      DIMENSION C(10000),C1(10000),SK(20)
      OPEN(6,FILE='DATA')
      OPEN(7,FILE='RESULT')
C
      READ(6,*) A,B,D,G1,G2
      WRITE(7,100) A,B,D,G1,G2
      READ(6,*) X,NX,CI,TH
      WRITE(7,200) X,NX,CI,TH
      READ(6,*) T0,NT
      WRITE(7,300) T0,NT
      READ(6,*) (SK(I),I=1,NT)
      WRITE(7,500) (SK(I),I=1,NT)
C
      T=0.0
      H=X/(NX-1)
      DO 10 I=1,NX
10    C1(I)=CI
      T=T+TH
      DO 20 I=1,NX
      IF(I.EQ.1) THEN
      IF (MOD(INT(T/TH),1000).EQ.0) WRITE(0,50) T

```

```

      TT=T/24000.
      C(1)=G1*(1.0-EXP(-TT))
ELSE IF(I.EQ.NX) THEN
      DDD=D*TH/(H*H)
      FF1=A*C1(NX-1)/(C1(NX-1)+B)
      FF2=A*C1(NX)/(C1(NX)+B)
      CCC=DDD*(FF1-FF2)+FF2+C1(NX)
      SS=A+B-CCC
      SSS=SS*SS+4.0*B*CCC
      C(NX)=0.5*(-SS+SQRT(SSS))
ELSE
      DD=D*TH/(H*H)
      F1=A*C1(I-1)/(C1(I-1)+B)
      F2=A*C1(I)/(C1(I)+B)
      F3=A*C1(I+1)/(C1(I+1)+B)
      CC=DD*(F1-2.0*F2+F3)+F2+C1(I)
      S=A+B-CC
      SS=S*S+4.0*B*CC
      C(I)=0.5*(-S+SQRT(SS))
END IF
20  CONTINUE
    IF(T.GE.T0) THEN
      WRITE(7,400) T,(C(I),I=1,NX)
    ELSE
      DO 30 I=1,NX
30    C1(I)=C(I)
50    FORMAT(1X,'T=',E20.5)
      J1=0
      DO 40 J=1,NT
      IF (ABS(T-SK(J)).LE.0.17) J1=J1+1
40    CONTINUE
      IF(J1.EQ.1) WRITE(7,400) T,(C(I),I=1,NX)
      GO TO 1
    END IF
C
100  FORMAT(1X,'A=',F15.9,2X,'B=',F15.9,2X,'D=',E15.9,2X,'G1=',

```

```
* F15.9,2X,'G2=',F15.9)
200  FORMAT(1X,'X=',F15.9,2X,'NX=',I5,2X,'CI=',F15.9,2X,'TH=',
* F15.9)
300  FORMAT(1X,'T0=',F15.9,2X,'NT=',I5)
400  FORMAT(5X,'CONCENTRATION VALUE ', 'T=',E20.9/(2X,F15.9))
500  FORMAT(1X,'SPECIFIC TIME TO PRINT OUT'/4(1X,E20.9))
STOP
END
```

**PROGRAM B.6:**

## PROGRAM MAIN

```

C -----
C  FORTRAN File:      BLOCK2.FOR
C  THIS A FORTRAN PROGRAM TO SIMULATE THE NUMERICAL RESULTS
C  OF DUAL-SORPTION MODEL WITH ONE SIDE OF SURFACE BLOCKED
C  (SCHEME II).

```

```

C              Created by:  Zhong Li
C                      Feburary, 1994
C -----

```

```

      DIMENSION C(10000),C1(10000),SK(20),W(10000),W1(10000)
      OPEN(6,FILE='DATA')
      OPEN(7,FILE='RESULT')
C
      READ(6,*) A,B,D,G1,G2,P1,P2,D1
      WRITE(7,100) A,B,D,G1,G2,P1,P2,D1
      READ(6,*) X,NX,CI,TH
      WRITE(7,200) X,NX,CI,TH
      READ(6,*) T0,NT
      WRITE(7,300) T0,NT
      READ(6,*) (SK(I),I=1,NT)
      WRITE(7,500) (SK(I),I=1,NT)
C
      T=0.0
      H=X/(NX-1)
      DO 10 I=1,NX
      W1(I)=0.0
10    C1(I)=CI
1    T=T+TH
      DO 20 I=1,NX
      IF(I.EQ.1) THEN

```

```

IF (MOD(INT(T/TH),1000).EQ.0) WRITE(0,50) T
  TT=T/12551.
  W(1)=P1*(1.0-0.6*EXP(-TT/1.4))
  C(1)=G1*(1.0-0.75*EXP(-TT))+W(1)
ELSE IF(I.EQ.NX) THEN
  DD=D*TH/(H*H)
  DW=D1*TH/(H*H)
  W(NX)=DW*(W1(NX-1)-W1(NX))+W1(NX)
  FF1=A*C1(NX-1)/(C1(NX-1)+B)
  FF2=A*C1(NX)/(C1(NX)+B)
  CCC=DD*(FF1-FF2)+FF2+C1(NX)
  SS=A+B-CCC
  SSS=SS*SS+4.0*B*CCC
  C(NX)=0.5*(-SS+SQRT(SSS))+W(NX)
ELSE
  DD=D*TH/(H*H)
  DW=D1*TH/(H*H)
  W(I)=DW*(W1(I-1)-2.0*W1(I)+W1(I+1))+W1(I)
  IF(C(I).LT.G1) THEN
    F1=A*C1(I-1)/(C1(I-1)+B)
    F2=A*C1(I)/(C1(I)+B)
    F3=A*C1(I+1)/(C1(I+1)+B)
    CC=DD*(F1-2.0*F2+F3)+F2+C1(I)
    S=A+B-CC
    SS=S*S+4.0*B*CC
    C(I)=0.5*(-S+SQRT(SS))+W(I)-W1(I)
  ELSE
    C(I)=W(I)-W1(I)+C1(I)
  END IF
END IF
20  CONTINUE
IF(T.GE.T0) THEN
  WRITE(7,400) T,(C(I),I=1,NX)
ELSE
  DO 30 I=1,NX
    C1(I)=C(I)

```



```

30      W1(I)=W(I)
50      FORMAT(1X,'T=',E20.5)
        J1=0
        DO 40 J=1,NT
          IF (ABS(T-SK(J)).LE.0.10) J1=J1+1
40      CONTINUE
          IF(J1.EQ.1) WRITE(7,400) T,(C(I),I=1,NX)
          GO TO 1
        END IF
C
100     FORMAT(1X,'A=',F15.9,2X,'B=',F15.9,2X,'D=',E15.9,2X,'G1=',
* F15.9,2X,'G2=',F15.9,2X,'P1=',F15.9,2X,'P2=',F15.9,2X,
* 'D1=',E15.9)
200     FORMAT(1X,'X=',F15.9,2X,'NX=',I5,2X,'CI=',F15.9,2X,'TH=',
* F15.9)
300     FORMAT(1X,'T0=',F15.9,2X,'NT=',I5)
400     FORMAT(5X,'CONCENTRATION VALUE ','T=',E20.9/(2X,F15.9))
500     FORMAT(1X,'SPECIFIC TIME TO PRINT OUT'/4(1X,E20.9))
        STOP
        END

```